UNIVERSIDADE D
COIMBRA

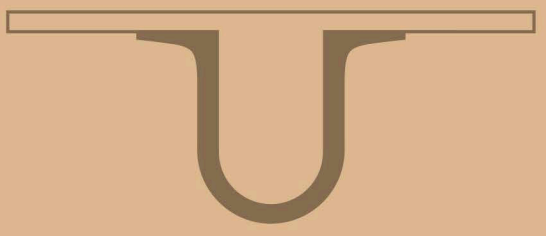

Emanuel Costa Duarte

ELECTRICAL IMPEDANCE SPECTROMETRY - APPLICATION TO PET (POLYETHYLENE TEREPHTHALATE) RELATIVE HUMIDITY DETECTION AND PRELIMINARY STUDIES TOWARDS PELOIDS CHARACTERIZATION

Thesis submitted to the University of Coimbra for the degree of Master in Engineering Physics, supervised by Professor Doctor Carlos Manuel Bolota Alexandre Correia, Professor Doctor José Paulo Pires Domingues and Professor Doctor João Manuel Rendeiro Cardoso

September 2018

UNIVERSIDADE D COIMBRA
FACULDADE DE CIÊNCIAS E TECNOLOGIA

Emanuel Costa Duarte

Electrical Impedance Spectrometry - Application to PET (Polyethylene Terephthalate) relative humidity detection and preliminary studies towards peloids characterization

Thesis submitted to the
University of Coimbra for the degree of
Master in Physics Engineering

Supervisors:
PhD José Paulo Domingues
PhD João Cardoso
PhD Carlos Correia[1]

Coimbra, 2018

This work was developped in collaboration with:

LIBPhys-UC

"Success is not final, failure is not fatal. It is the courage to continue that counts."

Winston Churchill

Aos meus pais

Acknowledgments

Gostaria de começar por deixar um agradecimento especial ao Prof. Dr. Carlos Correia por toda a sua paciência para comigo e por todos os seus contributos para o projeto. Gostaria de agradecer ao Prof. Dr. José Paulo Domingues por todo o apoio e paciência ao longo deste ano. Ao Prof. Dr. João Cardoso por todo o apoio nesta recta final do projeto e ao Tiago Marçal por todo o seu grande apoio. Gostaria de agradecer também a todos do GEI, especialmente à Ana Luísa e à Filipa pela partilha dos momentos de desespero.

Agradeço aos meus pais por terem tornado tudo isto possível e aos cromos dos meus irmãos por me chatearem e fazerem esquecer todas as preocupações.

Agradeço a toda a malta do "Maravilha Maravilha...". Todos eles especiais! Pelas sessões de estudo, pelos pequenos-almoços no Justiça, pelos cafezinhos no BM, pelas tardes de cartas na AAC e por todas as noitadas no Couraça! Muito Obrigado!

Agradeço aos PUTOS por serem todos uns cromos cada um à sua maneira especial e por todos os bons e maus momentos que passamos em Coimbra! Obrigado por terem partilhado casa comigo e por me terem dado as histórias para a vida! Somos uma verdadeira família!

Agradeço também ao Guerreiro e à Cristiana por terem lido este texto todo em busca das minhas aselhices.

Por fim, quero agradecer à minha Ana. Por me apoiar nas minhas crises existenciais e por sempre acreditar em mim.

Resumo

A Espectroscopia de Impedância Elétrica (EIE) é uma técnica com largo leque de aplicações na caracterização de propriedades de materiais sólidos e líquidos. Consiste na aplicação de uma tensão ou corrente variáveis a uma amostra e consequente medição da corrente induzida ou da queda de tensão na amostra, para assim determinar a sua impedância – a resposta em módulo e fase - numa gama definida de frequências.

O presente trabalho descreve um método baseado num impedancímetro composto por um dispositivo capaz de gerar e adquirir sinais analógicos e digitais – um osciloscópio USB comercial - Analog Discovery da Digilent, Inc - ao qual foi adicionado um interface hardware/software. O software de controlo, processamento e interface gráfico com o utilizador é baseado em Matlab.

O resultado é um instrumento de baixo custo adaptado à caracterização elétrica de um material polimérico, Polyethylene Terephthalate (PET). Este material primário é usado como dielétrico num contentor que funciona como um condensador integrado num circuito RLC e cuja temperatura pode ser controlada. Provou-se a relação entre essa caracterização elétrica (impedância) e o grau de Humidade Relativa (HR) contido em amostras desse material, característica importante para a sua aceitação/rejeição no processo industrial. Neste contexto a humidade relativa é definida como a relação entre o conteúdo, em massa, de água relativamente à massa do material seco. Os resultados apontam para níveis mínimos de deteção de humidade relativa de 0.04 $\%_{HR}$ com uma sensibilidade de 850 $Hz/\%_{HR}$ correspondendo a uma variação no pico de ressonância medida através da curva da fase em função da frequência. Considerando o interesse industrial, esta técnica distingue com clareza entre níveis de HR aceitáveis e não aceitáveis (no patamar dos 0.3 $\%_{HR}$). O sistema de elétrodos deverá sofrer evolução com foco na facilidade de acesso ao material em meio industrial.

O instrumento possui características de flexibilidade que permitem a adaptação a outro tipo de materiais como é o caso em curso da caracterização da mobilidade

iónica em pelóides. Neste caso de estudo é apresentado um aparato experimental adequado à caracterização pretendida. Numa fase inicial era importante definir alguns aspetos do sistema de medida, tais como as características dos elétrodos, o sistema de controlo de temperatura e o porta-amostras. Foi demonstrada a existência de uma dependência com a temperatura da mistura e com a concentração de argila terapêutica.

Palavras-Chave: Espectroscopia de Impedância Elétrica, Polyethylene Terephthalate, Pelóides.

Abstract

This project aims to apply a well studied technique, Electric Impedance Spectroscopy (EIS), to new fields of work. It consists of sample excitation with an alternating signal and the determination of sample's influence in the output signal to a specific range of frequencies.

The study is performed using an instrument composed by a commercial USB oscilloscope (Analog Discovery from Digilent, Inc), with a wave generator, and a control circuit. The software (user interface, control and signal processing) was developed on Matlab.

The importance of this project arose with the goal of developing a faster way to measure polymers moisture. The polymer under study was Polyethylene Terephthalate (PET). The main goal was to develop a prof of concept indicating that this technique is capable of measuring PET Relative Humidity (RH), which is here defined as the ratio of the sample water content, in mass, and the known initial mass of that sample when fully dry. P rof of concept was achieved by using the material as a dielectric in between two plates working as a capacitor integrated into an RLC circuit. So, the resonance effect as well as the influence of the material's RH on it, were studied. The results proved a relationship between impedance parameters and PET RH. It was possible to detect minimum values down to 0.04 $\%_{RH}$ with an overall sensibility of 850 $Hz/\%_{RH}$ when measuring the resonance effect in impedance's phase shift. Considering the industrial interest, this technique easily distinguishes between an acceptable and a non-acceptable level of moisture (lower or higher than 0.3 $\%_{RH}$). Electrodes should be improved to enable an easier access to the material in an industrial scene.

During PET's analysis, the interest for another case study arose: EIS of therapeutic peloid samples. In this case study, an experimental setup is provided. In this initial stage, it was important to define some proprieties of the measuring system, such as the sample holder, the heating system, and the electrodes characteristics. Some preliminary results were obtained such as: impedance dependency on temper-

ature and on peloid concentration in a mixture with distilled water.

Keywords: Electric Impedance Spectroscopy, Polyethylene Terephthalate, Peloids.

Contents

Acronyms

2D Two-Dimensional

3D Three-Dimensional

ABS Acrylonitrile Butadiene Styrene

AC Alternating Current

ADC Analog-to-Digital converter

Op-Amp Operational Amplifier

CEC Cation-Exchange Capacity

CMOS Complementary Metal-Oxide Semiconductor

CPE Constant Phase Element

DC Direct Current

DDL Diffuse Double Layer

DFT Discrete Fourier Transforms

EIS Electrical Impedance Spectroscopy

FFT Fast Fourier Transform

FRA Frequency Response Analysis

GEI Electronics and Instrumentation Group

LED Light-Emitting Diode

LOD Limit of Detection

MI Current Mode

MOSFET Metal-Oxide Semiconductor Field-Effect Transistor

MV Voltage Mode

PCB Printed Circuit Board

PET Polyethylene Terephthalate

PLA Polylactic Acid

PSD Phase-Sensitive Detection

RH Relative Humidity

USB Universal Serial Bus

List of Figures

List of Tables

CHAPTER 1

Introduction

The motivation and main objectives of this thesis are provided in this chapter. Here, it is presented an introduction related to each case study and their state of the art. Finally, a project contextualization is provided as well as the requirements analysis.

1.1 Motivation

Modern engineering, with the heritage of its long history, pursuits solutions capable of solving society's problems. Our society is living in a digital era and the role of an engineer is to answer society's demand on technological evolution, asking for faster and accurate measuring systems, with more features, but at a lower price.

In order to be able to successfully answer this demand, an engineer needs to evaluate and fully understand the environmental conditions. By doing an adequate study, engineers can achieve an instrument capable of correctly control, measure and manipulate almost everything, even if it takes longer than expected.

Technology has evolved to a point where the existing tools and methods need to be replaced by new techniques achieving the same result in a faster and more convenient way. Implementing Electrical Impedance Spectroscopy (EIS) to new fields of work could result in a new measurement method. This is due to impedance's big sensibility to electrochemical changes of an object.

1.2 Polyethylene Terephthalate

The first polyester related experiment was prepared by Carothers and Hill around 1932. It was discovered that mixing alcohols and carboxyl acids results in some sort of fibers [1]. Later, in 1941, further investigation was made in this area, discovering that higher melting points could be accomplished using terephthalic acid. This discovery was made by British Scientists, Whinfield and Dickson. In that same year, Terylene was created, being the first polyester fabric manufactured. DuPont bought out all polyester rights in 1946 and developed Dacron.

In 1966, Akzo company was the first to commercialize Polyethylene Terephthalate (PET) as a design material. Other companies, such as Hostadur or Crastin, introduced themselves in the market of injection-moldable PET. In the 90's polyester fiber had around 40 per cent of the total synthetic fiber production. But, in the last two decades, our society has been increasingly more concerned with environmental causes. It is easy to understand why this happens as plastic wastes can have a huge impact in natural ecosystems.

As the time passes more efforts are being done to reduce the use of non-recyclable or non-reusable materials. That is the main reason there is an huge market around recycling plastic waste [2].

Nowadays, developed countries seek to export their waste for other countries to recycle it. In 2016, China imported more than 7.3 mega tonnes of it, from countries such as the UK and the USA [3].

PET is a hygroscopic polyester with high strength and safe to use as a container material, that's why it has a big role in the world of plastic bottles and fabric [4, 5]. Between 75 °C and 255 °C, PET glass transition temperature and melting point, respectively, the material is extremely pliable, making it an ideal molding material for a wide application cluster [6]. PET also provides good protection from oxidation reactions and deterioration, due to high impermeability to CO_2 and O_2.

PET chemical formula is $C_{10}H_8O_4$ (Fig. 1.1) and its normal density is 1.38 g/cm^3, at 20 °C. When this polymer is exposed to very humid environments it will absorb water molecules with a rate up to 0.1 % in 24 hours [7, 8, 9].

Once PET reaches the end of its life cycle, the most common post-consumer technique used to recycle it is by mechanical methods [10]. After that, if the recycled material is exposed to air humidity, water is absorbed resulting in PET's moisture.

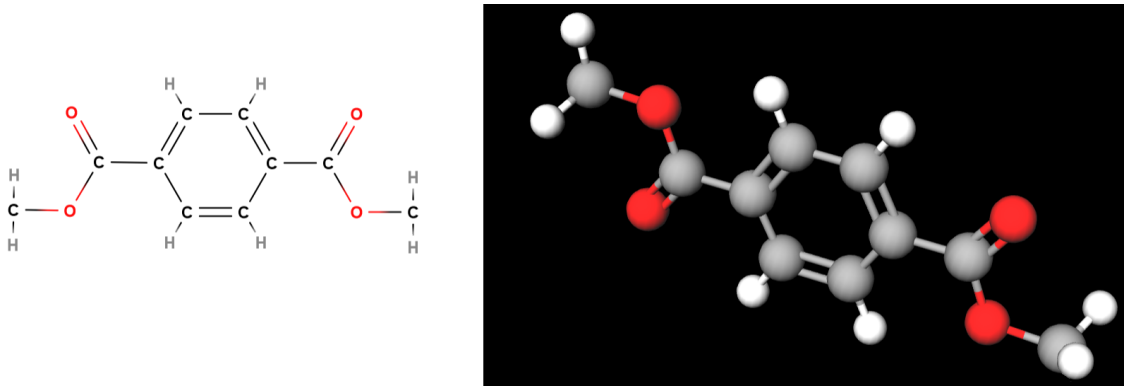

Figure 1.1: Two-dimensional (2D) and three-dimensional (3D) representation of the PET molecule. In 3D model, each sphere represents an atom: red spheres for Oxygen, gray spheres for Carbon and white spheres for Hydrogen.

The presence of water within polymer molecules can cause hydrolysis when molding the material [11, 12]. This molecular reaction reduces its strength and its density. Moreover, PET is more vulnerable to microbes.

PET films is nowadays used extensively as photographic and X-ray film, 3D printing material, and for packaging films [13, 14, 15].

Regardless of relative humidity being the ratio of the amount of water vapor to the value needed to air saturation (at the same pressure and temperature), every time it is referred to PET's Relative Humidity (RH) during this project, it is considered the amount of water absorbed by the sample (Eq. 1.1).

$$Relative\ Humidity = \frac{Mass_{absorbed\ water}}{Mass_{dry\ PET}} \times 100\ \% \tag{1.1}$$

State of the Art

Fortunately, plastic recycling has been increasing in the last years, and international organizations aim to keep it going. However, the moisture present in the material can't just be ignored. Before drying and molding PET, companies need to find out the exact RH present in the material. This will be the main goal of this project. In the market there are already options for this problem, but the majority of them are bench instruments. Therefore, they are not as practical as the one proposed here [16]. Furthermore, the solutions found are quite expensive.

Humidity detectors are based in physical principals, measuring variables such as resistance or capacitance [17]. Resistive detectors make use of thick-films polymers

(Ex. Carbon Polymers) in which the material shows a variation in resistance with humidity. On the other hand, capacitive detectors make use of thin-films as dielectric material. In both cases, the material absorbs water molecules, leading to a change in conductance.

One commercially available moisture meter is Aquatrac® - 3E, which measuring principle is based in the chemical equation: $CaH_2 + 2H_2O \longrightarrow Ca(OH)_2 + 2H_2$. The sample is placed in a low pressure vessel (lower than 10 $mbar$) and heated to a desired temperature (between 60 to 200 degrees Celsius). The evaporated water reacts with calcium hydride (placed above the sample) and from this reaction results hydrogen gas. The gas pressure is proportional to the water present in the sample and can be monitored using piezoelectric transducers. Thereby, the percentage of water is obtained by the ratio of pressure to sample weight [18]. Other types of gas moisture detection can be implemented, such as electrolysis [19].

Accordingly to Logoplaste, a multinational company that produces rigid plastic containers, with a production facility near Coimbra, the fastest and cheapest way to estimate PET moisture is to accurately weight the given sample (considering its density) and compare the value with a dry reference sample [20].

In order to optimize PET drying process, improving its temperature set-point and duration, this study must provide a better way to measure RH.

1.3 Peloids

Due to the healing properties of portuguese mineral waters, portuguese people have the tradition of going to spas. Other options appeared in the market making use of those same waters, which is the case of pelotherapy. It consists in the application of maturated muds, peloids, which are composed by mixtures of sea or mineral waters, materials with fine grains, and organic compounds [21]. Peloids' maturation process involves chemical, physical, and biological phenomena, from which results a material enrichment on organic compounds [22]. The necessary maturation time varies between these mixtures. Usually, peloids are directly applied into the skin for about 20 minutes at an initial temperature between 40 and 45 ^{o}C [23].

The most common fine-grained materials used in pelotherapy are clay minerals, which grains diameter are smaller than 2 μm. Their principal compounds are sodium, calcium, magnesium, iron, and potassium, but some organic compounds can also be found within the material, such as calcite, quartz particles, or soluble

salts [24]. In fact, to correctly characterize peloids, information about its pH, adsorption capacity, Cation-Exchange Capacity (CEC), plasticity, among others, need to be considered [21].

State of the Art

Edersensae is an R&D project being held by Exatronic, an instrumentation company based in Aveiro that develops new devices, with the collaboration of Universidade de Aveiro. The main focus of this project is to control and optimize peloids application [25]. At the moment, this is achieved by applying a DC current in the peloid during its skin application. The main objectives are:

- Development of a non-invasive medical device capable of providing a constant temperature while enabling transdermal transmission of peloids' active assets;
- Define the perfect material characteristics to use in this new device.

The second objective was already achieved, while the other one is still under study. Up to this point, this working device enables currents up to 6 mA and constant temperatures of 45 ^{o}C. The next step is to study peloids' behavior under the application of AC current. Therefore, it will be used EIS to study and identify cation exchange behavior alterations through the frequency spectrum.

Based on literature review and to the best of our knowledge, this is the first time that EIS is going to be applied to peloids. In fact, there are already other studies performing it into clay-materials, but the information gathered was related to clay strength or other properties changes [26, 27].

1.4 Requirements Analysis

The main focus of this project is the correlation between EIS parameters with new fields of work.

1.4.1 PET

In order to develop this proof of concept some requirements need to be defined, concerning points such as Moisture Profile, RH detection and hardware.

Data analysis needs to grant access to PET categorization, making possible the discrimination of non-acceptable PET RH.

A simple-to-use interface needs to be developed in order to make the process easy to reproduce. Moreover, a smart fitting algorithm capable of adapting to various test conditions needs to be achieved.

The output of this algorithm must fulfill the following requirements:

- 0.01 $\%_{RH}$ (0.1 g_{H_2O}/kg_{PET}) resolution
- Good linearity in frequency domain where PET as around 0.3 $\%_{RH}$ ($3g_{H_2O}/kg_{PET}$). That is the maximum acceptable limit from an economical perspective, according to Logoplaste.
- Amplitude range from 0 to 2 $\%_{RH_{PET}}$

1.4.2 Peloids

In this case study, the requirements diverge from the previous one. The main goal is to study the samples instead of the development of a prototype. Once this study is started, the main objective during this project becomes the definition of some aspects of the measuring system, which includes the heating system, sample holder and electrodes.

At the end of this project it is expected one system capable of stabilize the sample temperature at 45 ^{o}C with a easy-to-clean sample holder and reliable electrodes.

Considering the overall study, its main goal is to find a frequency (or a range of them) where peloids' active assets transmission is optimized.

1.4.3 Hardware

In a long term, the final goal of the overall project is to develop an inexpensive and user-friendly moisture detector. The final product should have a test time below one minute and, if possible, detect errors induced by test conditions. Regarding the electrode probe system, it needs to be easy-to-use, characterized by a good conductance and low-impedance. Made from a material that will not react with the sample under test.

Considering these requirements and taking into consideration that the final prototype must be portable, the maximum volume should be around 1.5 liters ($150 \times 100 \times 100\ mm$) and a weight up to 1 kg (not including the electrodes).

1.5 Project Contextualization

Although not indicated, formally, as a supervisor, the project is by Professor Dr. Carlos Correia, having been the main engine for the elaboration of the same

The present study took place within the Electronics and Instrumentation Group (GEI)[1]. The interest within the group in EIS dates back to 2008 and over time it had distinct fields of study, such as plant diseases, waste-water contaminants, malaria disease and impedance cardiography [20, 28, 29, 30]. The impedance measurement technique was also changed through time, evolving from a frequency domain method to the one present here (time domain method) [31, 32].

Tests were performed using an impedance meter based in the one used to study malaria disease [20, 28]. The initial tests consisted in the device debugging by performing EIS into passive components. After fully rely on the device's output, tests on samples were performed.

The results obtained during this study resulted in a scientific poster presented at *FÍSICA 2018 – 21ª Conferência Nacional de Física e 28º Encontro Ibérico para o Ensino da Física*, which abstract is available in Appendix A.

[1]This project was idealized by Professor Correia, who provided assistance during the early stage of this project.

CHAPTER 2

Theoretical Background

In this chapter the overall background of the measurement technique is described. Furthermore, some of its applications are here provided. The measurement principle here used is explained as well as some of the concerns around it. At the end, a study on clay-water mixture behavior is presented in order to better understand peloids' impedance.

2.1 Electrical Impedance Spectroscopy

In Alternating Current (AC) circuits, the concept of impedance arises. It characterizes the ability of an electrical circuit to oppose the flow of electric alternating current at a specific frequency [33].

This property is well described by Equation 2.1:

$$Z(\omega) = Z_0 sin(\omega t - \phi) \tag{2.1}$$

where ω is the angular frequency, given by $\omega = 2\pi f$, Z_0 is the voltage amplitude divided by current intensity, and ϕ is the phase shift.

The EIS technique takes advantage of two impedance attributes, phase shift, ϕ, and magnitude, $|Z|$. The first one represents the angular phase difference between voltage and current.

The impedance equation can be rearranged to:

$$Z = Z' + jZ'' \tag{2.2}$$

where Z' and Z'' are the real and imaginary part of impedance, respectively, and j is $\sqrt{-1}$. The first one is also know as resistance and Z'' as reactance.

So, impedance modulus is given by:

$$|Z| = \sqrt{Z'^2 + Z''^2} \tag{2.3}$$

and phase shift by:

$$\phi = arctg\frac{Z''}{Z'} \tag{2.4}$$

Figure 2.1 gives a proper representation of the complex impedance plane. In the horizontal axis is expressed the dissipated energy, $Re(Z)$, and in the vertical one is the stored energy, $Im(Z)$.

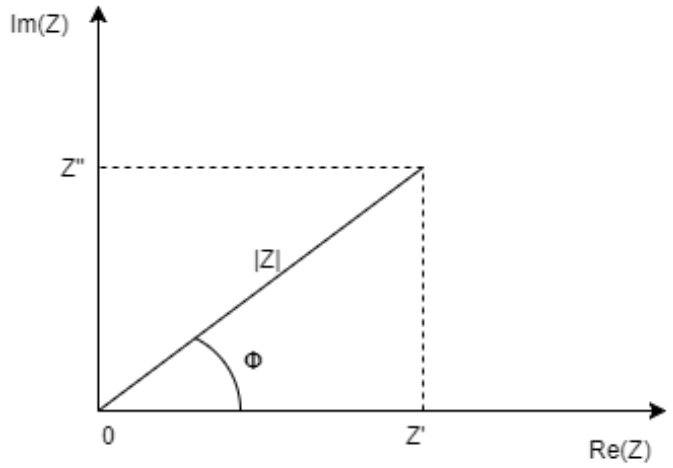

Figure 2.1: Graphical representation of the impedance plane.

These two features are given by:

$$Z' = |Z|cos(\phi) \tag{2.5}$$

$$Z'' = |Z|sin(\phi) \tag{2.6}$$

The advantage of using AC measurements rather than Direct Current (DC) ones

arises from the extra information gathered, the latter only provide the real component of impedance. In AC measurements the impedance of a system can be measured by making use of techniques such as Phase-Sensitive Detection (PSD) or Frequency Response Analysis (FRA), which fit in the category of frequency domain methods [31, 32, 34]. In contrast, the method applied here belongs to the time domain, as explained in Section 2.1.1 [35].

EIS is a sensitive technique that measures impedance properties of a material through a range of frequencies. Using this technique, it is possible to obtain information about dielectric values of the material [35]. It can therefore provide a non-invasive and radiation-free measurement. Making EIS an ideal candidate for Industrial applications (Fig. 2.2), such as material evaluation, study of electrochemical power sources components performance, study of fuel cells, among others [35].

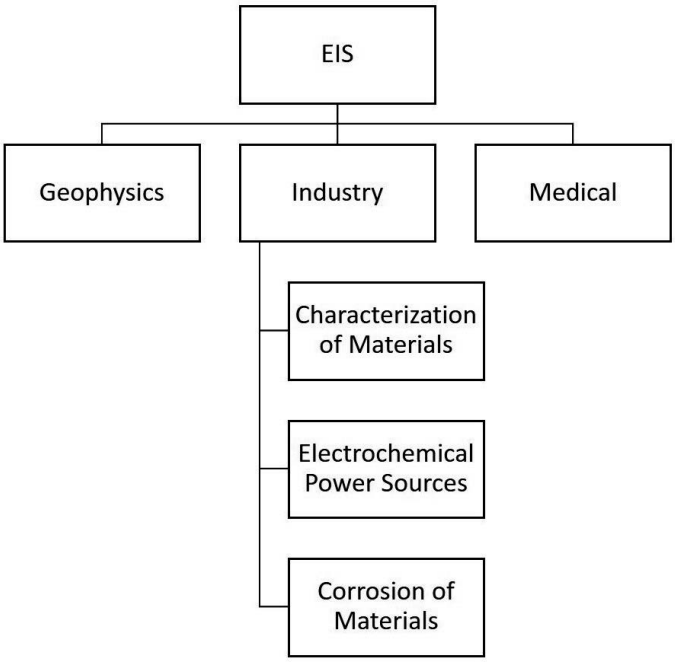

Figure 2.2: Some areas of application of EIS.

As mentioned in Chapter 1, the purpose of the overall project is to achieve a cheap, portable and reliable impedance meter. When searching for RLC meters or spectrum analyzers, one can find the most distinct devices. There are devices with just four measuring frequencies and others with ranges from 2 Hz up to 110 GHz [37, 38]. Considering expensive devices more features are available, also, more accuracy (up to 0.05 %) and better frequency resolutions (up to 0.01 Hz) [39]. In the market there are commercial instruments with high resolutions; however, for the case studies hereby presented most of these devices will not fit to our requirements, most of them

are bench meters, losing points in mobility, and the goal is not to develop the most accurate device, but rather a precise and reliable one [36].

2.1.1 Measurement Principles

Commonly, impedance measurements require excitation with current and measure a voltage, or the exact opposite. The nature of excitation signal varies depending on the application. The discussion on what mode is the most convenient to the application under study remains [40]. However, current sources need high-precision components and at higher frequencies accuracy decreases, while voltage sources can operate over a larger frequency range and are built with cheaper components [41, 42].

The excitation signal was given by a sinusoidal wave with 1 V of amplitude. The impedance meter used had two excitations modes: excitation by current (MI), when the material is placed in the feedback path of the amplifier, or by voltage (MV). The first excitation mode introduces a constant current in the sample and the second one a constant voltage [20]. Both equivalent circuits make use of an inverting Operational Amplifier (Op-Amp) configuration, as depicted in Figures 2.3 and 2.4.

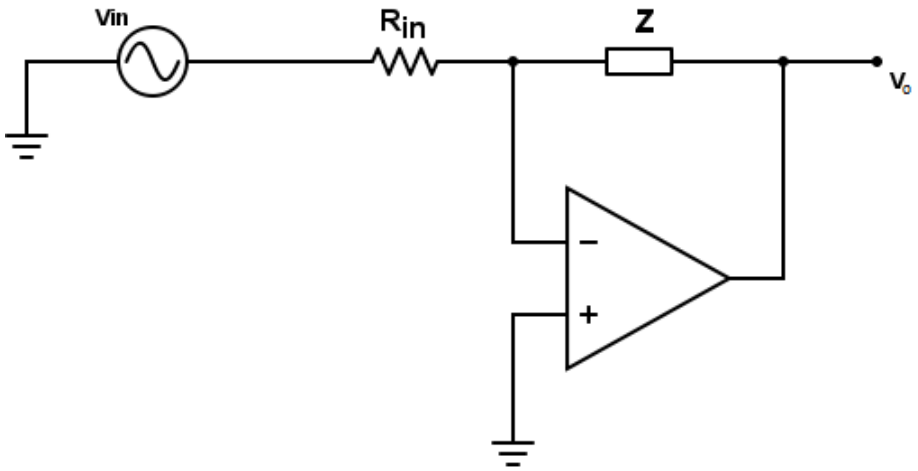

Figure 2.3: Inverting Op-Amp configuration for current mode excitation (MI).

In Figures 2.3 and 2.4 Z represents the sample between the electrodes and R_{in} is the resistance used to obtain a gain of approximately 1 at the output. For this type of Op-Amp configuration, the expected output signal in MI is:

$$V_o = -\frac{Z}{R_{in}} V_{in} \tag{2.7}$$

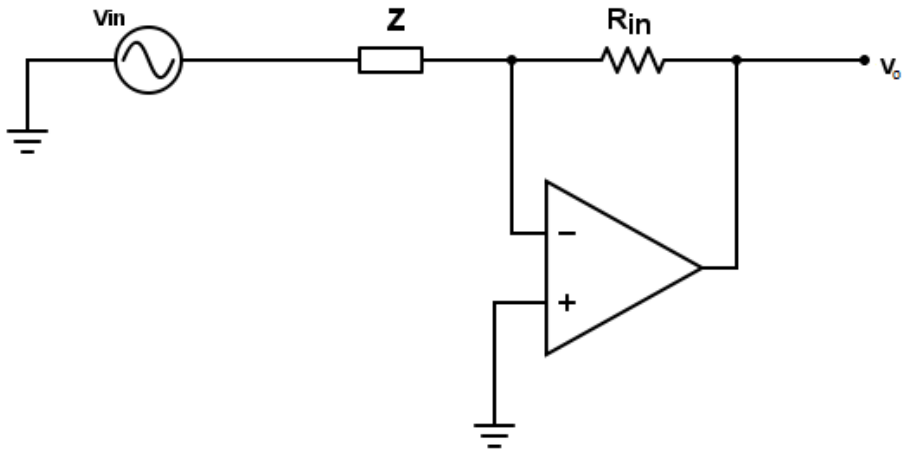

Figure 2.4: Inverting Op-Amp configuration for voltage mode excitation (MV).

and for MV it is:

$$V_o = -\frac{R_{in}}{Z}V_{in} \tag{2.8}$$

Since the Op-Amp saturates at $|V_0| > 15V$, the selection of the resistor R_{in} is an important decision to make. Therefore, it needs to be considered the Z impedance between the electrodes to adjust R_{in} to a Gain$\sim$1.

Knowing the excitation signal frequency, current, and voltage, enables the absence of reactance reference values. When analyzing the acquired data, it is important to take into consideration the presence of undesired signals. Those can arise from parasitic interferences, reactions between the electrode and the mass, among others [20].

Impedance data visualization can be achieved in distinct forms, such as Bode Plots, were impedance modulus and phase shift are plotted through a limited range of frequencies. Additionally, data can be depicted as shown in Figure 2.1, which are called Cole-Cole plots.

Data Analysis Method

The method applied in this project to obtain impedance is defined as a time domain method. It requires two major steps: input and response analog-to-digital conversion and their transformation from time domain into the frequency domain. The first step requires sampling and quantization of the signal, which is achieved using an Analog-to-Digital converter (ADC), and the latter requires mathematical transformations, such as Laplace's or Fourier's [35].

Considering that impedance is described as shown in Equation 2.9, where $V(t)$ and $I(t)$ are the voltage and current behavior in the time domain, respectively, by applying a Fourier transformation (Eq. 2.10) into the data acquired impedance is now calculated by Equation 2.11 [35].

$$Z(t) = \frac{V(t)}{I(t)} \tag{2.9}$$

$$F(jw) = \int_{-\infty}^{+\infty} F(t)e^{-jwt}dt \tag{2.10}$$

$$Z(jw) = \frac{V(jw)}{I(jw)} \tag{2.11}$$

A further explanation of this method is given in Section 3.1.2, where the MATLAB® functions used are explained and some limitations are provided.

2.1.2 EIS Errors

In order to succeed in data analysis, considering an appropriate algorithm, the data measured should be free from artifacts. The most common source of errors in impedance spectroscopy is capacitive leakage caused by stray capacitances in parallel with the measured load [43].

Other parameters can affect the data. Among them, the most relevant to consider is given by cables characteristics, which connect the Printed Circuit Board (PCB) to the electrode probe system. Considering that they present a resistive and capacitive behavior, they must be as short as possible.

Since stray capacitances are considered systematic errors, thus affecting all the measurements, their influence does not directly affect the intended analysis. However, it is important to consider the real equivalent circuit (Fig. 2.5), taking into account the effect of all parasitic elements.

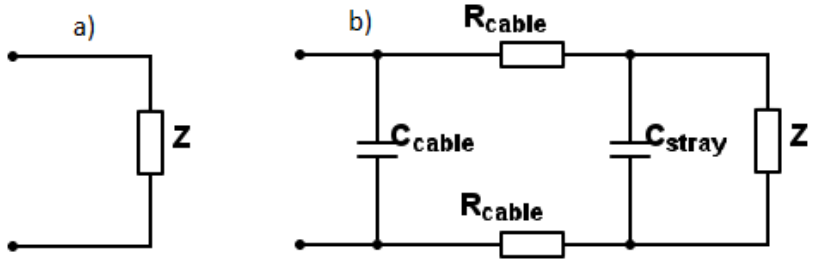

Figure 2.5: Electrode Probe system under "ideal" conditions (a) and under typical conditions (b). Showing stray capacitance (C_{stray}), load impedance (Z), cable capacitance (C_{cable}) and cable resistance (R_{cable}).

2.2 Clay-water mixtures

As an attempt to acquire as much information as possible about how the peloids results should look like, this section provides a study about non-maturated clay-water mixtures as there is not much information about peloids themselves.

When dry, clay-particles possess cations in the holes of their surfaces, which are helded by clay's negatively charged surfaces. After mixing them with water, a layer of adsorbed water molecules is created around it. In this layer, mixed with the water molecules, those same differently charged cations can be found [44, 45]. These elements work to balance the negatively charged clay surface; as a result, it is formed a Diffuse Double Layer (DDL).

The capacity of retaining those cations at its surface is measured by the CEC and it is presented in miliequivalent per 100 grams of mineral (meq/100g). Considering that the electrical conductivity depends on the excess of ions at the clay-particles surface, CEC should be a good indicator of how impedance changes between samples. Figure 2.6 provides a simple explanation of the cation exchange process [46, 45].

Taking into account the frequency spectrum, electrical conductivity behaves differently from sample to sample, increasing for some of them and decreasing in others. Moreover, it is also possible to take into consideration the changes in the dielectric permittivity, which, usually decreases as the frequency increases [46].

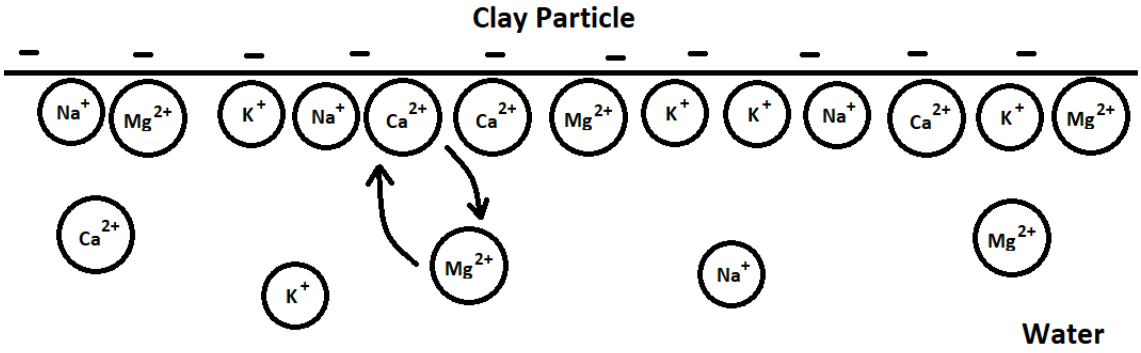

Figure 2.6: Cation exchange process in the DDL (adapted from [45]).

Impedance Models

In clay studies, impedance is usually plotted in Cole-Cole diagrams. Figure 2.7 provides some equivalent circuits that are commonly used to characterize clay-water mixtures behavior through frequency spectrum [47].

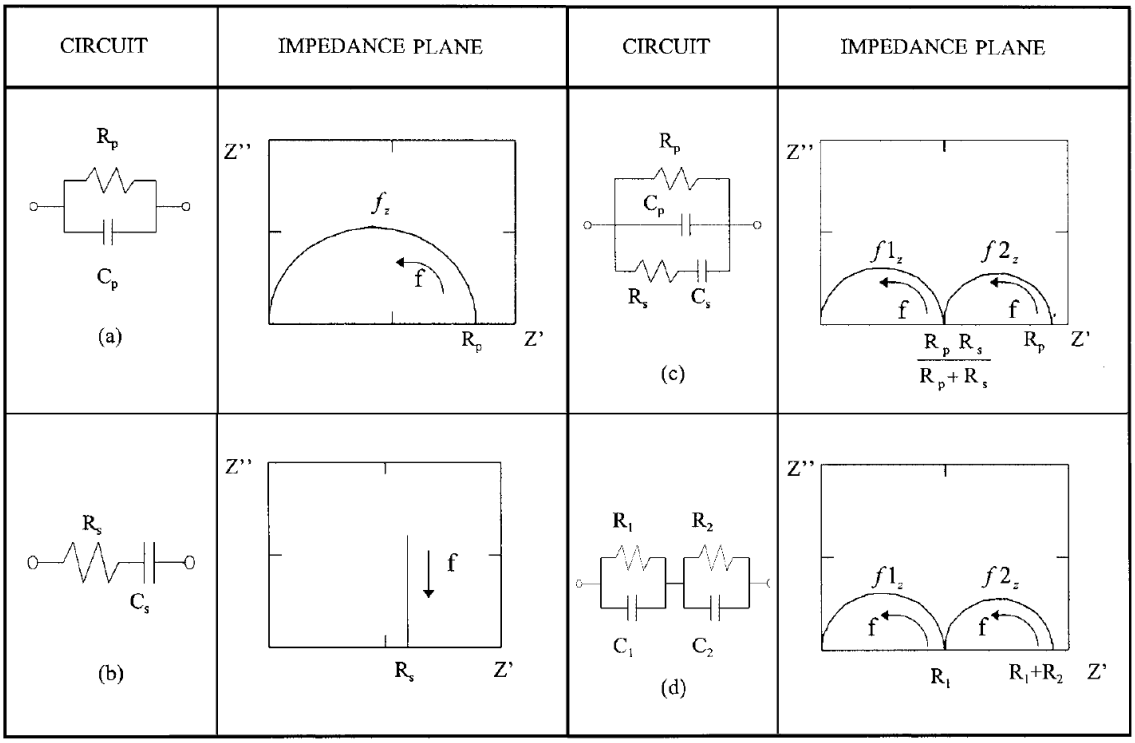

Figure 2.7: Clay-water mixtures basic equivalent circuits: (a) Parallel RC; (b) Series RC; (c) Debye equivalent circuit; (d) Maxwell-Wagner equivalent circuit. (Figure adapted from [47])

Considering the different equivalent circuits, the parallel RC circuit depicts a decrease in the real part of the impedance and a peak in the imaginary component.

Circuit (b) manifests a vertical line along the Cole-Cole plan, portraying a constant resistance through the frequency spectrum [47].

Both circuits (c) and (d) are used when the material presents more than one polarization mechanism as shown in Figure 2.7. Usually, impedance presents a more complex behavior, resulting in the overlapping of those semicircles in addition with some lines, resulting in a more complex analysis [47].

The resistors and capacitors depicted in Figure 2.7 describe the DDL behavior, which depend on the mixture's characteristics, such as temperature or electrolytes concentration [45].

In reality, it is usually added a resistor in series with these circuits, corresponding to the overall electrolyte resistance. Moreover, instead of the normal capacitors, Constant Phase Element (CPE) components are being used to portray the non-ideal capacitive response, which improves the overall fit [47].

CHAPTER 3

Materials and Methods

In this chapter the materials under study, the methods used and the main tools are presented. In the first section, a detailed description of all the hardware used is provided, as well as the overall software background. Additionally, the main tools and test objects are listed. The last section, contains the overall methods, including a detailed description of the measurement methods and the preparation procedures for the samples. Moreover, a technique for silver electroplating on copper is described.

3.1 Materials

3.1.1 Hardware

The necessary hardware to perform the measurements is summarized in Figure 3.1. The overall impedance measurement system is composed by a bench DC power supply, Digilent® - Analog Discovery (controlled using MATLAB®), an impedance measurement circuit, a temperature sensor, and the sample holder with electrodes incorporated.

3.1.1.1 Power Supply

Initially, the idea was to use an Universal Serial Bus (USB) port ($+5V$) to power all the system, and then use a DC/DC converter (*TMR 3-0523*) to power the impedance meter amplifier ($\pm 15V$). However, during tests, it was found that

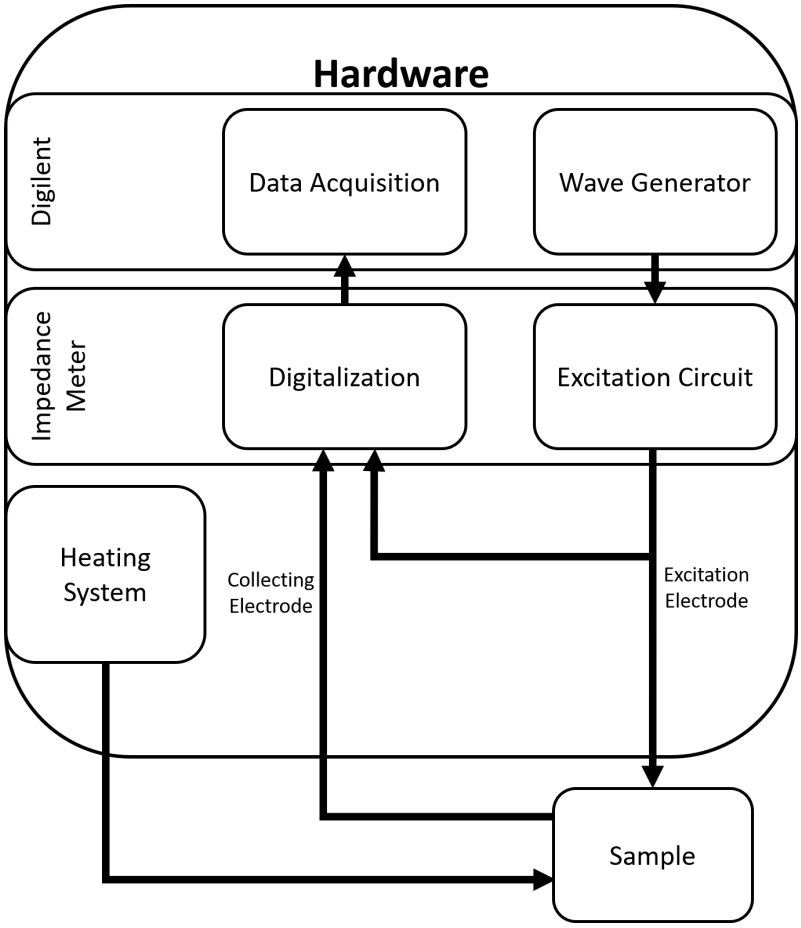

Figure 3.1: Hardware block diagram.

the current output of the USB port was not stable. This caused faulty DC/DC operation, which resulted in the Op-Amp saturation and, consequently, artifacts in impedance spectroscopy plots. Therefore, a midterm solution was to make use of a bench DC power supply (*PROTEC DF1731SL5A*).

3.1.1.2 Digilent® - Analog Discovery

Digilent® - Analog Discovery is an USB oscilloscope and multi-function instrument from *Digilent Inc* (Figure 3.2) [48]. The device is capable of measuring, recording, and generating analog and digital signals. In addition to the device's low price (around 230 €), the main reason to use it is its' portability [49].

The most important features to the project are:

- Two-channel Oscilloscope (Sampling up to 100 Msample/s);
- Two-channel waveform generator;

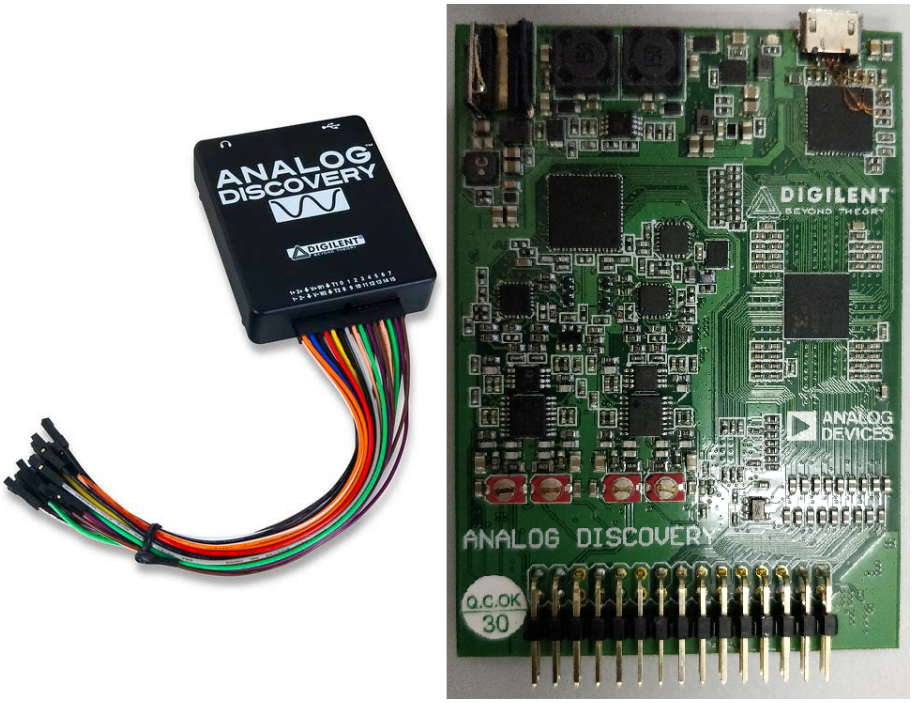

Figure 3.2: Left: Digilent® - Analog Discovery commercial package (extracted from [48]); Right: Digilent® - Analog Discovery board inside the black package (zoomed).

- Sixteen Digital I/O.

Moreover, Analog Discovery has a user-friendly interface (Digilent® - WaveForms) and can also be easily controlled with MATLAB® using the functions provided in the SDK file.

3.1.1.3 Impedance Meter

Figure 3.3 represents the circuit responsible for the precise impedance measurement[2]. The PCB where it was built is fully controlled using Digilent® - Analog Discovery, which is connected to the circuit by a 30-pin header.

From the schematics (Fig. 3.3) it is possible to identify two digitally controlled multiplexers, ADG1408 and ADG1409. The first one is used to adjust the internal resistance (R_{in} from Fig. 2.3 and 2.4), and the latter is responsible for excitation modes/temperature reading switching (case S1 - MV; case S2 -MI; Case S3 or S4 - Temperature) [50].

The referenced board is inside a 3D printed Polylactic Acid (PLA) box (Fig. 3.4)

[2]Developed under the framework of the global project. It was assembled, debugged, and tested during this thesis.

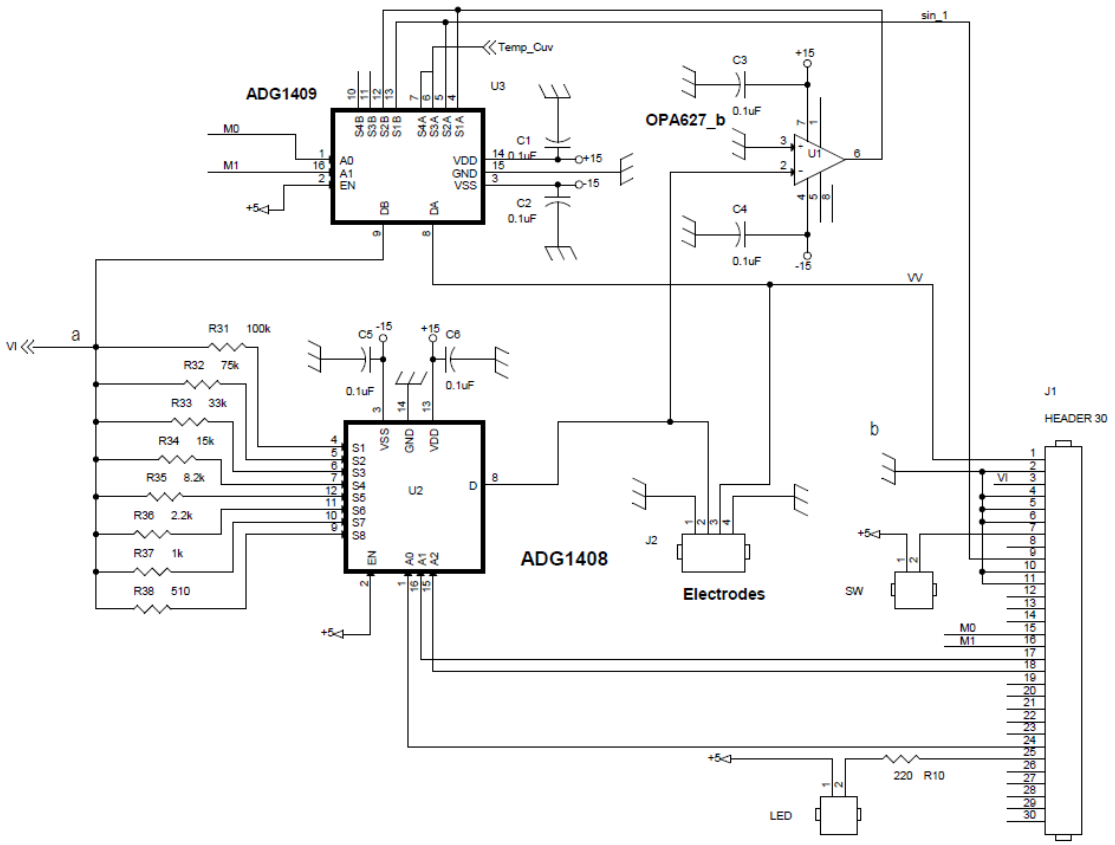

Figure 3.3: Impedance measuring circuit used for both excitation modes (MV and MI) and for temperature measurements.

(see Appendix B for the 2D drawings of the box). Two cables connect the board to the electrodes. Connected to this box is also a jack used for power supply and a micro-USB cable to communicate with the computer.

3.1.1.4 Temperature Sensor

Temperature is one important factor to take into account when making impedance measurements. Thus, one thermal resistance was added in order to measure this parameter. The thermometer circuit implemented (Fig. 3.5) makes use of a PT1000, a platinum temperature sensitive resistance.

PT1000 resistance, R_{PT1000}, can be obtained by Equation 3.1, where Z_{eq} is the resistance equivalent impedance from the parallel of R_{17} and C_9. Using a *LM4040A25I* as a shunt voltage reference, the input voltage is $V_i = -2.5V$ [51].

$$R_{PT1000} = -\frac{V_o}{V_i} R_{15} \frac{R_{16}}{Z_{eq} + R_{16}}, Z_{eq} = (R_{17}//C_9) \tag{3.1}$$

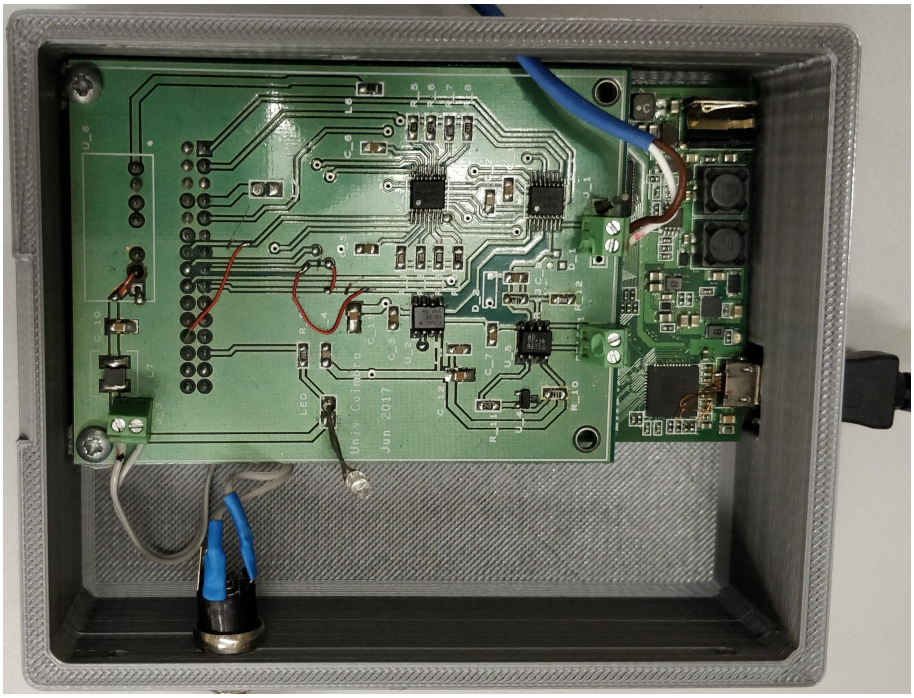

Figure 3.4: Impedance and temperature measurement circuits mounted in a PCB.

In this application only DC signals are expected, thus capacitor impedance can be ignored. Taking in consideration this change, the expected resistance is now given by Equation 3.2.

$$R_{PT1000} = \frac{-\frac{V_o}{V_i}R_{15}}{\frac{R_{17}}{R_{16}} + 1} \tag{3.2}$$

Accordingly to the components datasheet, temperature conversion is given by Equation 3.3.

$$T = -\frac{-R_0 A + \sqrt{(R_0 A)^2 - 4R_0 B(R_0 - R_{PT1000})}}{2R_0 B} \ [^oC] \tag{3.3}$$

Where R_0 is the sensor resistance at 0 ^oC, A and B are constants for a resistive temperature sensor with 3850 ppm/K (they are namely 3.9083×10^{-3} $^oC^{-1}$ and -5.775×10^{-7} $^oC^{-2}$).

Considering Equation 3.2 and the resistor values presented in Figure 3.5, the output gain can be easily calculated. In the second case study this parameter presented a problem: considering measurements from 0 up to 50 ^oC, the output variation would be of 0.22 V from end to end, which introduced measurement errors due to

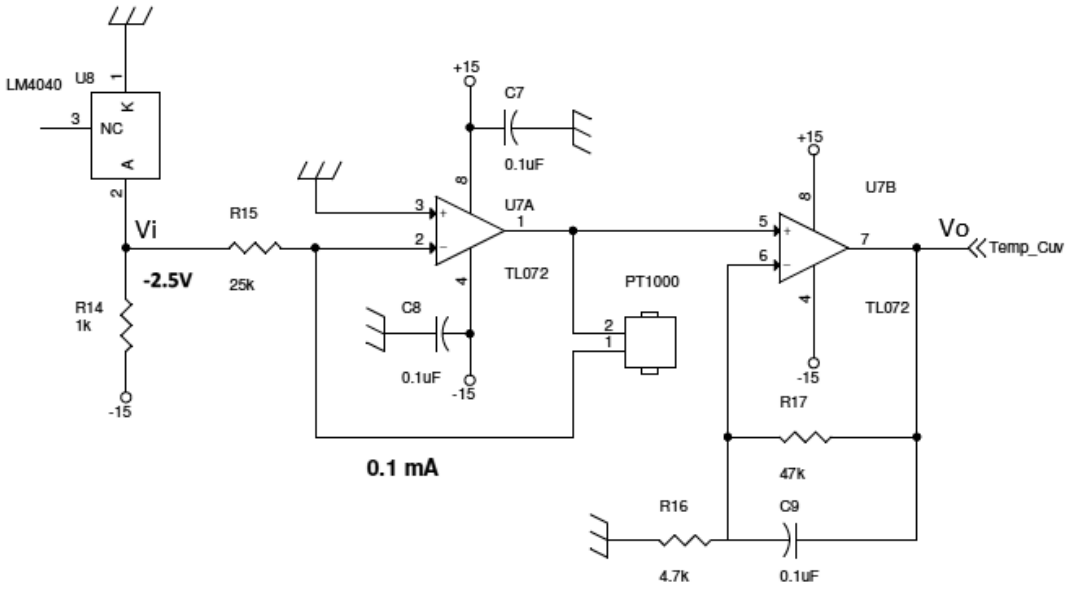

Figure 3.5: Temperature measurement circuit.

voltage fluctuations. The mid-term solution was to increase the output gain, by changing the resistors values and making sure that the Op-Amp didn't reach saturation. The final temperature measurement circuit was soldered with: $R_{15} = 24\ k\Omega$, $R_{16} = 2\ k\Omega$, and $R_{17} = 180\ k\Omega$.

3.1.1.5 Sample Holder

PET

PET's sampler holder was printed with white PLA and can be filled with a volume of PET up to 0.2 l.

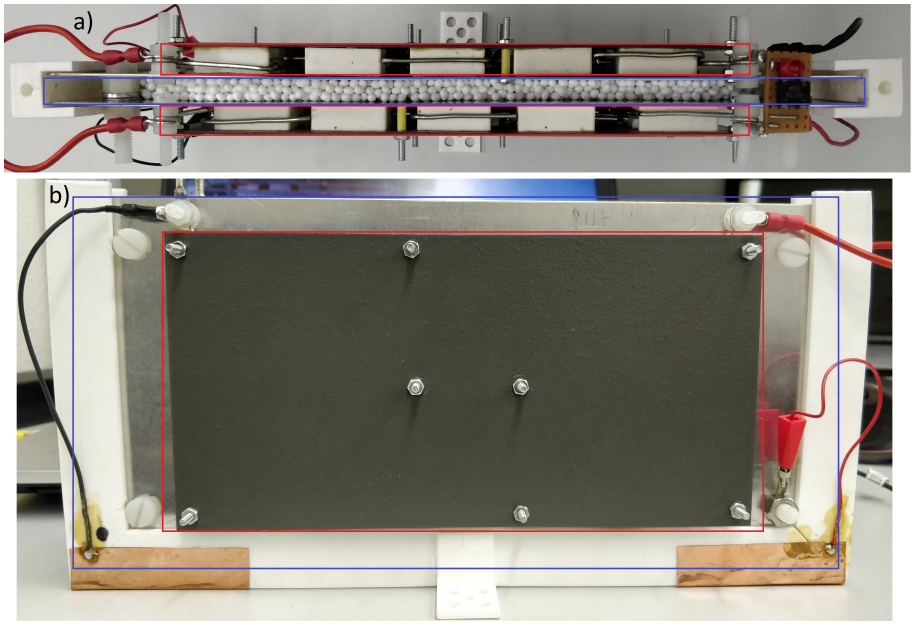

Figure 3.6: PET Heating System, Sample Holder, and Electrodes. (a) Top View (b) Front View (Red Boxes: Heating System; Blue Boxes: Sample holders and electrodes).

Peloids

Initially, peloid sample holder was fully printed with grey PLA and then treated in order to prevent liquid (water) leaks. The container's inside was coated with ethyl acetate to avoid reactions between PLA and the samples. All the possible leak points were glued using an epoxy adhesive (Araldite® Standard) and the box capacity was up to 1.7×10^{-2} l.

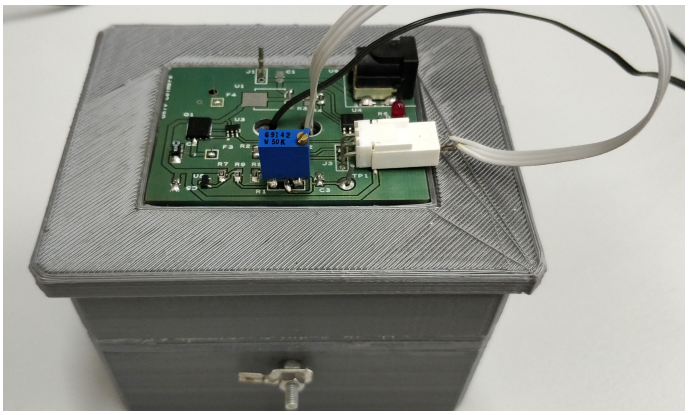

Figure 3.7: Box system peloid sample holder and heating controller circuit board.

However, this box presented some concerns with respect to heat dissipation and tests' range of temperatures. Seeing as those tests were performed at temperatures around 45 ^{o}C and PLA starts to be malleable at 60 ^{o}C (glass transition temperature) an upgrade was considered necessary. In this realm, it was reckoned that the

next container should be composed by (Fig. 3.7): an inner box, with the same internal volume, printed in Acrylonitrile Butadiene Styrene (ABS) (which starts to be malleable at 105 ^{o}C), isolated with a layer of sphincter and, finally, another box of PLA (see Appendix C for the 2D drawings of Peloid Sample holder). This container was also treated with epoxy adhesive.

Unfortunately, as shown in Section 4.3.1, this box wasn't fitted to use as our system, which led to the system shown in Figure 3.9 (water bath system). In this final solution, the sample holder is a 50 ml beaker where the electrodes are inserted (Fig. 3.9).

3.1.1.6 Electrodes

PET

In PET's moisture detection, in supplement to the electrodes, it was introduced another component: a buffer circuit[3] (Fig. 3.8). At low frequencies capacitors introduce high impedance, for high frequencies it behaves in an opposite way. The series resistor eliminates short circuit at high frequencies and the parallel coil eliminates open loop at low frequencies.

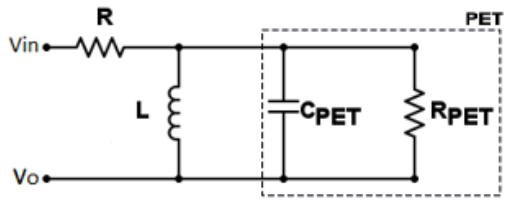

Figure 3.8: Buffer circuit schematic need to avoid short circuit and open loop behavior from PET pellets.

Although PET's characterization is represented as a capacitor in parallel with a resistor (Fig. 3.8), the resistive behavior can be ignored. This approximation arises from the high resistance value shown by the material (with a resistivity around 10^{12} $\Omega.cm$) [52]. Another important aspect to consider is the coil value. As shown in Section 4.2.2, PET capacitance varies approximately 15 pF from 1 $\%_{RH}$ to dry. From Equation 3.4, lower values of inductance produce higher sensibility to capacitance

[3]By definition, a buffer circuit produce an electrical impedance transformation between its input and output. In this case, this circuit is labeled as buffer because it enables a wider range of frequency measurements [20].

changes.

$$f_{ressonance} = \frac{1}{2\pi}\sqrt{\frac{1}{LC}} \tag{3.4}$$

Regarding the electrodes, two aluminum plates (width = 12 cm; length = 25 cm) separated by 0.7 cm make possible the measurement of material's impedance behavior (Fig. 3.6). Connecting the electrodes to the PCB is a double cable. A coaxial cable was also considered, but was decided that this approach was adequate to the tests conditions (laboratory).

Peloids

Initially, the electrodes developed to study peloid samples were two aluminum plates (width = 1.9 cm; height = 6.0 cm) separated by 2.0 cm. This configuration was then changed to two coper plates separated by 0.2 cm (width = 2.0 cm; height = 6.0 cm) (Fig. 3.9), increasing the capacity. These copper electrodes were also painted with varnish to eliminate electrical conduction between the plates, as explained in Section 4.3.2.2. It is important to consider that the sample will only have between 0.5 and 1 cm of height.

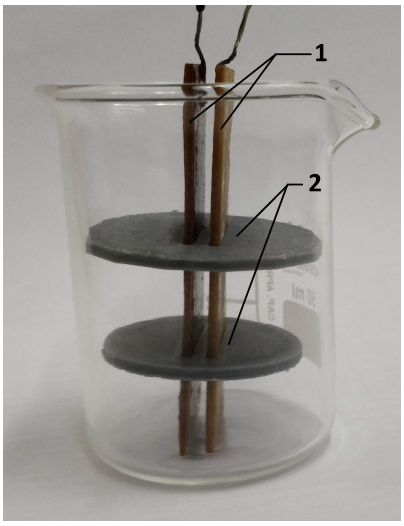

Figure 3.9: Water bath sample holder and electrodes: 1 - Copper plates; 2- 3D printed plates used to secure the distance between the electrodes.

Moreover, some of these copper plates were electroplated with silver as explained in Section 3.2.1. However, as shown in Section 4.3.2.2, the simple copper plates provided better results, and then being the elected solution.

3.1.1.7 Heating System

PET

In order to obtain a faster evaporation of moisture a heating system around the PET's sample holder was assembled, which can be observed inside the red boxes in Figure 3.6. It is composed by 50 ceramic cased 5 W resistors, which are mounted as showed in Figure 3.10 [53].

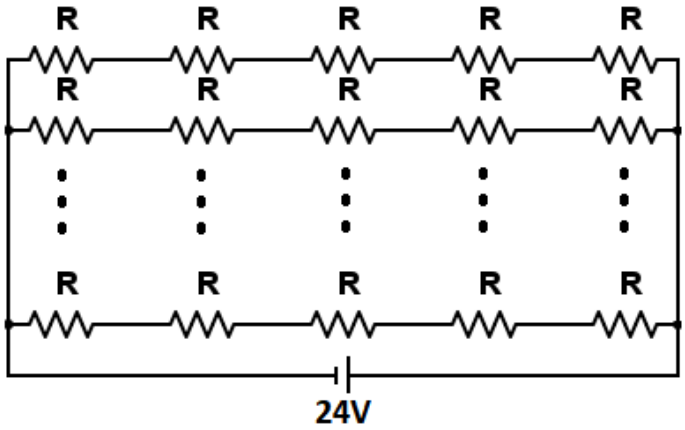

Figure 3.10: Schematics of PET's heating System: resistors configuration and power supply.

When the circuit is supplied with 24 V and 1.72 A, the maximum temperature achieved with the system is thereabout 69.9 ± 0.1 ^{o}C. Parallel to the heating system is a control Light-Emitting Diode (LED) to check when the heating system is turned on.

Peloids

Regarding the second case study, the sample temperature must be controlled and stable through the test's duration. Therefore, it was started by implementing the thermostat[4] shown in Figure 3.11. The main component responsible for temperature manipulation is the *LMT86* (right tube of Fig. 3.12), which is a precision Complementary Metal-Oxide Semiconductor (CMOS) analog temperature sensor with a linear output voltage inversely proportional to temperature (2616 mV at -50 ^{o}C up to 420 mV at 150 ^{o}C) [54].

Temperature is calculated using the parabolic expression obtained in the com-

[4]Developed under the framework of this Case Study.

ponent's datasheet:

$$T = \frac{10.888 - \sqrt{(-10.888)^2 + 4 \times 0.00347 \times (1777.3 - V_{TEMP}(mV))}}{2 \times (-0.00347)} + 30 \quad (3.5)$$

In the given application, Equation 3.5 will not be necessary. Our circuit requires a reference voltage corresponding to a certain temperature, which can be achieved with a calibration test.

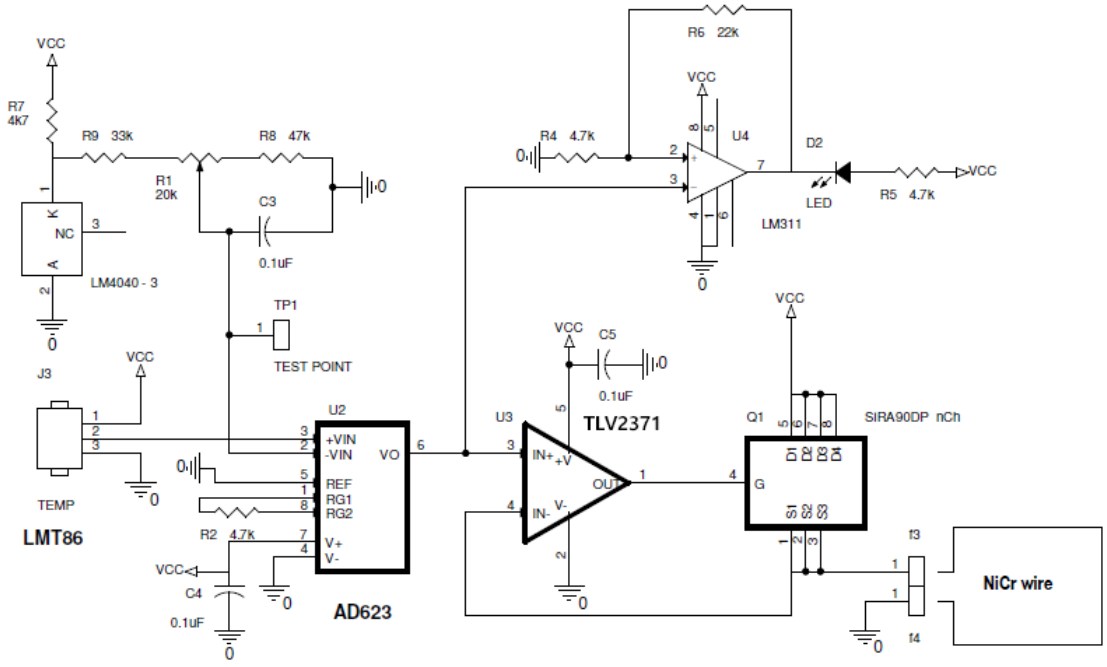

Figure 3.11: Thermostat used to control and stabilize internal temperature of Peloid sample holder (box system).

AD623 is a low cost instrumentation amplifier, which purpose is to compare the output voltage from LMT86 (V_{IN}^{+}) with the reference (V_{IN}^{-}). When V_{REF} is lower than the sensor output voltage the heating system is turned on. The output of this amplifier will be as expressed in Equation 3.6 [55].

$$V_o = (1 + \frac{100\ k\Omega}{R_2})(V_{IN}^{+} - V_{IN}^{-}) \quad (3.6)$$

The control LED is turned on when the inverting input of this Op-Amp is higher than $V_{CC}\dfrac{R_4}{R_4 + R_6}\ (V)$ and switched off when it is smaller than $0\ V$. When the LED is turned on, it means that current flows through the n-channel formed between the

drain and source of the Metal-Oxide Semiconductor Field-Effect Transistor (MOSFET) (SiRA90DP) [56]. Moreover, it means that occurs heat dissipation in the Nickel-Chromium wire which is the heating element in this system (0.25 mm diameter). The total length of wire used was approximately 1.0 meter (Fig. 3.12) which has a linear resistance of 22 Ω/m.

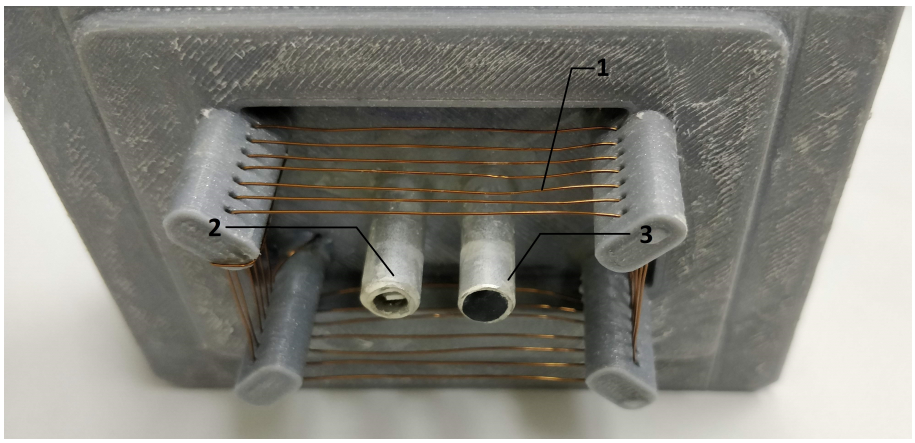

Figure 3.12: Box system heating apparatus (bottom view): 1- Nickel-Chromium wire; 2- PT1000; 3- LMT86.

After some tests, it was decided to change R_2 to 1 $k\Omega$. This gain increase enables a faster channel saturation in the MOSFET.

When it was changed to the water bath system, the overall heating technique was also changed to a more traditional solution. Figure 3.13 depicts the final solution where peloids impedance was acquired. This solution consists of inserting the sample holder in a water bath at a controlled temperature. The device responsible for controlling the water temperature is the *CHEERLINK MH1210W* which turns on the heating resistor (kettle) when the measured temperature is lower than the set-point and turn it off whenever it passes that same point. This controller has an accuracy of ± 1 ^{o}C and can be configured to temperatures up to 99.9 ^{o}C [57].

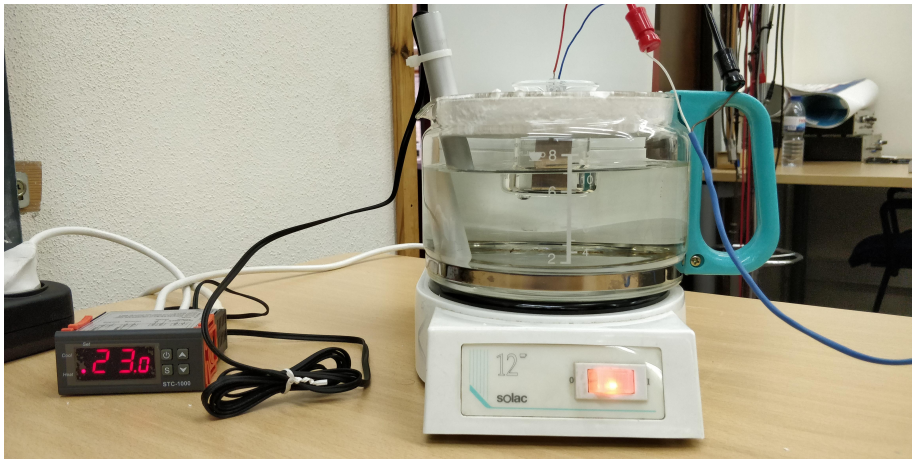

Figure 3.13: Water bath measurement and heating system.

3.1.2 Software

In order to control the Analog Discovery using MATLAB® it is required the previous installation of Digilent® drivers and the download of the SDK file. The software was first developed using MATLAB® R2015b, and then substantially adapted and manipulated during this project using MATLAB® R2017b[5]. The main difference between this impedance meter and its older versions is the replacement of the manual switches by digitally controlled multiplexers (ADG1408 and ADG1409). This required the implementation of control algorithms in order to set the values of Digilent®'s digital pins (Fig. 3.14).

[5]In an early stage of this thesis the hole code was studied and fully understood, which permitted its high adaptation to the desired application.

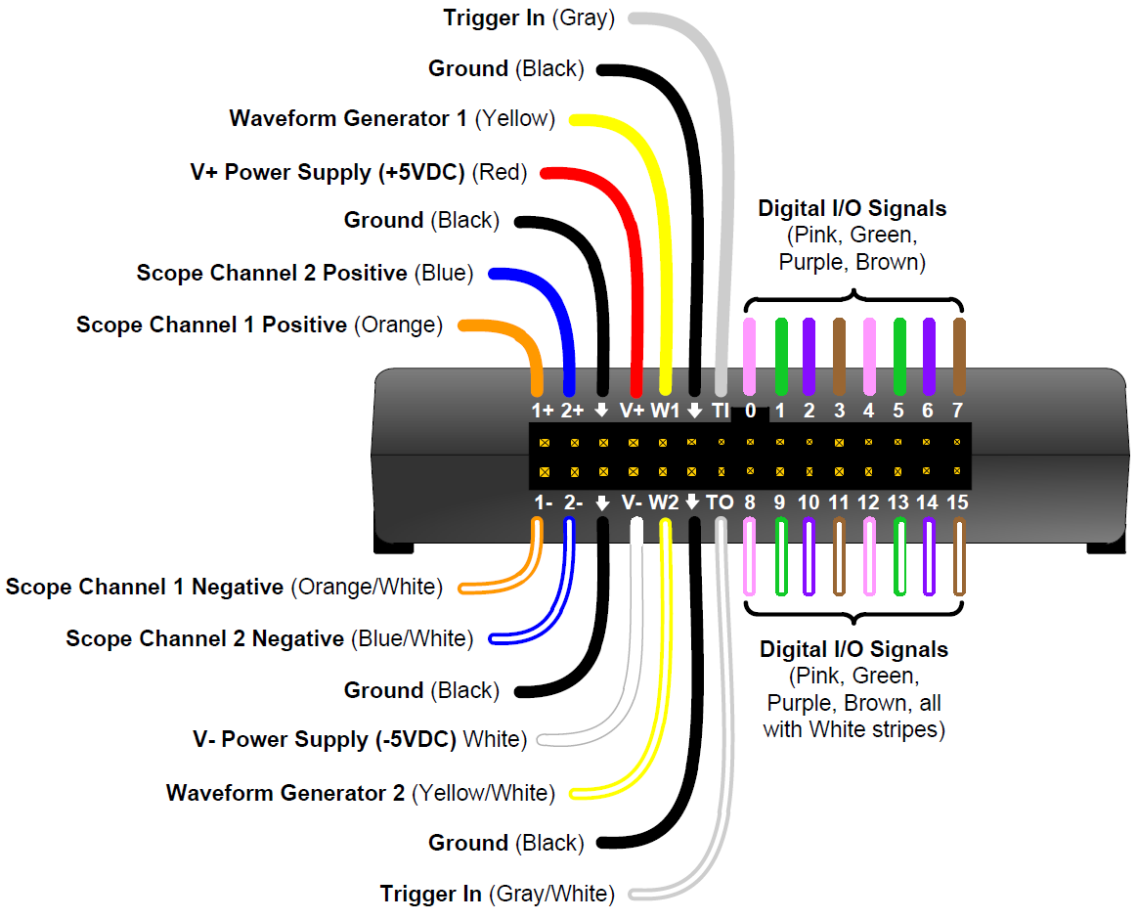

Figure 3.14: Digilent® Pin-Out scheme.

The user interface implemented to control the acquisition system is shown in Figure 3.15. Using the options inside the green box, the type of data to acquire is chosen. Selecting "Impedance" mode, the next step is to select the excitation mode (blue box), the internal resistance (brown box), signal's characteristics (orange box) and the type of acquisition (purple box). Inside the latter it is possible to choose between single frequency analysis or a sweep of all frequencies inside the red box. These frequencies are previously set and can't be changed after the Digilent® has been turned on.

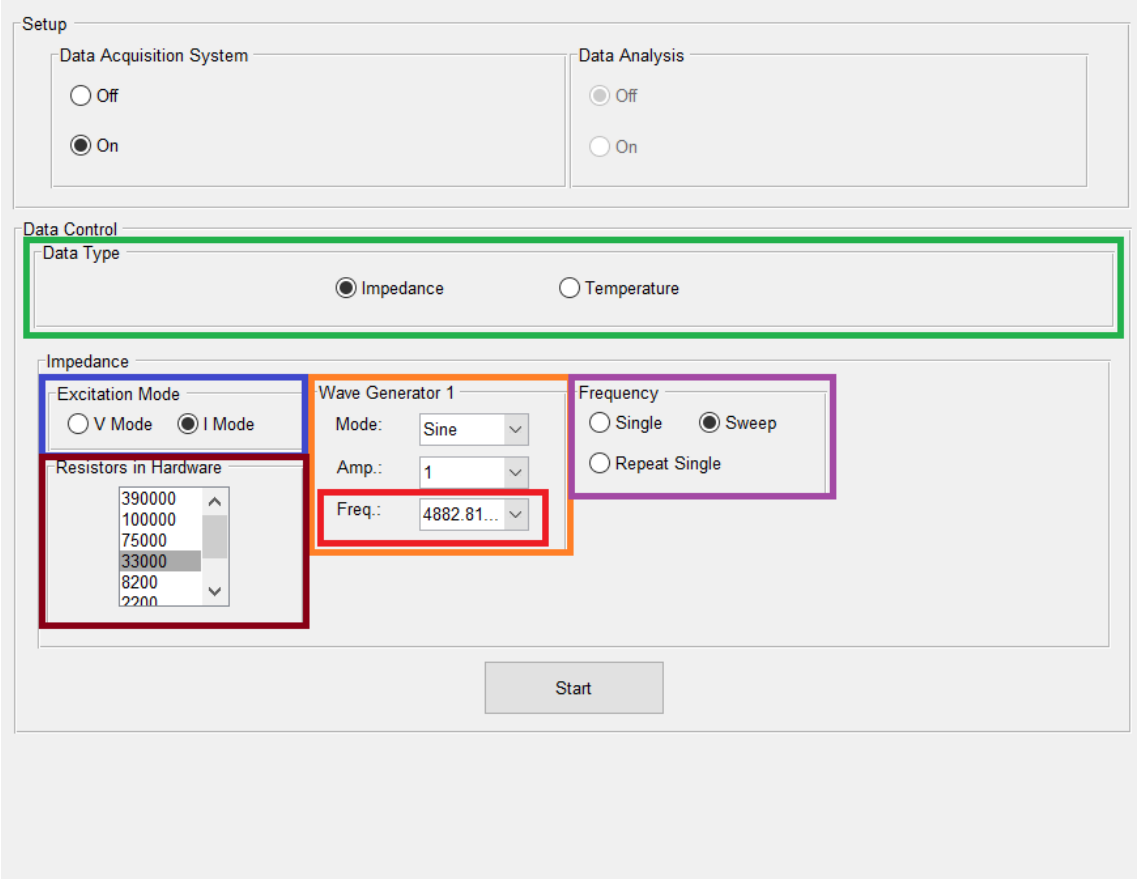

Figure 3.15: MATLAB® user interface adapted from previous projects.

Data Processing

Figure 3.16 depicts the algorithm flowchart responsible for the data acquisition and processing behind the interface. Signal processing is based in Discrete Fourier Transforms (DFT) (Eq. 3.7), which is accomplished with a MATLAB® function that uses a Fast Fourier Transform (FFT) algorithm [58, 59]. This allows signal manipulation in order to find the dominant frequency. Knowing that it is possible to calculate signal's phase angle and amplitude [58].

$$X_k = \sum_{n=0}^{N-1} x_n . e^{-\frac{2\pi j}{N} kn}, \; N \; points, \; k \in [0, N-1] \tag{3.7}$$

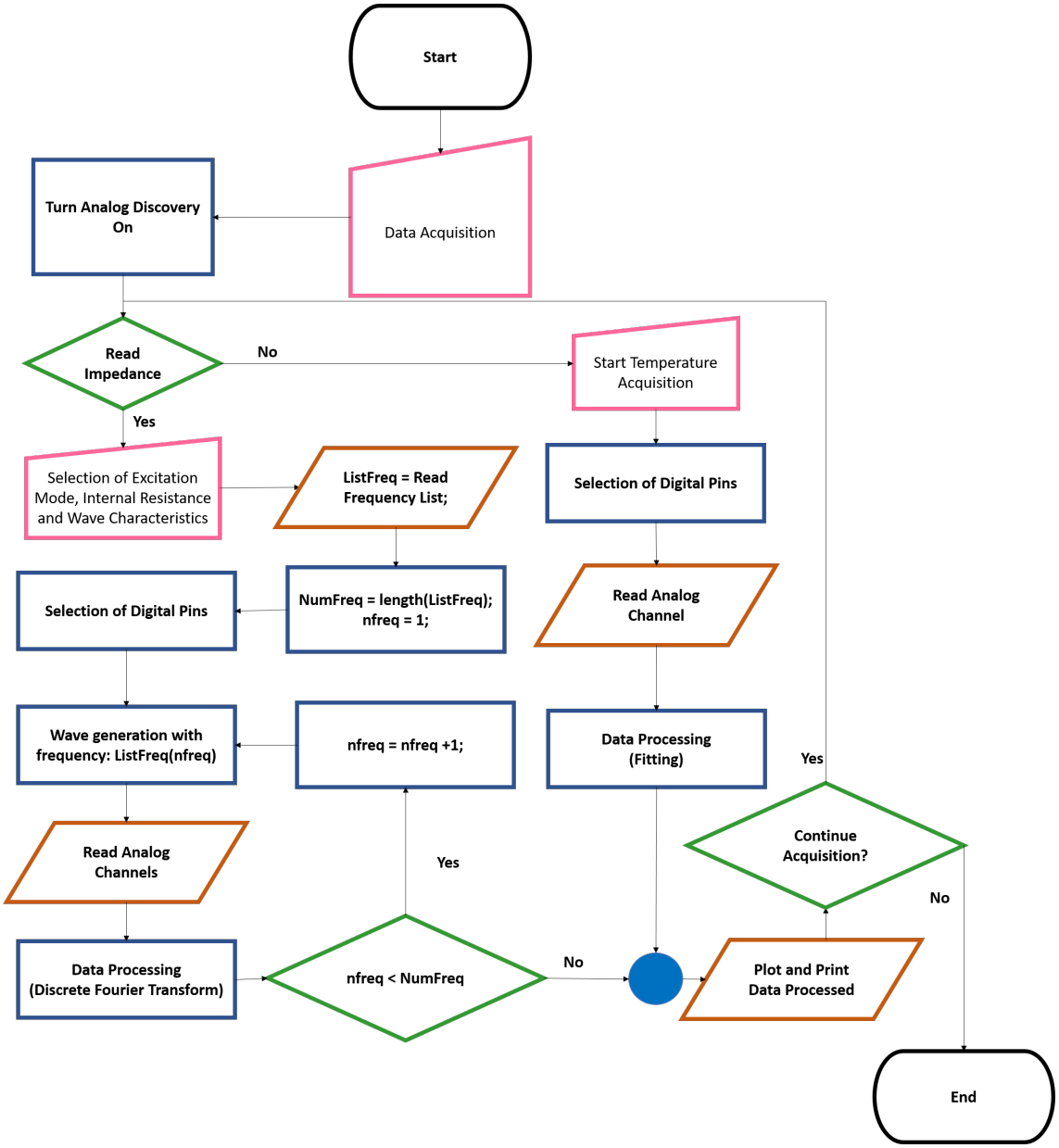

Figure 3.16: Flow chart of the implemented code used in data Acquisition.

The use of FFT for data processing requires the acquired data to be periodic and to have an integer number of periods in the given time interval [60]. To assure that it happens, excitation signal frequency must take into consideration Analog Discovery's buffer size and the sampling frequency, which are adjusted using Equation 3.8.

$$f_{signal} = \frac{f_{sampling} \times N_{periods}}{buffer\ size} \tag{3.8}$$

By using this formula it is ensured that the maximum number of data points are used (buffer size - 2^{13}) for an integer number of periods (at least 10), these conditions

were necessary to avoid frequency leakage.

3.1.3 Test Samples

Aiming to study and fully understand the impedance meter developed in the laboratory, some tests were performed using commercial passive components. Afterwards, some performance parameters were assessed. To do so, it was soldered an RLC circuit with one variable capacitance.

PET

In order to achieve the moisture measurement two shapes of PET were studied, which were obtained from different providers. Two distinct shapes were at hand, round (Fig. 3.17 (a)) and cylinder (Fig. 3.17 (b)). Thus, it can be ensured that PET shape does not affect moisture detection by EIS.

Figure 3.17: Different PET pellet shapes at hand: (a) round (b) cylinders.

Peloids

The goal of this part of the project is simple to define the overall specific measuring system. This was possible using a commercial clay (Fig. 3.18) [61]. The remaining samples are the object under study which were chosen from a group of 23 samples provided by Exatronic, which only provided the mass necessary to one test per sample. Their characteristics are presented in Table 3.1.

Figure 3.18: Different peloid samples tested and (in the brown paper bag) the commercial clay.

Table 3.1: Physiochemical properties of each sample (data provided by Exatronic, Lda).

Sample	Origin	pH	CEC $(meq/100g)$	Specific heat capacity $(J/kg \cdot K)$
M1	Synthesized	10.29	34.4	638.06
M2	Natural	7.60	10.8	104.44
M3	Synthesized	3.96	0.6	90.49
M4	Synthesized	6.21	4.2	166.45
M5	Natural	8.60	49.6	2,930.00

From these samples, the most important is sample M5, which is the one selected to be used in the Edersensae project (Sec. 1.3). Table 3.2 contains more detailed information about the CEC of each sample.

Table 3.2: Main exchangeable cation of each sample (data provided by Exatronic, Lda).

Sample	Main Exchangeable Cation	Value (mg/l)
M1	Ca^{2+}	251.57
M2	Ca^{2+}	53.73
M3	Na^{+}	163.24
M4	Ca^{2+}	451.99
M5	Ca^{2+}	13,237.00

3.1.4 Tools

Some instruments and software were used in order to measure environment and system variables or to create tools used during the project:

- PEAK® Atlas LCR40: this instrument is an advanced tool that automatically detects the type of passive element between the probes and analyzes it (measure their value);
- Testo 110 - Probe Thermometer: precise temperature instrument used for calibration;
- Simple bench temperature and humidity sensor, used to register the test's environment conditions;
- KERN® CKE 2000-2: Laboratory scale used to measure PET's mass;
- Inventor®: 3D CAD software used to develop the 3D printed parts;
- Ultimaker 2+: 3D printer.

3.2 Methods

3.2.1 Silver Electroplating

As stated in Section 3.1.1.6, silver electroplated copper plates were also tested. The process of plating those electrodes was performed within the laboratory using silver nitrate, copper plates, and silver foils. The overall plating process consists in a redox reaction: $Cu + 2AgNO_3 \longrightarrow Cu(NO_3)2 + 2Ag$.

To perform the electroplating a low quantity of silver nitrate crystals (concentration lower than 0.02 mg/ml) was added to a beaker with 200 ml of ultra-pure water. Both the silver foils (anode) and the copper plate (cathode) were submerged in this solution and a voltage of 10 V was applied. This procedure (Fig. 3.19) took about 3 hours to complete and required cleaning the copper plate from time to time to remove the copper (II) nitrate accumulated around it.

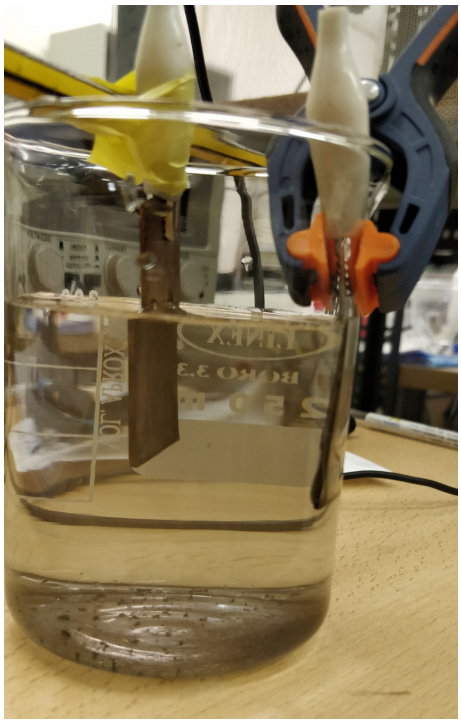

Figure 3.19: Electroplating process used to plate copper with silver. On the left crocodile clip is the copper plate and on the right the silver foils. On the bottom of the beaker it is possible to observe some copper (II) nitrate removed from the copper plate.

3.2.2 Data Acquisition

In Chapter 2 two excitation modes were mentioned, **MV** and **MI**. However, the proof of concept and peloid analysis were developed using only **MI**, due to its stability and less sensibility to parasitic interferences, as showed in Section 4.2.1.1.

Frequency Sweep

Digilent®'s Analog Discovery is capable of generate and analyze signals from 1 Hz up to 10 MHz. As previously stated (Sec. 3.1.2), these frequencies need to be carefully calculated to avoid processing errors. In this method the program implements the frequency list presented in the red box (Fig. 3.15) and calculates impedance modulus and phase shift for each one of those frequencies. From these two impedance characteristics, Resistance and Reactance are also calculated.

3.2.3 Samples Preparation

PET

To study the relation between PET's relative humidity and its impedance characteristics, one started by making the polymer absorb water. The easiest way to do so is to maintain the polymer on an humid environment. Therefore, the sample is submitted to water evaporation, which is absorbed by the material [62].

The next important step is to measure the water content ratio in each sample. Knowing sample's dry weight it is possible to calculate the exact amount of water present after evaporation. In this study, more focus was given to PET's RH from 0 to 1 $\%_{RH}$ range, considering the initial objectives.

Finally, impedance characteristics are obtained for a reduced frequency interval, between 5 kHz and 200 kHz (taking into consideration the reduction of each sweep duration). This process is done for various percentages of PET's RH. The results are then analyzed in order to develop the proof of concept. Once impedance is temperature dependent, all the tests were performed at a constant temperature of 70 ^{o}C (provided by the heating system).

Peloids

Impedance characteristics were obtained for a larger range of frequencies, from 1 Hz up to 1 MHz. This process is done for different concentration and temperatures. After those parameters were defined, distinct samples were submitted to EIS.

All mixtures were prepared using 10 g of sample and 5 ml of distilled water at a temperature of 60 ^{o}C, which enable an higher initial temperature. Having obtained an homogenized mixture, the electrodes were placed inside the beaker and the sample holder was put in the bath heating system. The tests were performed at 45 ^{o}C, which required an interval of 5 *minutes* for stabilization. Each test was performed for an additional 20 *minutes*, allowing a total of five frequency sweeps during that.

CHAPTER 4

Results and Discussion

The presented chapter contains the obtained results regarding the methods described. It is divided in 3 major sections: Instrument Analysis, PET RH Detection, and Peloid Ionic Conductivity. The first refers to instrument statistical analysis. Then, the overall PET study is arranged. Finally, peloid preliminary tests are presented.

4.1 Instrument Analysis

4.1.1 Simulation

One viable way to predict the buffer circuit behavior is to simulate it using appropriate software. In this case, it was used National Instruments^{TM}Multisim 12.0 and the results from this simulation are presented in Figure 4.1.

Taking into account Figures 2.3 and 2.4 and considering Z as a buffer circuit (Fig. 3.8 with negligible R_{PET}), for MI impedance expressions are:

$$\frac{V_o}{V_i} = -\frac{R}{R_{in}} + j\frac{wL}{R_{in}(w^2LC-1)} \tag{4.1}$$

$$|Z| = \frac{1}{R_{in}(w^2LC-1)}\sqrt{R^2(w^2LC-1)^2 + w^2L^2} \tag{4.2}$$

$$\phi = \text{arctg}\left(\frac{wL}{R - w^2LRC}\right) \tag{4.3}$$

and for MV:

$$\frac{V_o}{V_i} = \frac{R_{in}(1 - w^2LC)}{R^2(w^2LC - 1)^2 + w^2L^2}[R(w^2LC - 1) + jwL] \tag{4.4}$$

$$|Z| = \frac{R_{in}(1 - w^2LC)}{R^2(w^2LC - 1)^2 + w^2L^2}\sqrt{R^2(w^2LC - 1)^2 + w^2L^2} \tag{4.5}$$

$$\phi = \text{arctg}\left(\frac{wL}{w^2LRC - R}\right) \tag{4.6}$$

From Equations 4.3 and 4.6, it is clear that phase shift is symmetrical. This behavior is confirmed in the following images (Fig. 4.1 and 4.2). Another important aspect to notice is that the internal resistance (R_{in}) used to adjust the output gain does not affect the phase shift. However, it influences impedance modulus in both modes. Considering this, the next results were obtain for an internal resistance of 33 $k\Omega$ and 2.2 $k\Omega$ for MI and MV, respectively.

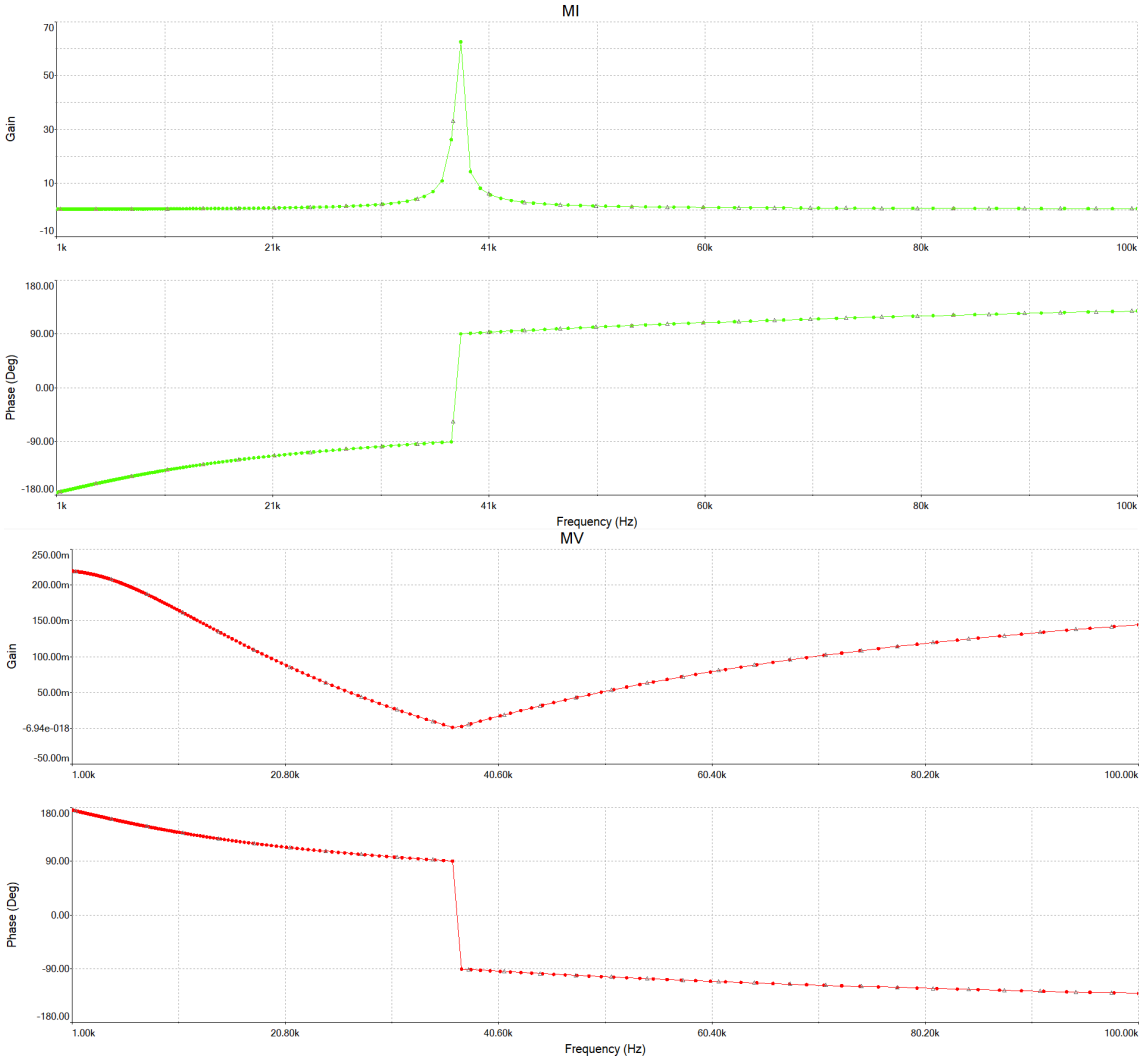

Figure 4.1: Simulation of Impedance Meter behavior [**MI** (green data) and **MV** (red data)] for PET's measurements (buffer circuit: R $= 10 \pm 0.1$ $K\Omega$; L $= 118.2 \pm 0.1$ mH; C$= 160 \pm 0.1$ pF).

Comparing Figures 4.1 and 4.2 it is possible to identify that the results obtained comply with each other for both excitation modes. One can notice the effect of changing between excitation modes just by comparing the modulus behavior of both them. In MI the gain is maximum at the resonant frequency, on the other hand it is minimum for MV. This outcome can be explained using Equations 2.7 and 2.8. When acquiring data using the impedance meter this MV behavior can be overcome due to the data analysis that takes place using MATLAB® functions.

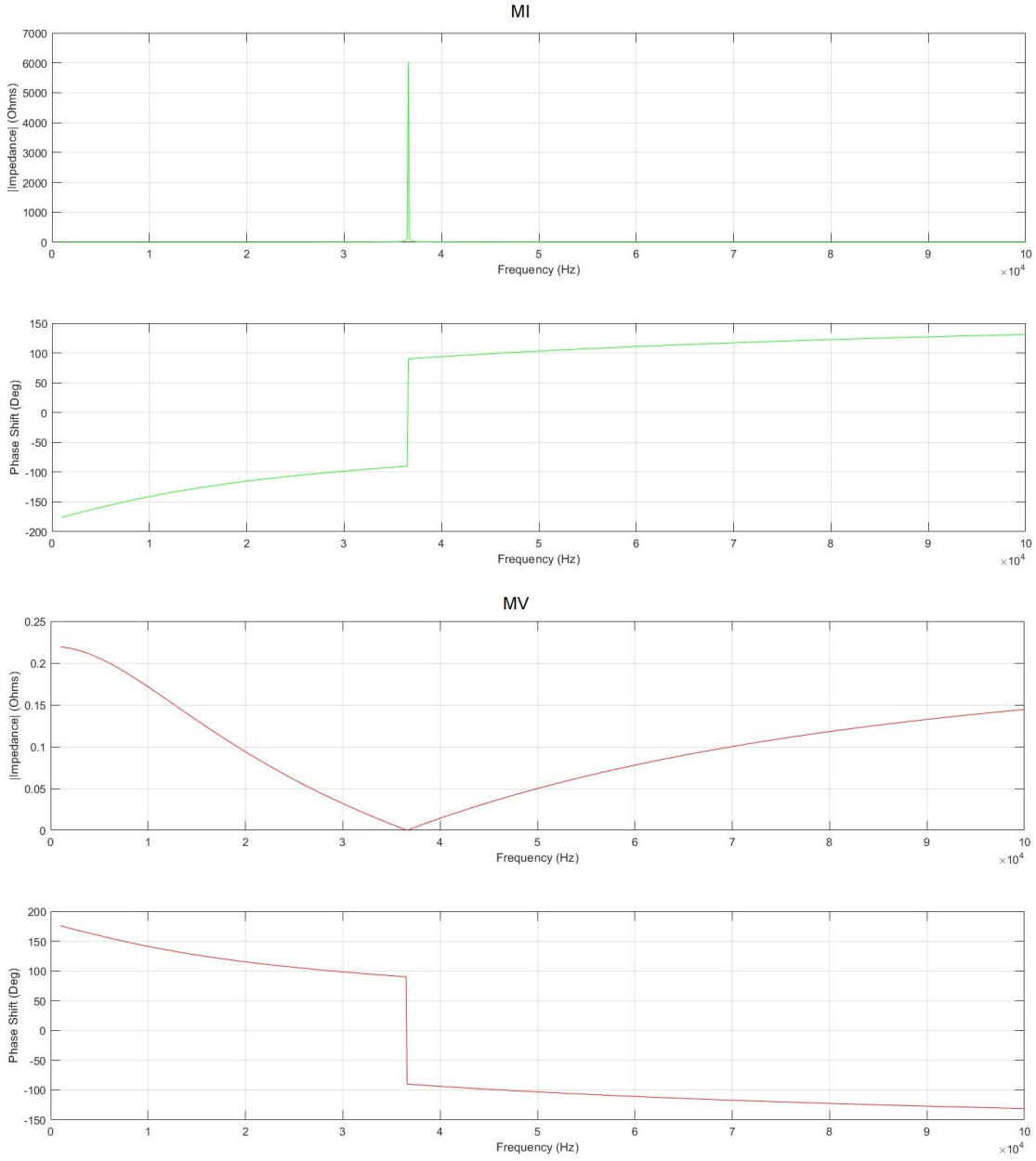

Figure 4.2: Expected behavior using theoretical expressions (Eq. 4.1 to 4.6) [**MI** (green lines) and **MV** (red lines)] for PET's measurements (buffer circuit: R = 10 ± 0.1 $K\Omega$; C = 118.2 ± 0.1 mH; C= 160 ± 0.1 pF).

4.1.2 Impedance Meter Performance Evaluation

In order to know the characteristics of the instrument, some performance parameters were evaluated. The tests provided information about instrument's behavior in measuring the position of resonance frequency. To do so, an RLC circuit with a variable capacitance was tested (Fig. 4.3).

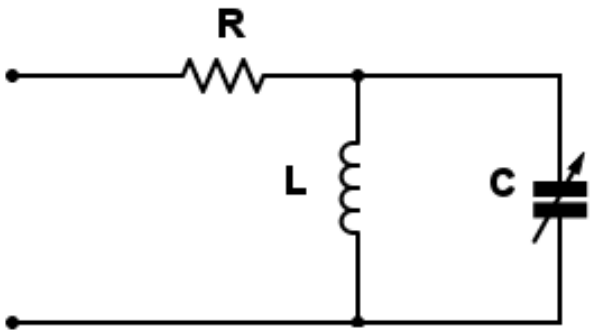

Figure 4.3: RLC circuit used in instrument analysis (R = 10±0.1 $K\Omega$; L = 105.7±0.1 mH ; C represents a capacitor with variable capacitance)

At this point the main focus was on changes of the resonance's frequency position and the value of impedance modulus. Therefore, the results obtained in phase shift are not analyzed. In order to obtain a better value for resonance frequency, modulus peak was fitted to the expression represented by Equation 4.7. This mathematical expression is the *Lorentzian probability density* function with an height offset (d) added for better fitting results ($R^2 > 0.95$). μ is the mean and Γ is the width at half height [63].

$$p_L(x;\mu,\Gamma) = \frac{1}{\pi}\frac{\Gamma/2}{(x-\mu)^2 + (\Gamma/2)^2} + d \tag{4.7}$$

The result of fitting the data to this model is shown in Figure 4.4 for a capacitance value of 42.6 pF. From it, one can observe that the fitting method should be changed for future data analysis. Table 4.1 gives the results obtained for linearity tests. For each value of capacitance were performed five frequency sweeps from 30 up to 150 kHz. Measurements repetition made possible the assess of the standard deviation, which corresponds to the uncertainty in a single measurement [63].

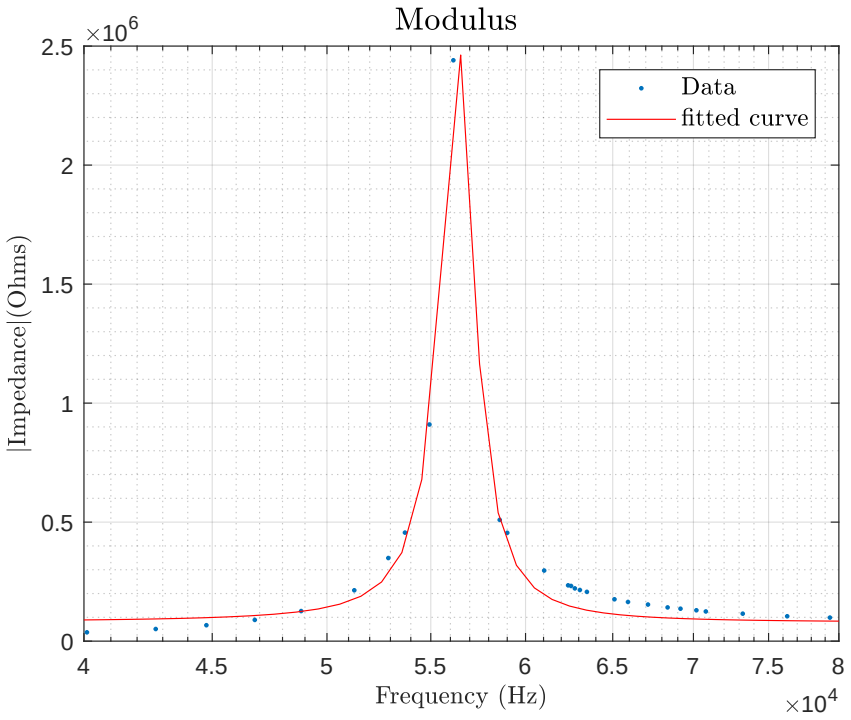

Figure 4.4: Impedance resonant peak fit example to *Lorentz probability density* function (C = 42.6 ± 0.1 pF).

Table 4.1: Resonant frequency obtained for different values of Capacitance (1st column: measured capacitance using PEAK® Atlas LCR40; 2nd column: Expected resonance frequency (Eq. 3.4); 3rd column: Obtained resonance frequency; 4th column: Relative Percent Error).

$C \pm \triangle C$ (pF)	$f_{theoretical} \pm \triangle f$ (kHz)	$f_{experimental} \pm \triangle f$ (kHz)	Relative Error (%)
32.6 ± 0.1	85.74 ± 0.28	60.25 ± 0.11	29.75
35.6 ± 0.1	82.05 ± 0.24	59.48 ± 0.13	27.50
37.2 ± 0.1	80.26 ± 0.23	59.02 ± 0.11	26.46
38.2 ± 0.1	79.21 ± 0.22	58.22 ± 0.18	26.49
40.5 ± 0.1	76.92 ± 0.20	56.83 ± 0.13	26.12
42.2 ± 0.1	75.36 ± 0.19	56.53 ± 0.12	24.98
42.6 ± 0.1	75.00 ± 0.19	56.36 ± 0.12	24.85
46.4 ± 0.1	71.87 ± 0.17	54.85 ± 0.08	23.67
48.4 ± 0.1	70.36 ± 0.16	53.85 ± 0.06	23.47

Figure 4.5 shows a graphical representation of Table's 4.1 data. This data was fitted to a linear equation using standard least-squares method with Gaussian statistics (95% confidence interval).

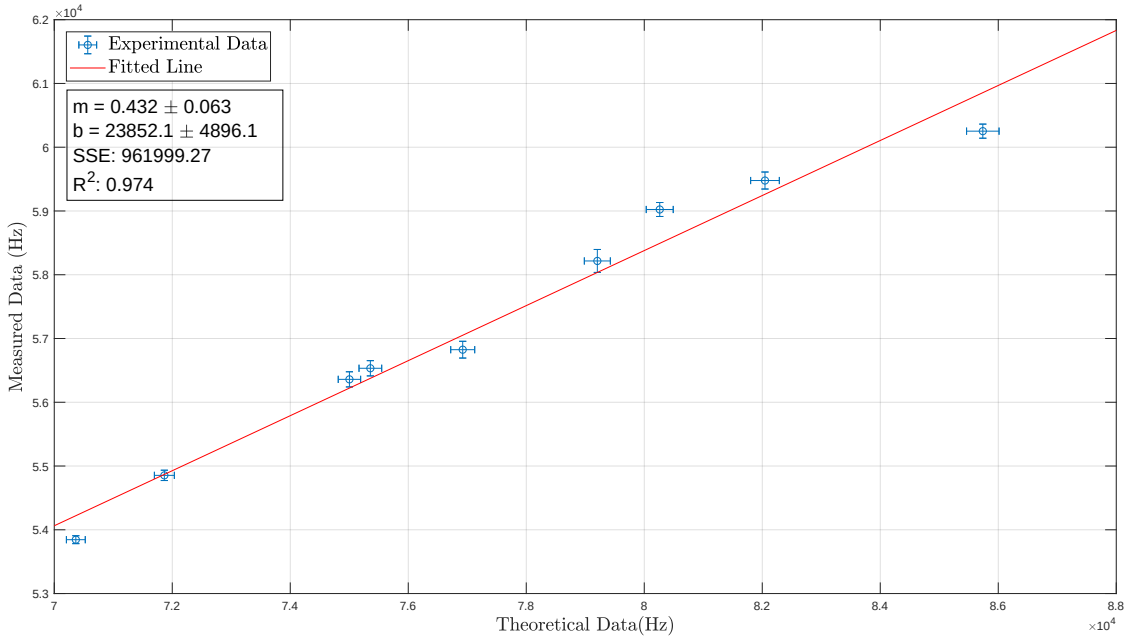

Figure 4.5: Theoretical vs Experimental Resonant Frequency (Data fitted using standard least-squares method with Gaussian statistics).

Repeatability is one good way to evaluate the performance of an instrument. For the same observer and location, 10 measurements were performed for a capacitance of $42.6 \pm 0.1\ pF$. After verifying that the results followed a normal distribution, using a Kolmogorov-Smirnov and a Shapiro-Wilk normality test, the estimated repeatability coefficient obtained was 163 Hz for a 95 % confidence interval (Eq. 4.8) [64, 65, 66].

$$Repeatability = \sqrt{2} \times 1.96 \times Standard\ Deviation \tag{4.8}$$

Discussion

Taking into account the relative errors (provided in Tab. 4.1) it is possible to identify an error higher than 20 %, which is not the most desirable feature for a measuring instrument. These results suggest that there are errors associated with our measurements. These systematic errors are due to instrumentation artifacts, such as resistive behavior in the connectors or capacitance between the electrodes. It is also possible to identify that as capacitance increases the obtained error decreases (Tab. 4.1). This means that for PET's measurements (C around 160 pF) relative

percent error is expected to be even lower than 20 %.

Focusing on the minimum detectable variation, one can study the results obtained for capacitance values of 42.2 and 42.6 pF. Consulting the experimental frequency and the measurement's uncertainty for 42.2 pF one can expect to obtain values from 56.413 up to 56.653 kHz; and for 42.6 pF: 56.240 up to 56.478 kHz. Comparing those intervals, the impedance meter has a minimum detectable variation of at least 0.4 pF. The output gain obtained for these measurements was $0.406 \pm 0.027\ kHz/pF$.

Considering Figure 4.5, the obtained output for the linearity study gives us a linear function of: $f_{experimental} = 0.43159 * f_{theoretical} + 23852\ (kHz)$.

Despite the low accuracy of the impedance meter, it shows high precision, which is compatible with our main measurement objectives for relative humidity.

Device's characteristics are summed up in Table 4.2.

Table 4.2: Device's measured parameters.

Parameter	Value
Minimum Detectable Variation (pF)	0.4
Repeatability (Hz)	163
Max Error (%)	29.75
Gain (Hz/pF)	406

4.2 PET RH Detection

For the purpose of extract more precise values from impedance modulus and phase shift, was considered necessary the upgrade of the fitting method. Thus, in this section, the results are obtained by fitting a 12th-degree polynomial to the impedance meter output [67]. Perhaps the same results could be obtained with a smaller polynomial degree, but as this fitting process implemented in MATLAB® did not require much processing power it was considered viable.

4.2.1 Preliminary Results

In first instance it is important to understand the sample's behavior. Thus, the necessity of the following tests arose.

4.2.1.1 Excitation Mode

To reduce the amount of data collected in the proof of concept, was decided that all the tests should be performed using only one excitation mode. Figure 4.6 shows the obtained results with both modes. Those tests were performed on a dry sample, using 95 frequencies between 5 kHz and 600 kHz.

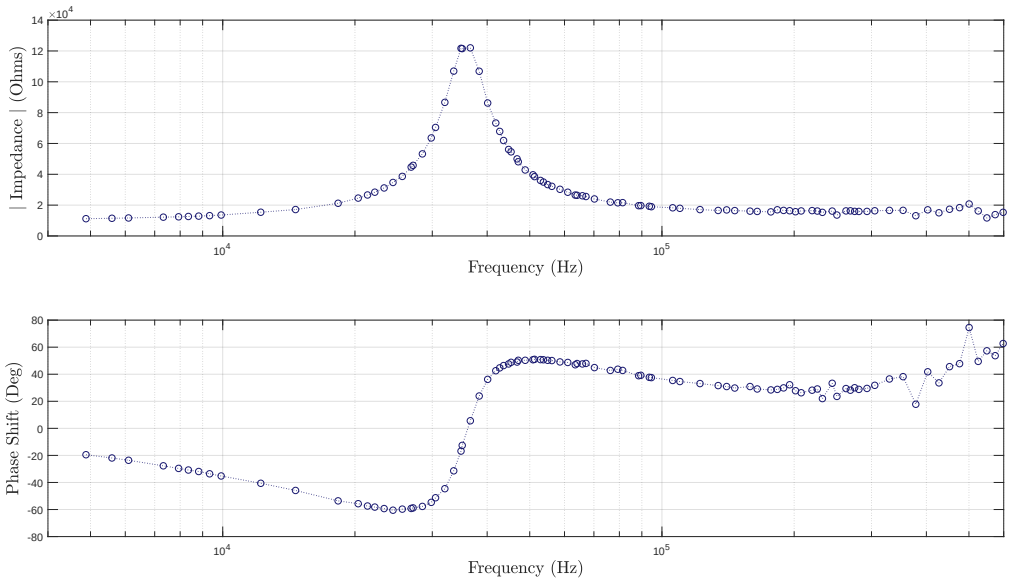

(a) MI

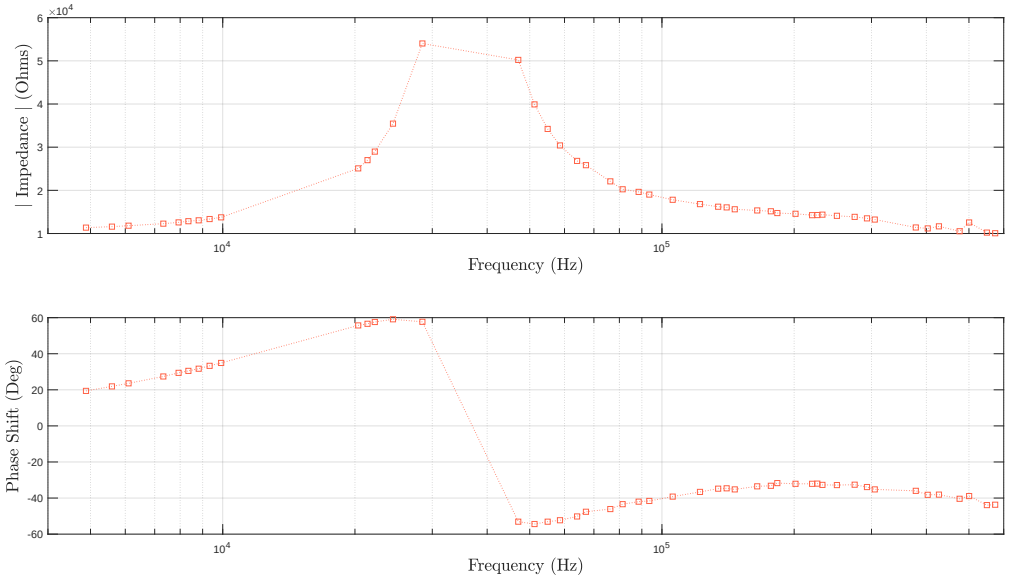

(b) MV

Figure 4.6: Comparison between excitation modes (Sample: 157.28 ± 0.01 g of dry round shaped PET; $L = 118.2 \pm 0.1$ mH; External Conditions: 19 ^{o}C and 49 $\%_{humidity}$).

The results here present are already filtered from artifacts, it is possible to notice that MV has fewer points after the filtration process, particularly near resonance frequency. This fact is explained by considering the gain formula for each mode: at resonance frequency using MI it reaches its maximum and for MV its minimum (Fig. 4.2). Taking these results into consideration, further tests will be given only by MI excitation mode.

4.2.1.2 PET Initial Tests

Figure 4.7 shows impedance behavior for different pellets' shapes in comparison with air, this test was used to define the frequency range to apply during the proof of concept, by studying electrodes performance.

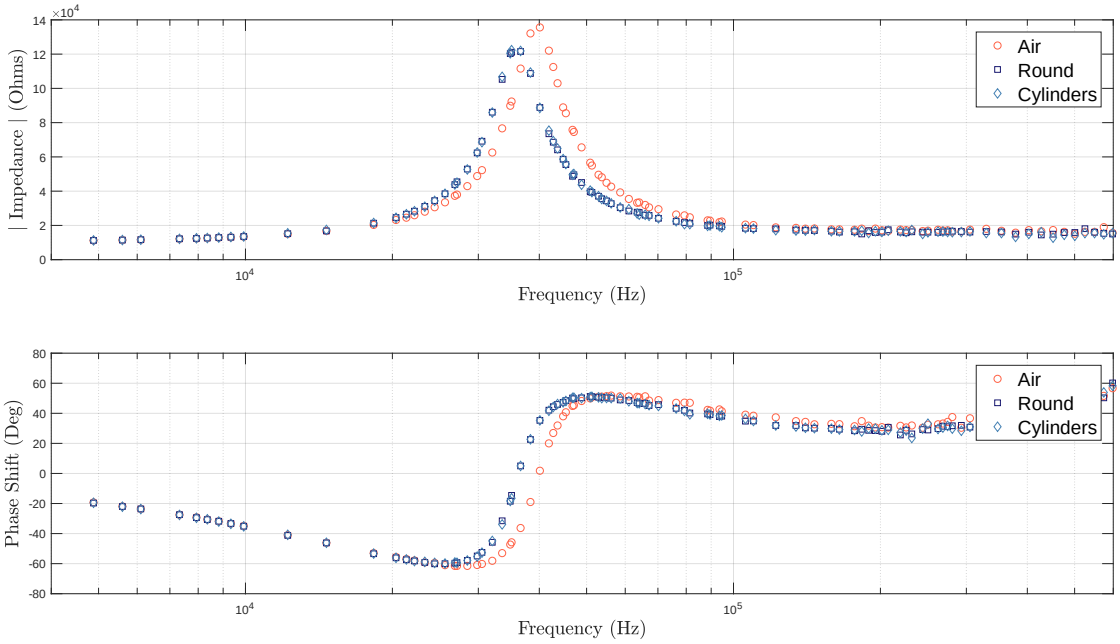

Figure 4.7: Comparison between dielectric materials: Red: Air; Dark Blue: Round shaped PET; Light Blue: Cylindrical shaped PET ($L = 118.2 \pm 0.1\ mH$; External Conditions: 20 ^{o}C and 45 $\%_{humidity}$).

The plot above showed that PET's shape does not affect electrical impedance behavior at all. On the other hand, inserting the PET between the electrodes causes a deviation of approximately 3.82 kHz for the resonant frequency. This is a good indicator that it will probably be possible to detect dielectric changes using this system. Similar results were obtained in previous works [20].

4.2.1.3 Buffer Circuit Inductance Value

In this section the focus was to study the influence of the inductance's value. Figure 4.8 depicts the initial results for two distinct coil values, in red is the data gathered with a $638.8 \pm 0.01\ mH$ coil and in blue with a $118.2 \pm 0.01\ mH$ coil.

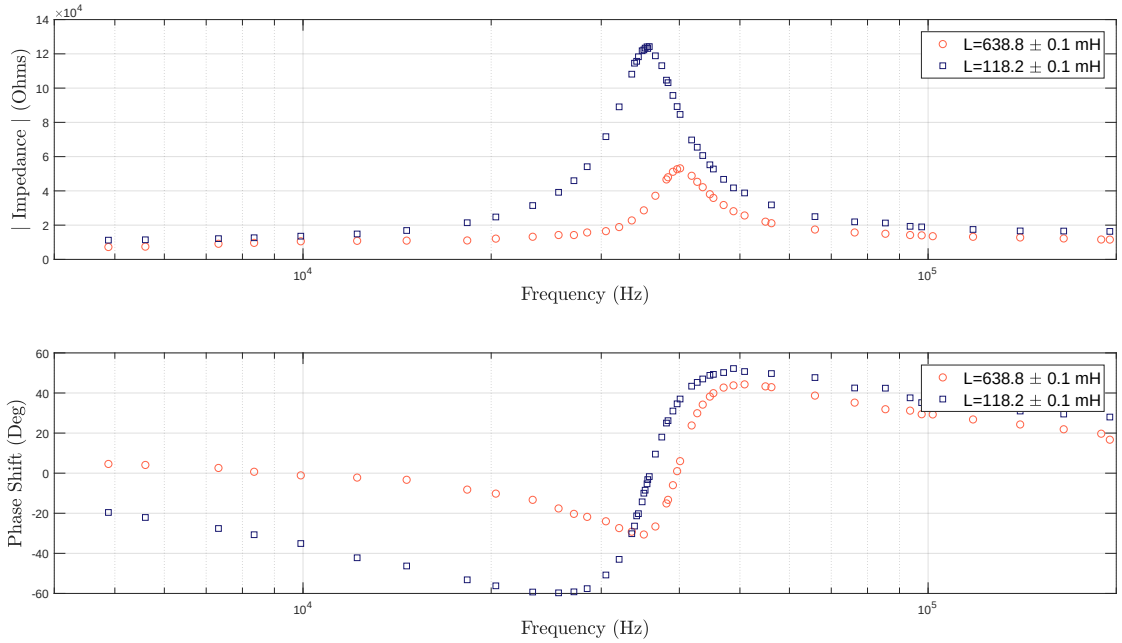

Figure 4.8: Data acquired with different coil values: Red: $L = 638.8 \pm 0.1\ mH$; Dark Blue: $L = 118.2 \pm 0.1\ mH$ (External Conditions: 19 ^{o}C and 53 $\%_{humidity}$).

These results depict the coil influence in our buffer circuit. These two cases reveal one difference of approximately 4.18 kHz. Considering impedance's modulus amplitude, it can be noticed a major difference between the resonance peaks. In order to choose the more adequate value to use, some additional tests were performed, namely to identify the less dispersive test set. Thus, the resonance's frequency position and amplitude were studied for impedance modulus, and for phase shift only the resonance's position was studied.

The following results were obtained from performing one hundred tests using each coil and a dry sample of PET. The main goal of these tests is the calculation of the standard deviation of each measured parameter. From these results it will be decided which coil should be used. These values will also be used (Sec. 4.2.2) to calculate the Limit of Detection (LOD). Table 4.3 and Figure 4.9 were obtained after verifying data's normal distribution, using a normality test (z-test) [68]

Table 4.3: Mean and Standard deviation obtained for 3 different parameters for distinct coil values.

Parameter	$L = 118.2 \pm 0.1\ mH$ $(\mu \pm \sigma)$	$L = 638.8 \pm 0.1\ mH$ $(\mu \pm \sigma)$
Resonance Frequency: Phase Shift (Hz)	$35{,}956 \pm 11$	$39{,}516 \pm 17$
Modulus Maximum (Ω)	$121{,}411 \pm 244$	$52{,}917 \pm 88$
Resonance Frequency: Modulus (Hz)	$35{,}597 \pm 30$	$40{,}165 \pm 32$

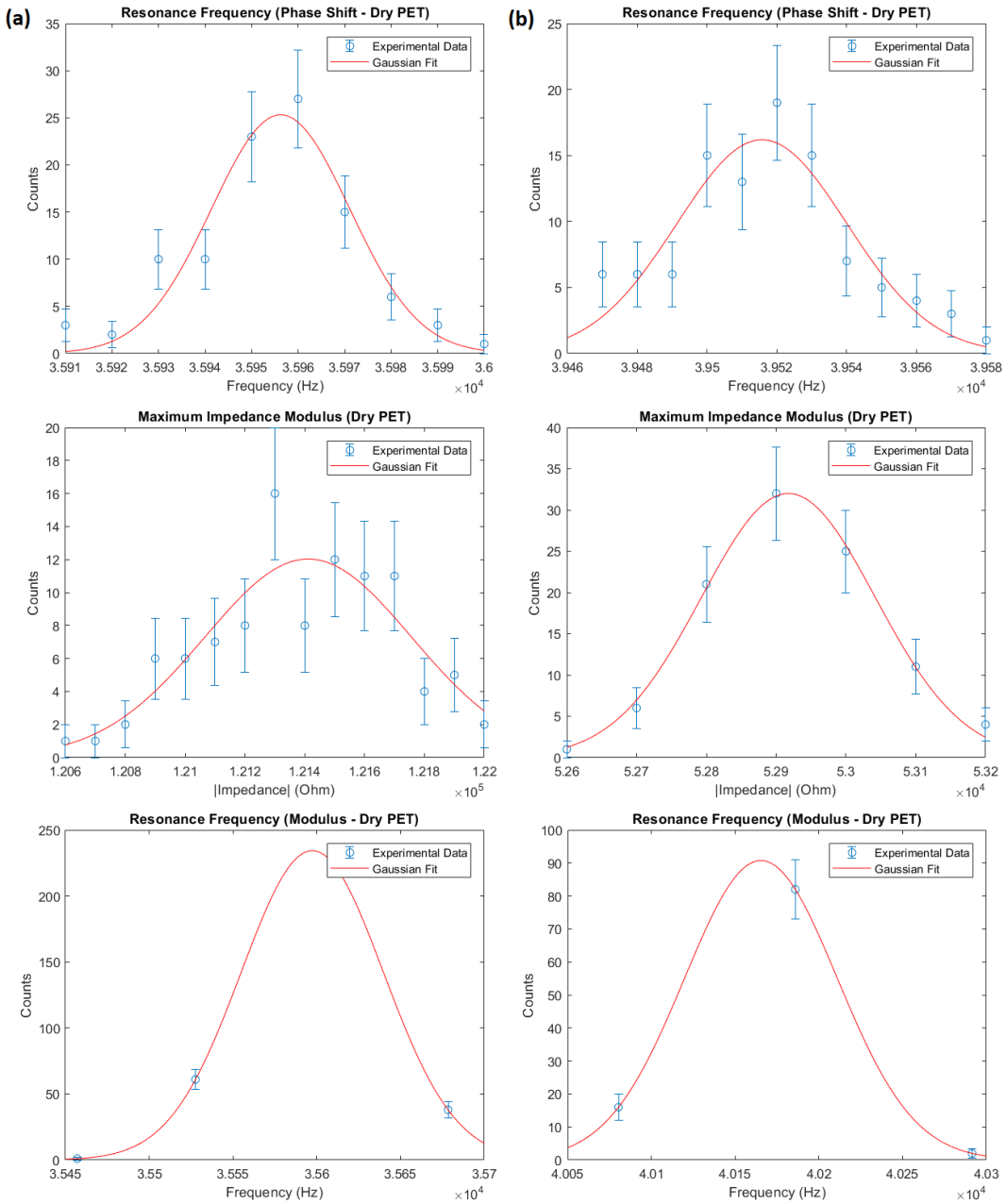

Figure 4.9: Gaussian distribution obtained for null phase frequency (top), for modulus maximum value (middle), and modulus resonance frequency (bottom) to study standard deviation for distinct coil values: (a) $L = 118.2 \pm 0.1\ mH$; (b) $L = 638.8 \pm 0.1\ mH$ (External Conditions: 19 ^{o}C and 53 $\%_{humidity}$).

Table 4.4: Repeatability values obtained using Equation 4.8.

Parameter	Repeatability ($L = 118.2 \pm 0.1\ mH$)	Repeatability ($L = 638.8 \pm 0.1\ mH$)
Resonance Frequency: Phase Shift (Hz)	29.10	47.84
Modulus Maximum (Ω)	677.36	244.15
Resonance Frequency: Modulus (Hz)	84.54	89.45

Figure 4.9 and Tables 4.3 and 4.4 report the obtained results using distinct coil values. Comparing the distributions, it is identified that both coil values present results which can easily be fitted to a *Gaussian Distribution*. Considering the values of the mean and the standard deviation one can state that using inductors with a smaller value lead to slightly better values of standard deviation (taking in consideration means' magnitudes). Another aspect to denote is that the values obtained for resonant frequency position are marginally modified when considering impedance phase shift or modulus.

Considering Equation 3.4, it is expected an higher change in resonant frequency position through RH study for a smaller value of inductance. Based on that and in Table 4.4, the coil with the smaller inductive value was the one chosen to perform the proof of concept.

These tests were taken under the most stable conditions to PET's RH (dry and only exposed to environment humidity). As it is harder to stabilize these conditions to other RH percentages, the obtained values for standard deviation will be considered the same for all of the humidity values.

4.2.2 Proof of concept

Figure 4.10 represents output data from the impedance meter through RH changes.

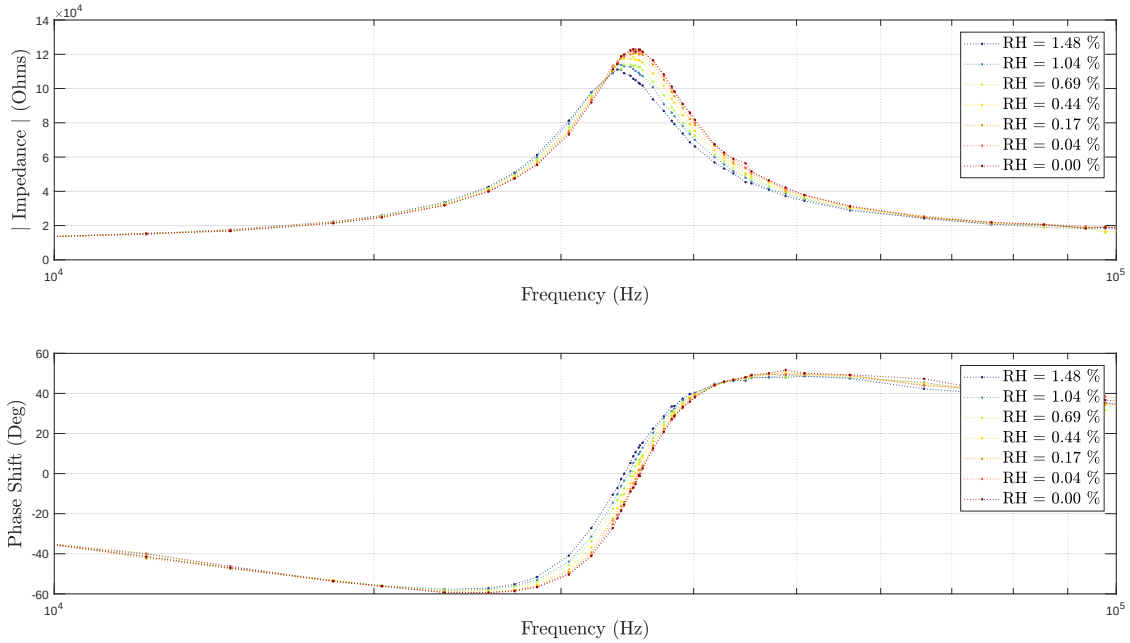

Figure 4.10: Impedance behavior through RH variation: Dark Red: 0.00 ± 0.01 $\%_{RH}$ (dry sample); Dark Blue: 1.48 ± 0.01 $\%_{RH}$ (Sample: 157.23 ± 0.01 g of dry round shaped PET; $L = 118.2 \pm 0.1$ mH; External Conditions: 21 ^{o}C and 53 $\%_{humidity}$).

Table 4.5 shows PET behavior through time after turning on the heating system. The initial time delay was given to let it achieve its maximum temperature (70 ^{o}C) and stabilize. One can observe the mass variation over time (Fig. 4.11) and the continuous capacitance variation (Tab. 4.5) (container capacitance measured with PEAK® Atlas LCR40). As expected, more water content means an higher capacitance value. This can be explained by water relative permittivity which is higher than PET's relative permittivity [69]. However, it is possible to identify some capacitance fluctuations which can be due to the measurement technique applied: to measure the capacitance values the container was removed from the platform and the capacitance meter was reconnected (PEAK® Atlas LCR40).

Table 4.5: Mass and capacitance variation after the heating system is turned on (Sample: 157.23±0.01 g of dry round shaped PET; $L = 118.2 \pm 0.1\ mH$; External Conditions: 21 ^{o}C and 53 $\%_{humidity}$).

Sweep	Time (min)	Sample Mass (g)	Relative Humidity ($\%_{RH}$)	Container Capacitance (pF)
01	20	159.77 ± 0.01	1.616 ± 0.013	170.2 ± 0.1
02	30	159.55 ± 0.01	1.476 ± 0.013	170.4 ± 0.1
03	40	159.34 ± 0.01	1.342 ± 0.013	169.8 ± 0.1
04	50	159.06 ± 0.01	1.164 ± 0.013	166.8 ± 0.1
05	60	158.87 ± 0.01	1.043 ± 0.013	167.9 ± 0.1
06	70	158.65 ± 0.01	0.903 ± 0.013	166.2 ± 0.1
07	80	158.51 ± 0.01	0.814 ± 0.013	166.4 ± 0.1
08	90	158.31 ± 0.01	0.687 ± 0.013	164.4 ± 0.1
09	100	158.17 ± 0.01	0.598 ± 0.013	162.7 ± 0.1
10	110	158.04 ± 0.01	0.515 ± 0.013	163.5 ± 0.1
11	120	157.92 ± 0.01	0.439 ± 0.013	161.0 ± 0.1
12	130	157.74 ± 0.01	0.324 ± 0.013	161.1 ± 0.1
13	140	157.63 ± 0.01	0.254 ± 0.013	160.1 ± 0.1
14	150	157.50 ± 0.01	0.172 ± 0.013	160.5 ± 0.1
15	160	157.38 ± 0.01	0.095 ± 0.013	159.6 ± 0.1
16	170	157.30 ± 0.01	0.045 ± 0.013	158.9 ± 0.1
17	180	157.25 ± 0.01	0.013 ± 0.013	158.3 ± 0.1
18	190	157.23 ± 0.01	0.000 ± 0.013	159.0 ± 0.1

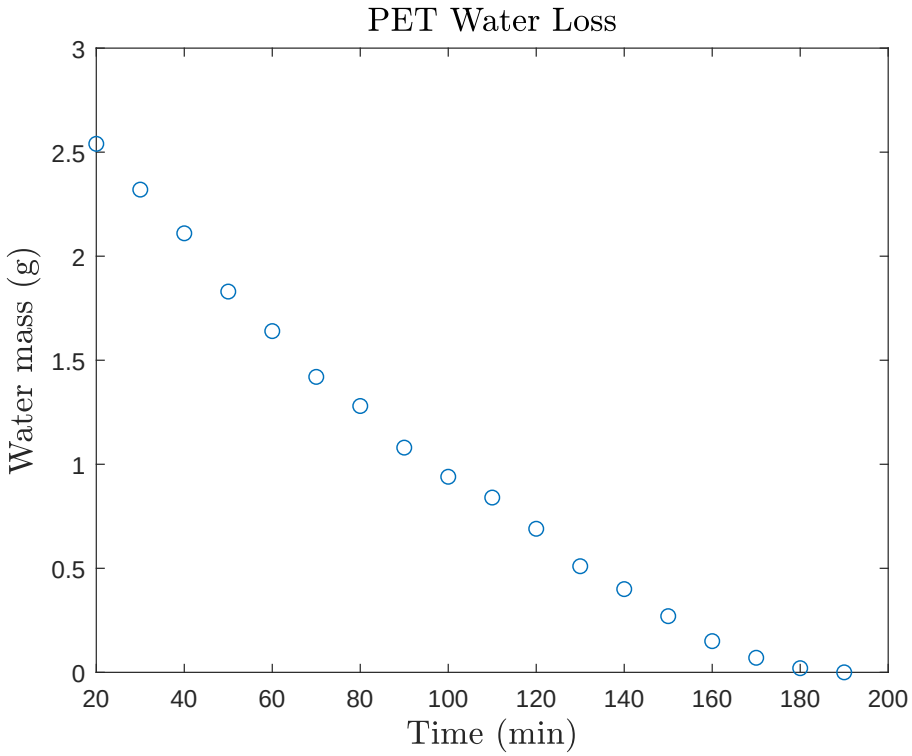

Figure 4.11: PET water loss throughout time (Time counted after turning the heating system ON) (Sample: $157.23 \pm 0.01\ g$ of dry round shaped PET; $L = 118.2 \pm 0.1\ mH$; External Conditions: 21 ^{o}C and 53 $\%_{humidity}$).

The following Table (4.6) was obtained using the impedance meter together with the fitting algorithms already described.

Table 4.6: Calculated impedance parameters from acquired data using least-squares fitting to a 12th-degree polynomial (Sample: 157.23 ± 0.01 g of dry round shaped PET; $L = 118.2 \pm 0.1$ mH; External Conditions: 21 ^{o}C and 53 $\%_{humidity}$).

Sweep	Relative Humidity ($\%_{RH}$)	Resonance Frequency: Phase Shift (Hz)	Modulus Maximum (Ω)	Resonance Frequency: Modulus (Hz)
01	1.616 ± 0.013	34,289.5	107,582.0	34,020.1
02	1.476 ± 0.013	34,403.7	108,483.9	34,020.1
03	1.342 ± 0.013	34,492.6	109,646.6	34,170.9
04	1.164 ± 0.013	34,624.6	110,285.4	34,321.6
05	1.043 ± 0.013	34,714.5	111,908.6	34,321.6
06	0.903 ± 0.013	34,862.1	112,293.2	34,472.4
07	0.814 ± 0.013	34,912.4	112,468.9	34,472.4
08	0.687 ± 0.013	35,010.5	113,283.6	34,623.1
09	0.598 ± 0.013	35,062.2	113,651.7	34,773.9
10	0.515 ± 0.013	35,132.0	115,223.3	34,773.9
11	0.439 ± 0.013	35,253.6	116,579.0	34,924.6
12	0.324 ± 0.013	35,350.0	117,734.3	34,924.6
13	0.254 ± 0.013	35,408.6	118,863.5	35,075.4
14	0.172 ± 0.013	35,495.4	119,268.4	35,075.8
15	0.095 ± 0.013	35,552.7	119,302.0	35,226.1
16	0.045 ± 0.013	35,634.1	120,630.1	35,226.1
17	0.013 ± 0.013	35,654.5	120,935.0	35,226.1
18	0.000 ± 0.013	35,667.3	120,829.9	35,226.1

The data dispersion was considered to be equal to 2σ, where σ is the standard deviation previously calculated. From these results one can denote a linear behavior through RH variation. This led to Figure 4.12 where data from Table 4.6 was fitted to a linear equation using standard least-squares method with Gaussian statistics.

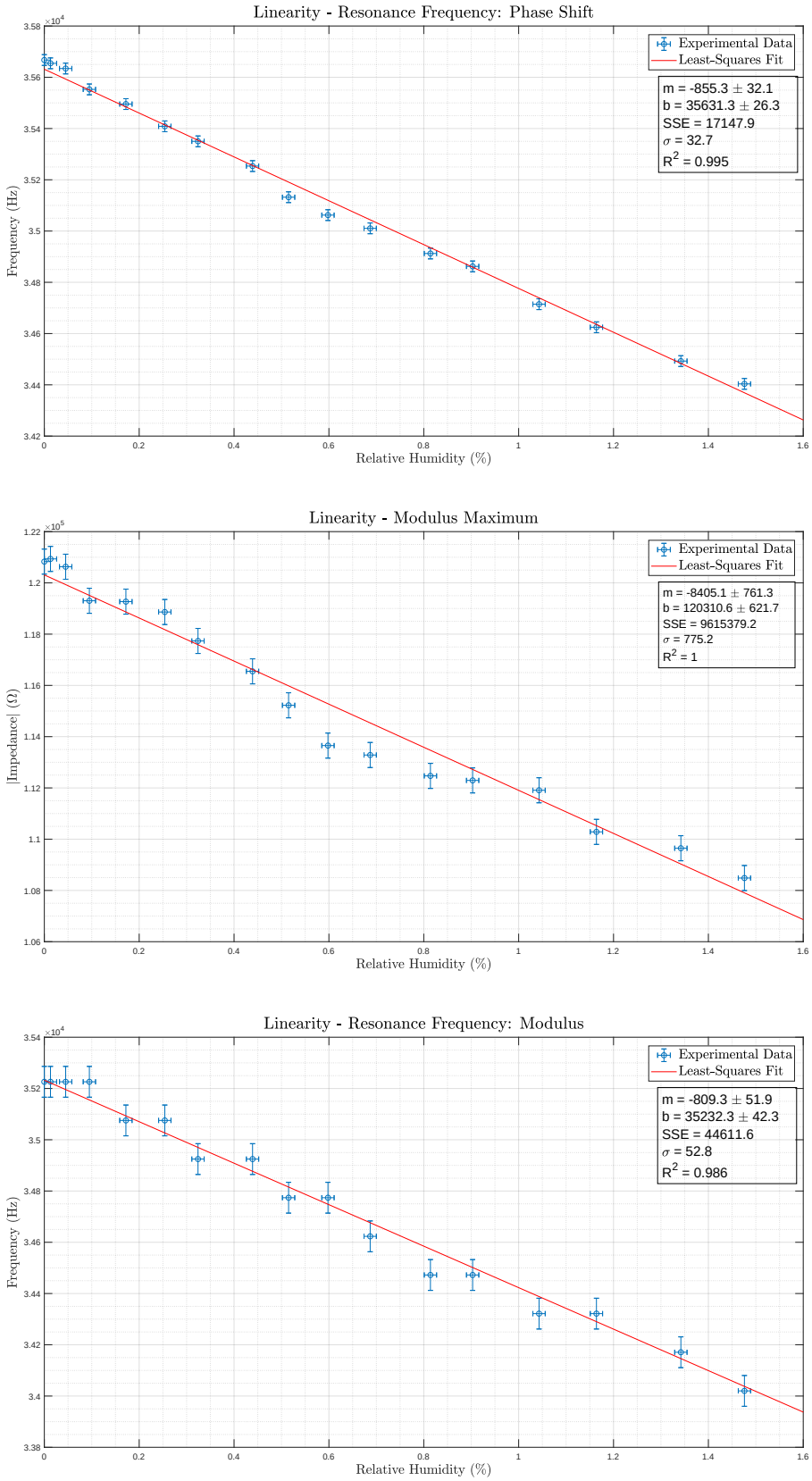

Figure 4.12: Impedance linearity through RH variation (Data fitted using standard least-squares method with Gaussian statistics; Sample: 157.23 ± 0.01 g of dry round shaped PET; $L = 118.2 \pm 0.1$ mH; External Conditions: 21 ^{o}C and 53 $\%_{humidity}$).

From these fits, it is possible to extract the information stated in Tables 4.7 and 4.8.

Table 4.7: Impedance linearity properties (Data fitted using standard least-squares method with Gaussian statistics; Sample: 157.23 ± 0.01 g of dry round shaped PET; $L = 118.2 \pm 0.1$ mH; External Conditions: 21 ^{o}C and 53 $\%_{humidity}$).

Parameter	Linear Equation ($y = mx + b$)	Limit of Detection
Resonance Frequency: Phase Shift (Hz)	$y = (-855 \pm 32)x + (35{,}631 \pm 26)$	0.037 $\%_{RH}$
Modulus Maximum (Ω)	$y = (-8{,}405 \pm 761)x + (120{,}311 \pm 622)$	0.087 $\%_{RH}$
Resonance Frequency: Modulus (Hz)	$y = (-809 \pm 52)x + (35{,}232 \pm 42)$	0.111 $\%_{RH}$

Table 4.8: Impedance fit performance parameters (Sample: 157.23 ± 0.01 g of dry round shaped PET; $L = 118.2 \pm 0.1$ mH; External Conditions: 21 ^{o}C and 53 $\%_{humidity}$).

Parameter	Sensitivity	Resolution
Resonance Frequency: Phase Shift	855 $Hz/\%_{RH}$	0.016 $\%_{RH}$
Modulus Maximum	8,405 $\Omega/\%_{RH}$	0.099 $\%_{RH}$
Resonance Frequency: Modulus	809 $Hz/\%_{RH}$	0.136 $\%_{RH}$

Considering that the main objective is to use this study to develop one measuring instrument, data related with tests repeatability was gathered. The following data (Tab. 4.9) represent the results of 5 additional complete tests in different environment conditions.

Table 4.9: Linear equations obtained in different tests.

Test	Dry Mass (g)	Resonance Frequency: Phase Shift (Hz)	Modulus Maximum (Ω)	Resonance Frequency: Modulus (Hz)
01	157.57 ± 0.01	$y = -749x + 35{,}705$	$y = -7{,}400x + 117{,}553$	$y = -668x + 35{,}343$
02	157.58 ± 0.01	$y = -788x + 35{,}675$	$y = -9{,}598x + 122{,}375$	$y = -746x + 35{,}294$
03	157.27 ± 0.01	$y = -901x + 35{,}723$	$y = -7{,}862x + 121{,}905$	$y = -793x + 35{,}286$
04	155.34 ± 0.01	$y = -916x + 35{,}900$	$y = -8{,}045x + 121{,}966$	$y = -864x + 35{,}488$
05	155.16 ± 0.01	$y = -883x + 35{,}877$	$y = -9{,}159x + 122{,}204$	$y = -866x + 35{,}490$

Table 4.10 depicts the parameters' calculation obtained for a RH of 0.3 % (maximum acceptable limit).

4.2.3 Discussion

Initial tests showed that MI was the more adequate mode to perform the tests on PET. It was also proved that pellet's shape does not affect PET's dielectric properties. Moreover, from the impedance's point of view they are indistinguishable. Taking into account performance parameters, it was decided that a lower inductance value was the best approach to achieve the main goals.

Table 4.10: Parameter calculation for maximum RH acceptable limit,values at 0.3 $\%_{RH}$ (Test 00 is the one previously analyzed).

Test	Dry Mass (g)	Resonance Frequency: Phase Shift (Hz)	Modulus Maximum (Ω)	Resonance Frequency: Modulus (Hz)
00	157.23 ± 0.01	35,375	117,790	34,989
01	157.57 ± 0.01	35,481	115,330	35,143
02	157.58 ± 0.01	35,439	119,500	35,071
03	157.27 ± 0.01	35,453	119,550	35,049
04	155.34 ± 0.01	35,625	119,550	35,229
05	155.16 ± 0.01	35,612	119,460	35,231

It was instantly observed that the proof of concept was possible as soon as measurements with humidity variations were performed. Table 4.5 and Figure 4.11 depict that water loss is approximately linear through time, with the exception of the last $20 - 30$ minutes. It was also denoted that capacitance decreases with water loss, which is expected according to the theoretical expressions.

Taking into consideration impedance modulus and phase shift, it was observed that there is a deviation up to 500 Hz on the resonance frequency of both of them. However, one can verify that they behave in similar way: decreasing relative humidity increases the resonance frequency. Bearing in mind sweep number 16 ($C = 158.9 \pm 0.01\ pF$), the expected resonance frequency value should be $36{,}724 \pm 19\ Hz$. If it is considered the phase shift parameter, the relative error is 2.97 %, and 4.01 % if impedance modulus is considered. As predicted in Section 4.1.2, as capacitance increased the relative error decreased.

Figure 4.12 proves that the considered PET's impedance characteristics are correlated with its relative humidity. These properties assume a linear behavior as water content changes. One disadvantage that one can identify is the lack of accuracy at low RH percentages. Taking in consideration the data obtained in Section 4.2.1.3, Tables 4.7 and 4.8, and the relative error here calculated, we can state that the best impedance parameter to measure PET's RH is resonance frequency using phase shift data.

Table 4.10 illustrates the parameters' dependency on sample's mass. Changes in mass produce deviations in these parameters. However, it can be stated that, for our setup, the maximum acceptable limit (0.3 $\%_{RH}$) is easily defined when the sample's dry mass is constant. Slope does not manifest any obvious dependency, further tests should be performed to correlate this parameter with other characteristics. Perhaps by gathering additional information it can be correlated with environmental relative humidity or temperature and can be properly calibrated accordingly to those.

4.3 Peloid Ionic Conductivity

In this section it is provided a preliminary study on peloids impedance measurements. Some initial tests need to be performed concerning the measuring system, taking into account temperature control, electrodes and the sample holder (Sec. 1.4.2).

4.3.1 Box System

4.3.1.1 Temperature Calibration

Due to temperature influence in peloid samples, it is important to have constant conditions during all tests. In Section 3.1.1.7, the initial system responsible for temperature control was introduced. The first step is to calibrate PT1000 and LMT86. Both sensors (Fig. 3.12) were submerged in hot water and their output was measured through time. Temperature values were calculated using Equations 3.3 and 3.5, and then compared with a precision temperature sensor (*testo 110*). The relation between water temperature and the obtained values is represented in Figures 4.13 and 4.14.

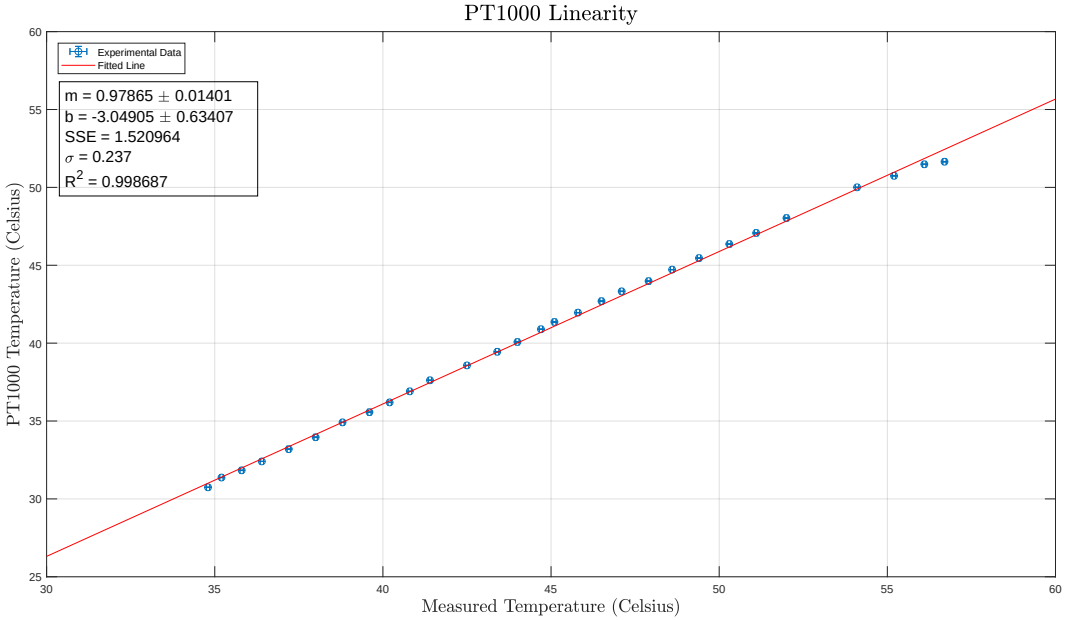

Figure 4.13: PT1000 linearity: PT1000 results vs. water temperature value obtained with *testo 110* (precision thermometer).

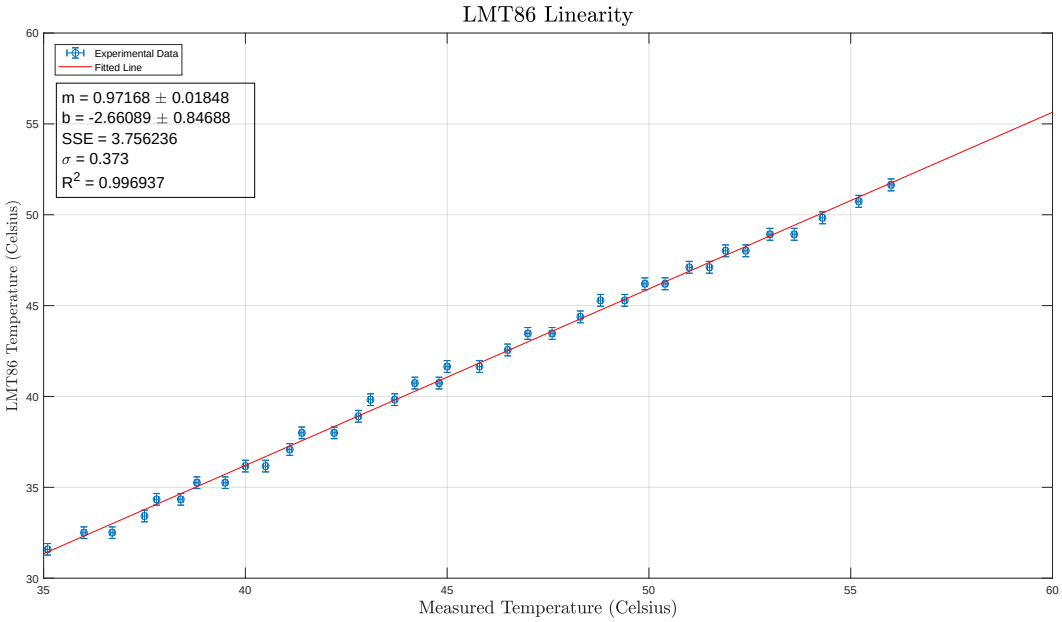

Figure 4.14: LMT86 linearity: LMT86 results vs. water temperature value obtained with *testo 110* (precision thermometer).

The relation between water temperature and the calculated using PT100 is given by $T_{PT1000} = 0.979\, T_{water} - 3.049$. For LMT86 it is given by $T_{LMT86} = 0.972\, T_{water} - 2.661$. These results confirm both sensors linearity, and show that they behave likewise. The offset obtained in the linear regression can be due to lack of isolation in the top end of both tubes (Fig. 3.12). Taking into account that the offset is constant in our temperature range, this systematic error is easy to overtake.

4.3.1.2 Heating System

Considering that the sample's temperature is an important parameter in this case study, it is necessary to access information relative to the heat dissipation of the sample holder. Data is depicted in Figure 4.15, using water.

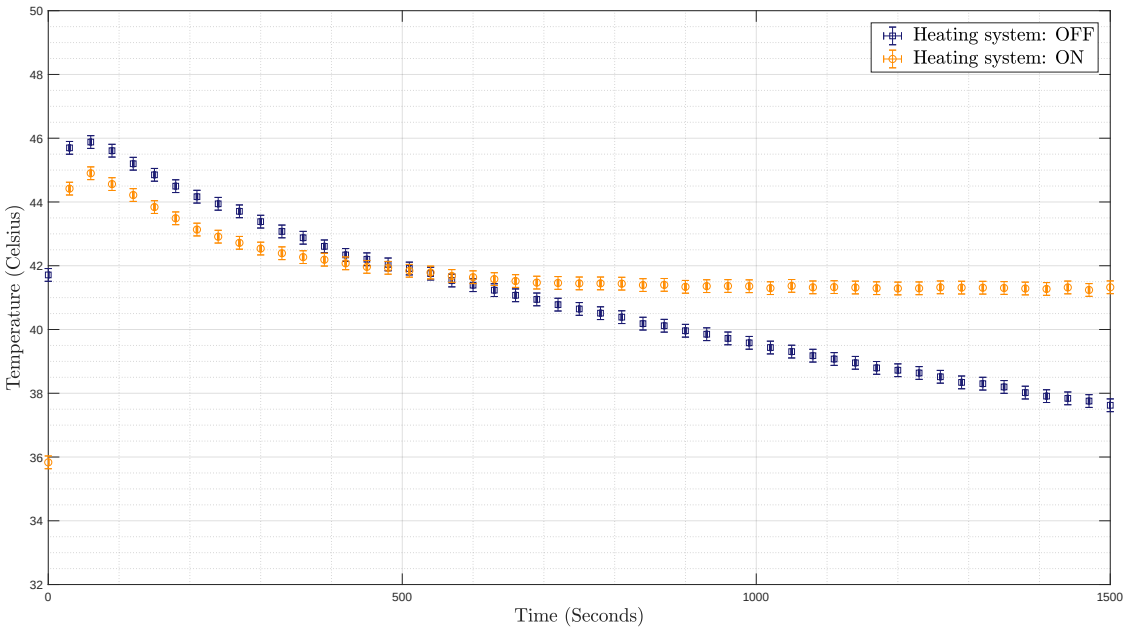

Figure 4.15: Sample holder heat dissipation using water.

It is possible to notice an enormous difference when the heating system is turned ON. The temperature will stabilize at 41 $^{\circ}C$ after 660 seconds, which is a long time period. This time interval is the one needed to stabilize the heat exchange between the sample, the container, and the heating system.

The next step was to study the heating system's performance with a clay-water mixture. Figure 4.16 portrays the sample temperature through time (clay used in the initial tests was obtained in a supermarket [61]).

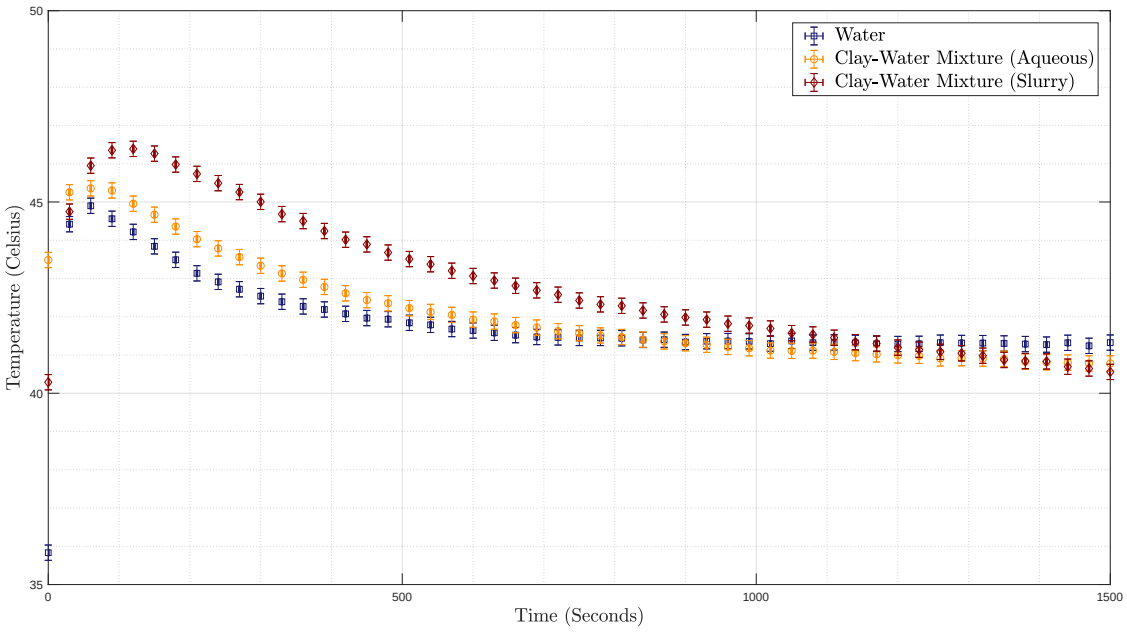

Figure 4.16: Comparison between water and clay-water mixtures (25 *minutes*).

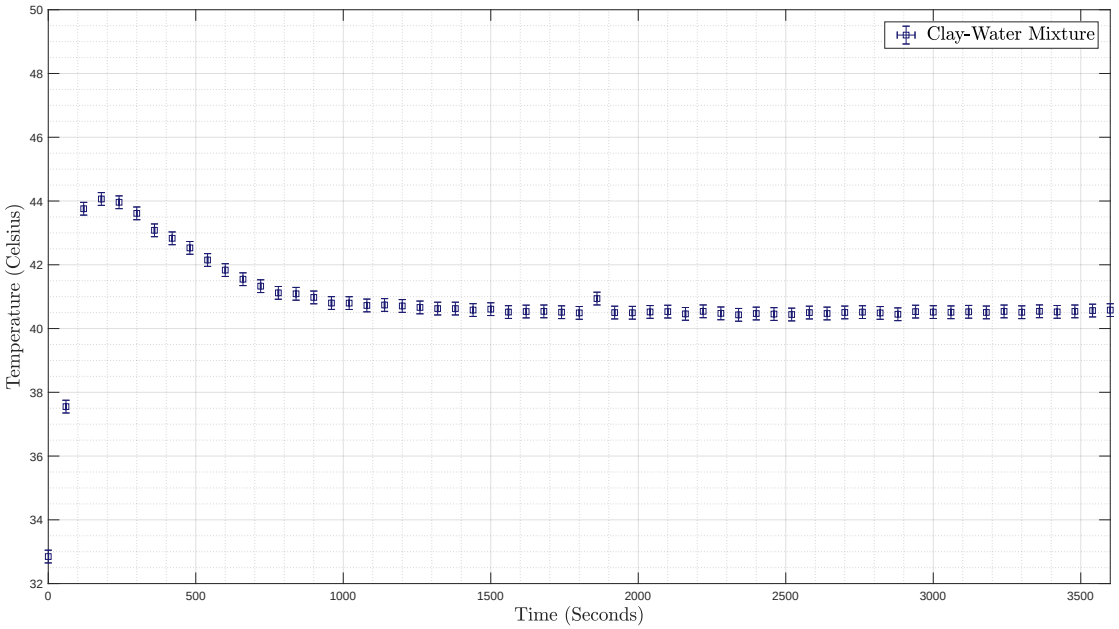

Figure 4.17: Clay-water mixtures temperature behavior for a 60 *minutes* period.

In Figure 4.16, it was possible to notice that water-clay mixtures behave differently when compared to water. From Figure 4.17, it is denoted that the mixture

stabilized at a temperature smaller than 41 ^{o}C. From this section one can immediately point out one disadvantage in this heating system: it cannot stabilize at a temperature higher than 41 ^{o}C. Considering our range of temperatures ($40-50\ ^{o}C$), this system does not fit our requirements.

Some effort was made to improve this solution: it was changed the length of the heating element, instrumentation's amplifier (Fig. 3.11) gain was increased, and the initial wire was replaced by others available in the laboratory, without any remarkable difference.

In addition to this limitation, this box-type system demands a large stabilization period and a time consuming cleaning process. These limitations led to a completely different system (Fig. 3.13).

4.3.2 Water Bath System

4.3.2.1 Heating System

The previous tests were repeated in a new system. Here, the temperature measuring instrument used was the *testo 110* due to its higher precision. The results obtained are depicted in Figures 4.18, 4.19, and 4.20.

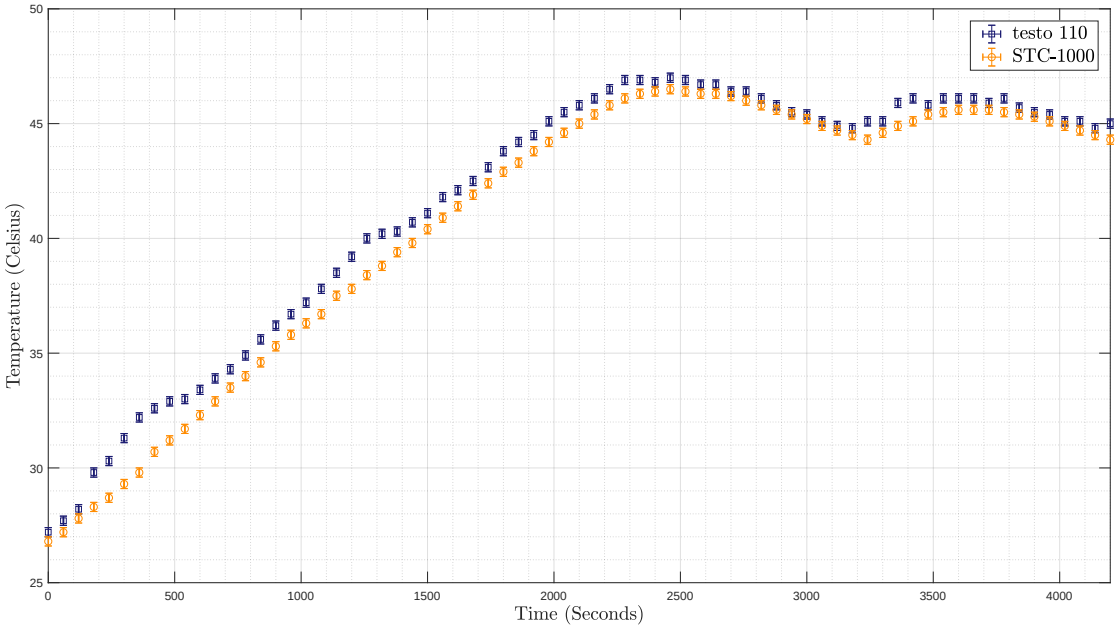

Figure 4.18: Water heating process from room temperature to 45 ^{o}C: comparison between *testo 110* and *STC-1000* (temperature control/meter) (70 minutes).

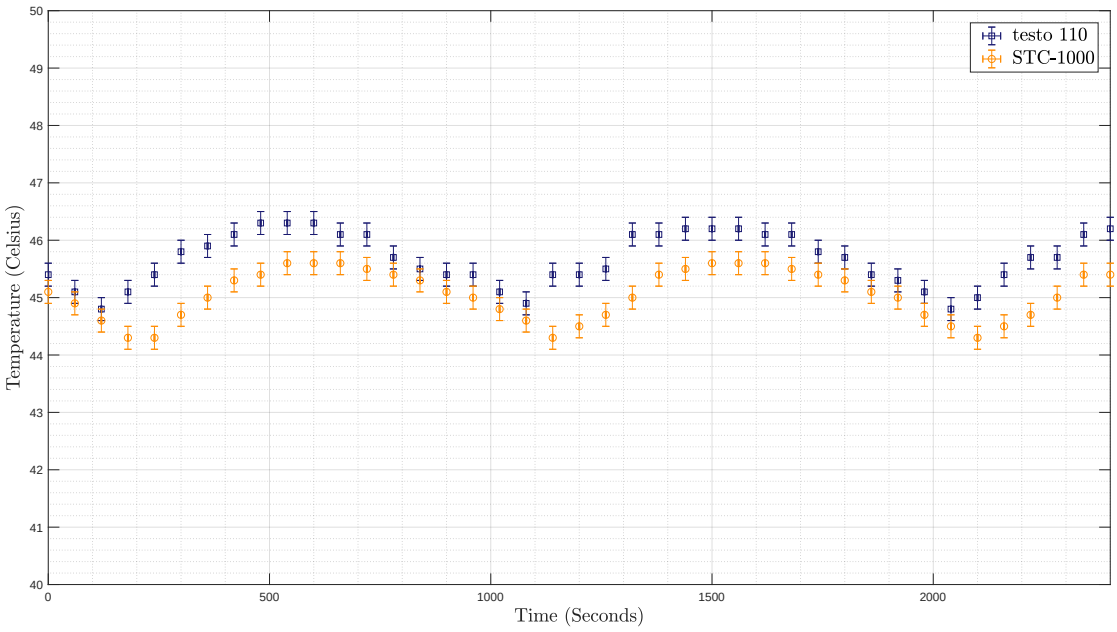

Figure 4.19: Water temperature stabilization at 45 ^{o}C: sensor comparison (40 minutes).

From the acquired data it is verified the viability of this new heating system, being capable of stabilizing at temperatures higher than 41 ^{o}C (with an accuracy of ± 1 ^{o}C). When comparing the two used sensors (*stc-1000* and *testo 110*), it was observed a difference due to the tube where the *stc-1000* probe was inserted. Taking this into account, we used the *testo 110* to acquire the temperature dependency on concentration (Fig. 4.20). Setting the temperature to 45 ^{o}C, the highest registered value was 46.3 ^{o}C and the lowest 44.8 ^{o}C, which indicates that our system is able to maintain a stable temperature with the accuracy stated in its datasheet (± 1 ^{o}C).

In contrast to the previous system, the stabilization time required is just 5 minutes. Evaluating by Figure 4.20, it was verified that temperature and stabilization time is independent of the mixture's concentration.

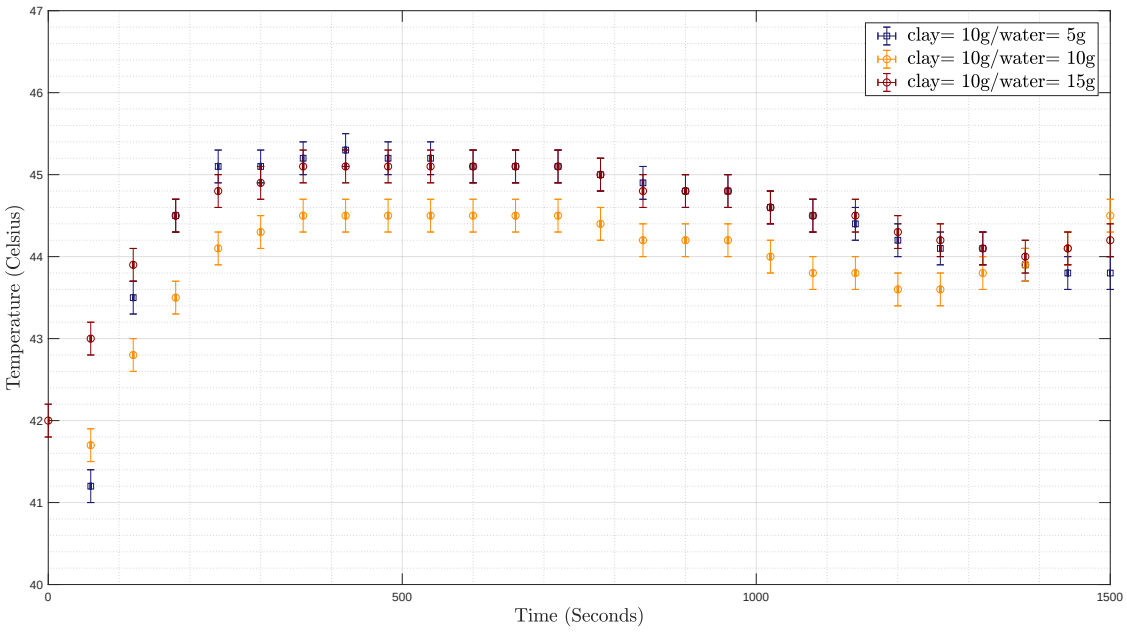

Figure 4.20: Clay-water mixtures heating process and stabilization at 45 ^{o}C: concentration comparison (25 minutes).

4.3.2.2 Electrodes

In view of defining the overall measuring system, the electrodes are one important issue. Several aspects needed to be considered, such as shape, size, and separation distance. Initially, it was considered to use aluminum plates (60×20 mm). When calculating some common material's relative permittivity, they proved not to be suited to liquid materials due to electrical conduction between the two plates.

The next electrodes considered were two copper plates (60×20 mm) painted with varnish. The results obtained with these new electrodes were as expected ($\varepsilon_{r_{paper}} = 2.64$; $\varepsilon_{r_{distilled\ water}} = 70.24$).

Figures 4.21 to 4.23 depict the initial impedance results obtained for the commercial clay-water mixture and the copper electrodes.

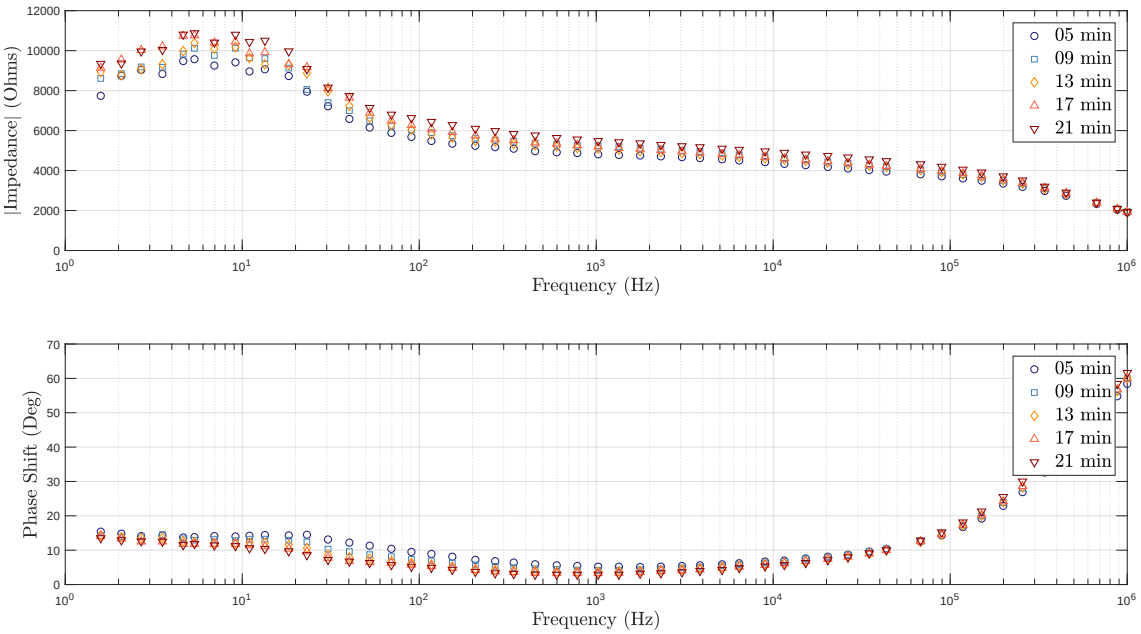

Figure 4.21: Clay-water mixture impedance behavior through time. Sample temperature was set to 45 ^{o}C and mixture was prepared with 10 g of clay and 5 ml of distilled water.

From Figure 4.21 it was verified that throughout the course of time the mixture's impedance changes. Focusing in its modulus it is easily observed that the latter increases with time which is due to water evaporation. Phase shift decreases to low frequencies, which is also verified in Figure 4.22.

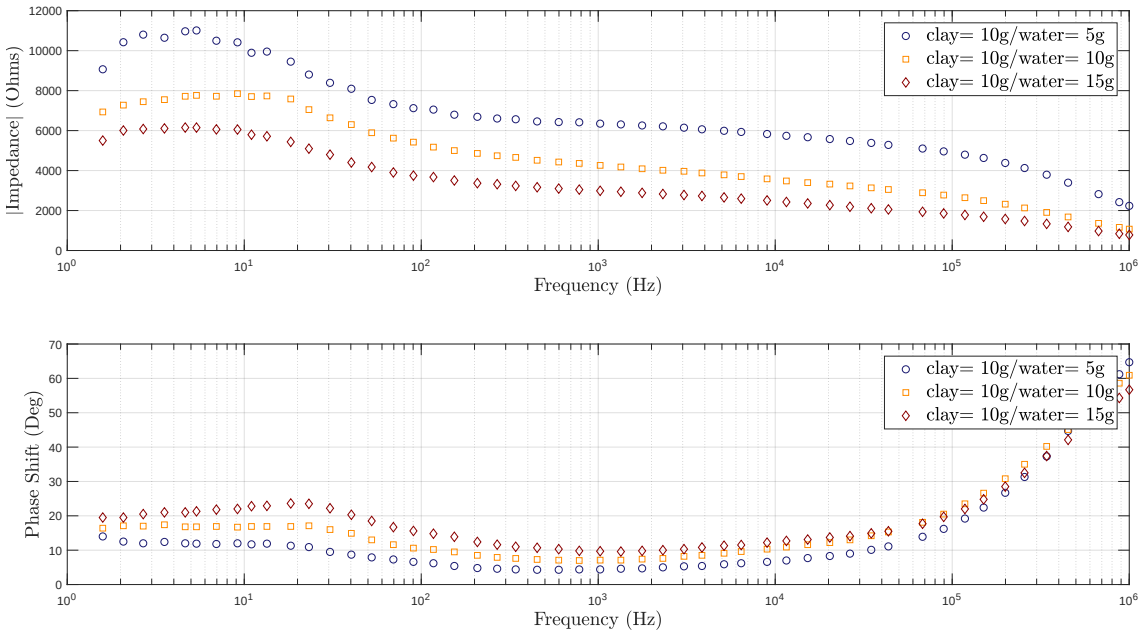

Figure 4.22: Clay-water mixtures impedance dependency with material concentration. Sample temperature was set to 45 ^{o}C.

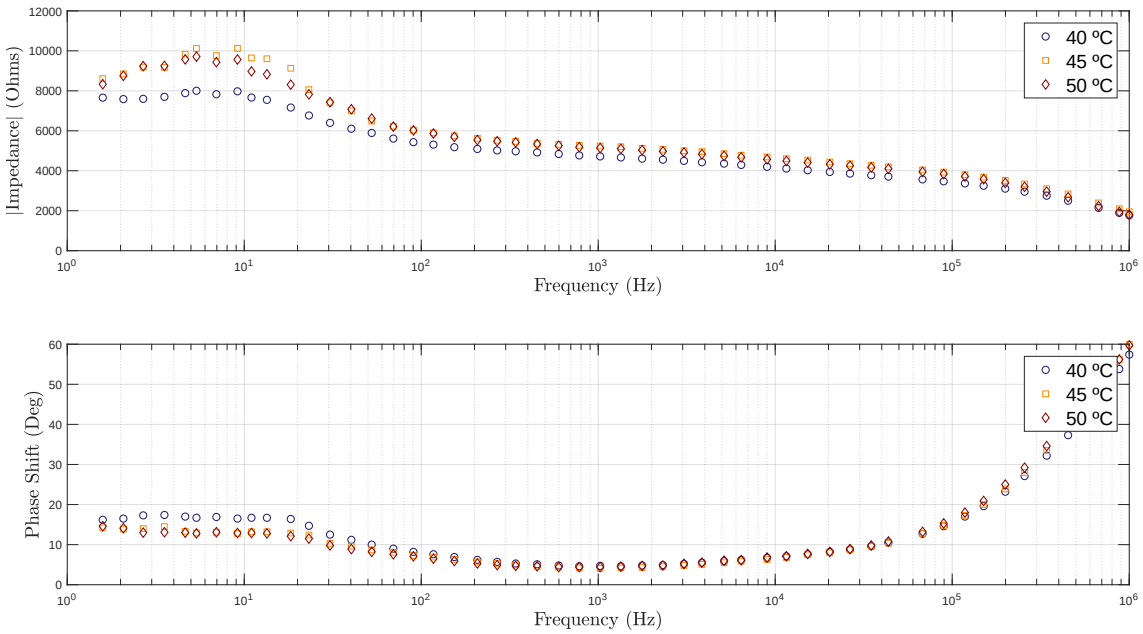

Figure 4.23: Clay-water mixtures impedance dependency with sample temperature. Mixtures were prepared with 10 g of clay and 5 ml of distilled water.

Figure 4.22 shows that impedance modulus increases with clay concentration,

which is in accordance with the results from Figure 4.21: less water equals to higher modulus (and in this case, resistance). From Figure 4.23 it is observed that the modulus is almost the same for 45 and 50 ^{o}C and lower to 40 ^{o}C.

In Figure 4.24 one can see the clay-water mixture behavior using the two silver plated electrodes. The relative permittivity constants obtained with these electrodes were $\varepsilon_{r_{paper}} = 2.36$ and $\varepsilon_{r_{distilled\ water}} = 455.36$.

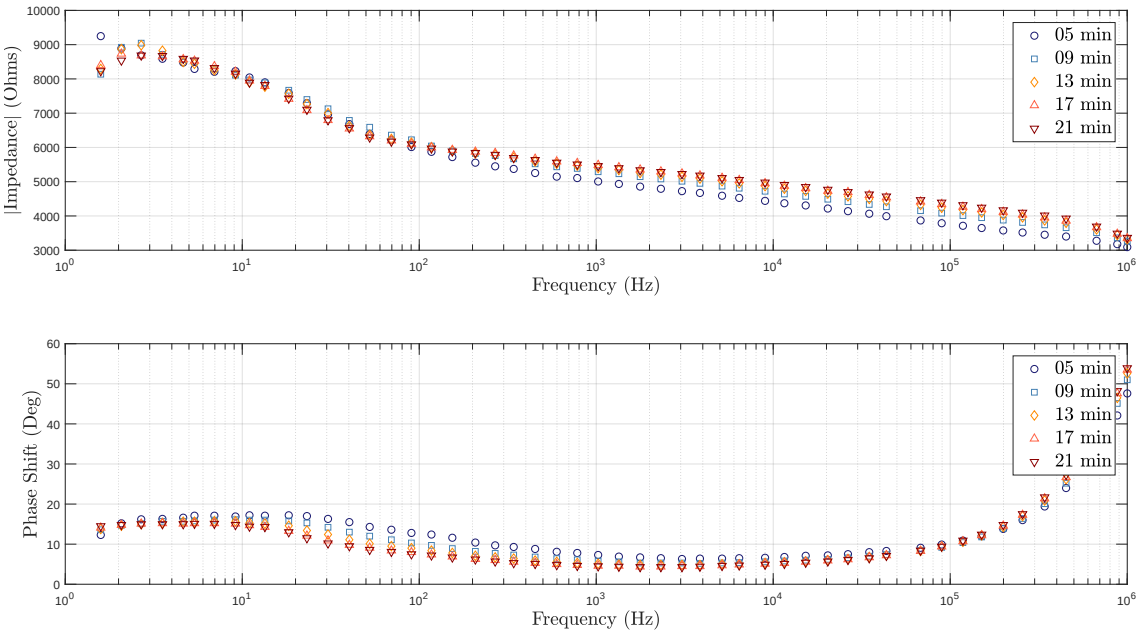

Figure 4.24: Clay-water mixture impedance behavior through time using silver plated electrodes. Sample temperature was set to 45 ^{o}C and mixture was prepared with 10 g of clay and 5 ml of distilled water.

One can conclude that the impedance spectrum is similar using both types of electrodes. However, when calculating the relative permittivity, the non-plated plates provided more accurate results. Therefore, the copper plates were the ones selected to this study.

4.3.2.3 Sample Analysis: Peloids Preliminary Results

Figure 4.25 depicts peloids modulus and phase shift behavior over the frequency spectrum.

By simple observation of the raw data, differences between samples' outputs can immediately be noticed. In the tested frequency range they decreased in modulus,

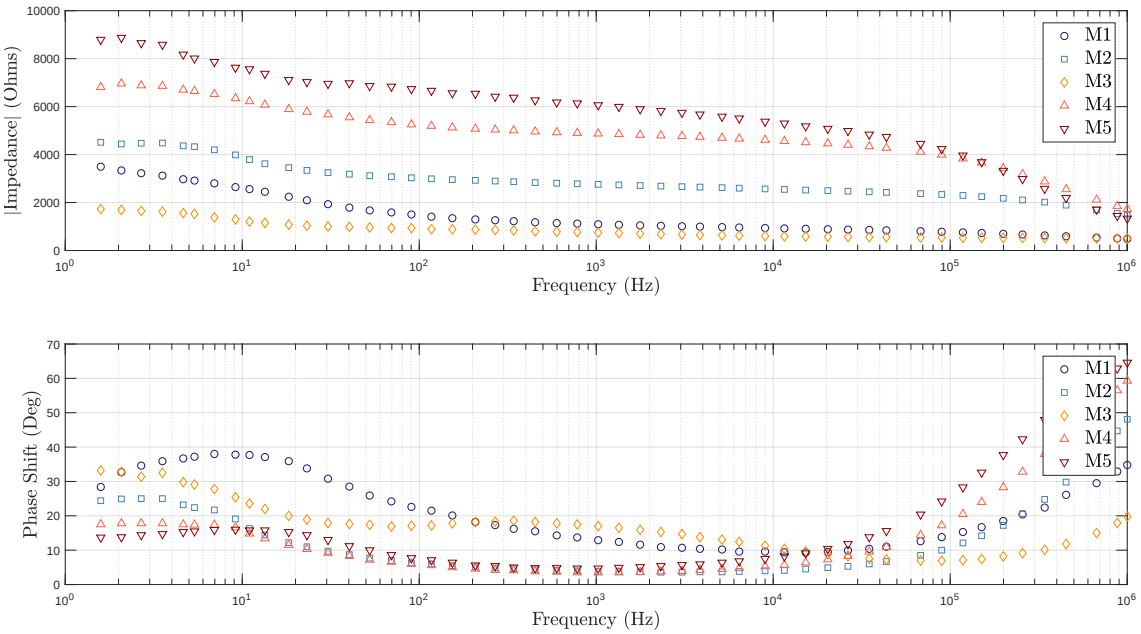

Figure 4.25: Peloid-water mixtures impedance behavior throughout time using copper electrodes. Samples temperature was set to 45 ^{o}C and mixtures were prepared with 10 g of peloid and 5 ml of distilled water.

which is expected from a capacitor, but their initial value is different for each sample. From a first impression, it seems that there is not any correlation between each sample's characteristics (such as pH or CEC) and these results. Figure 4.26 is introduced here to compare the sample results with the impedance planes from Figure 2.7 (Sec. 2.2).

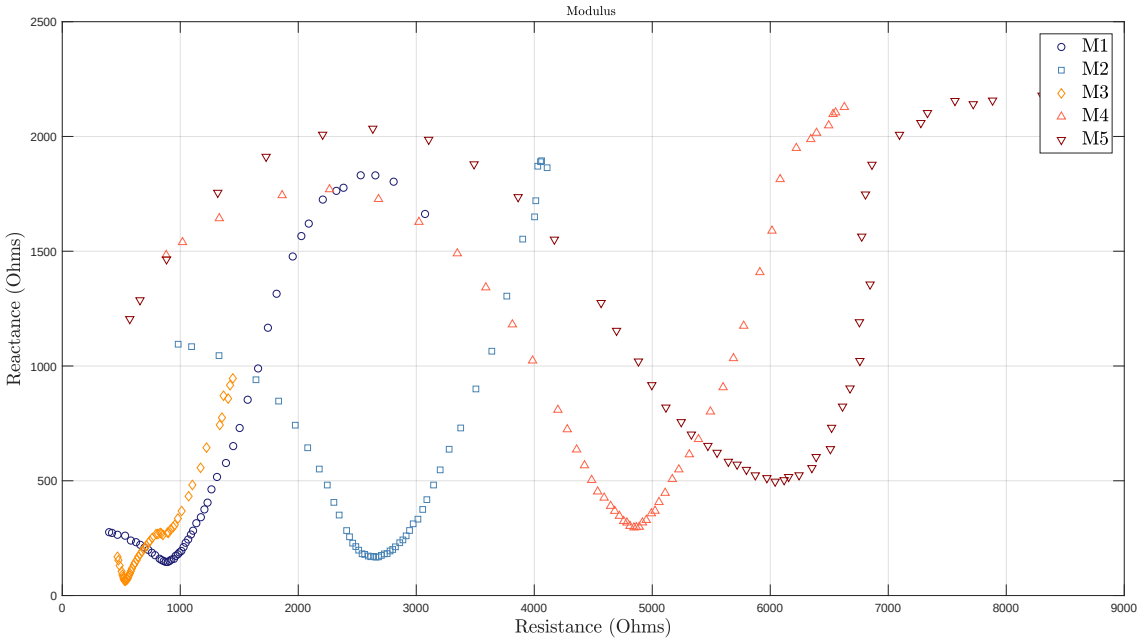

Figure 4.26: Peloid-water mixtures Cole-Cole plots using copper electrodes. Samples temperature was set to 45 ^{o}C and mixtures were prepared with 10 g of peloid and 5 ml of distilled water.

These results are similar to the expected ones from Figure 2.7, specially to samples M4 and M5. It can be easily identified that a semi-circle and the begin of another (for low-frequencies). With a larger range of frequencies the reader would probably be observing two semi-circles, which should be enough to analyze this data using Debye or Maxwell-Wagner equivalent circuits. This analysis should allow the extraction of the different variables (Fig. 2.7).

4.3.3 Discussion

In a first instance, the definition of the measuring system was crucial. It was important to provide an initial definition of the sample holder's material, the electrodes' main characteristics, and the heating system. All these aspects were studied in this project and it was provided a viable solution even though there is plenty room for improvements.

If it is analyzed each sample reactance (Fig. 4.26), it is easy to identify that all of them present a minimum value. This phenomenon occurs around 1 kHz and, taking into account Exatronic's main goal, this frequency would probably be a good starting point for them to study peloids' ionic conduction changes.

Some conclusions can already be taken from these preliminary results: EIS is affected by the sample's temperature and it can easily discriminate between sample's concentration (higher water content results in lower modulus). By increasing the range of frequencies, one should be able to fit our data to the equivalent circuits (Fig. 2.7), extract sample parameters, and correlate them with their known characteristics (pH, CEC, or particle surface area).

With this study it was not possible to achieve any constant correlation peloids' characteristics and their impedance. Off course much remains to be done following this preliminary approach. Cooperation with Exatronic or other developers should proceed in order to correlate scientifically therapeutic effects of peloids and their chemical/physical characteristics.

CHAPTER 5

Conclusions

The studies developed during this project showed that the efforts to build a low cost impedance spectroscopy meter resulted in a precise device. Moreover, the overall device characteristics make of it an ideal candidate for a wide range of applications where portability is a key factor.

PET moisture analysis revealed a linear relation with impedance characteristics. In fact, it was demonstrated that EIS provide good linearity around the maximum acceptable value of water content. In general, phase shift parameters proved to be more reliable in PET RH measurements. Further investigation should be performed in order to correlate the results with environmental temperature.

Taking into account the second case study, the measuring system main characteristics were defined. Furthermore, it was proved that the EIS system is capable of identifying different peloid samples according to their impedance dependency. Although, it is expected that it will be possible to correlate the impedance parameters with peloids' physiochemical characteristics by increasing the frequency range in the future.

It can be stated that the final result is a trustworthy measuring device that, with the appropriate electrodes and data analysis, may measure almost any material properties that affect impedance.

5.1 Future Work

5.1.1 Tests

- PET's RH detection was tested using an heating system and the outcome results were achieved under high temperatures (70 ^{o}C). In order to improve those results, further tests should be performed at a controlled environment (constant humidity at room temperature);
- Another approach to PET's RH detection should take into account slopes variation: more data must be gathered during each test to correlate these variations with other parameters (such as air relative humidity and external temperature);
- Additional PET testes should be performed at controlled PET RHs;
- Should be increased peloids' frequency range and fit the data to the equations presented in Figure 2.7;
- All the tests presented here should be repeated with a commercial impedance meter and compare both of them. At the moment, the laboratory is waiting for the arrival of a spectrum analyzer (*RIGOL DSA832-TG* [70]).

5.1.2 Hardware

- As stated in Section 4.2.3 PET's RH detection depends on the sample's mass. Electrodes should be improved in order to secure a constant mass between them and to make them more suitable for the final application (fast industrial measurements);
- Should be developed a supply circuit based on a battery to make it viable for industrial environments;
- Should be developed a new glass sample holder for peloids, that permits ultrasound cleaning and a constant sample volume between the electrodes.

5.1.3 Software

- One section just for PET RH measurement should be added in the user interface, including a proper frequency range and, in the end of each sweep, present

the RH estimation;

- A new section should be created in the interface that automatically calculates the correct frequencies by choosing the frequency range and the number of points.

Publication

Emanuel Duarte, J. P. P. Domingues, João Cardoso, *GRAU DE HUMIDADE EM POLYETHYLENE TEREPHTALATE (PET) POR ESPECTROSCOPIA DE IMPEDÂNCIA ELÉTRICA*, *FÍSICA 2018 – 21ª Conferência Nacional de Física e 28º Encontro Ibérico para o Ensino da Física*, August 30, 2018

Bibliography

[1] Y. Banat and Z. A. El-Rub, "A technical and economic feasibility study of: Production of Polyethylene Terephthalate by direct esterification using pervaporation," *University of Twente*, 2001.

[2] D. Boffey, "EU declares war on plastic waste." `https://www.theguardian.com/environment/2018/jan/16/eu-declares-war-on-plastic-waste-2030`, Jan 2018. Date accessed: 05, Feb 2018.

[3] S. Laville, "Chinese ban on plastic waste imports could see UK pollution rise." `https://www.theguardian.com/environment/2017/dec/07/chinese-ban-on-plastic-waste-imports-could-see-uk-pollution-rise`, Dec 2017. Date accessed: 07, Feb 2018.

[4] R. López-Fonseca, I. Duque-Ingunza, B. de Rivas, L. Flores-Giraldo, and J. I. Gutiérrez-Ortiz, "Kinetics of catalytic glycolysis of PET wastes with sodium carbonate," *Chemical Engineering Journal*, vol. 168, no. 1, pp. 312 – 320, 2011.

[5] L. N. Ji, "Study on preparation process and properties of Polyethylene Terephthalate (PET)," *Applied Mechanics and Materials*, vol. 312, pp. 406–410, 2013.

[6] G. Thomas, "Recycling of polyethylene terephthalate (PET or PETE)." `https://www.azocleantech.com/article.aspx?ArticleID=254`, Feb 2017. Date accessed: 28, Jan 2018.

[7] www.goodfellow.com, "Polyethylene terephthalate (polyester, PET, PETP)." `http://www.goodfellow.com/E/Polyethylene-terephthalate.html`. Date accessed: 09, Feb 2018.

[8] P. P. INC, "PET(polyethylene terephalate)." `http://www.plastic-products.com/engineered-plastics/pet/`. Date accessed: 17, Jul 2018.

[9] S. A. Jabarin and E. A. Lofgren, "Effects of water absorption on physical properties and degree of molecular orientation of poly(ethylene terephthalate)," *Polymer Engineering & Science*, vol. 26, no. 9, pp. 620–625, 1986.

[10] D. Lazarevic, E. Aoustin, N. Buclet, and N. Brandt, "Plastic waste management in the context of a european recycling society," vol. 55, pp. 246–259, 12 2010.

[11] J. R. Campanelli, M. R. Kamal, and D. G. Cooper, "A kinetic study of the hydrolytic degradation of polyethylene terephthalate at high temperatures," *Journal of Applied Polymer Science*, vol. 48, no. 3, pp. 443–451, 1993.

[12] D. Ravens and I. Ward, "Chemical reactivity of polyethylene terephthalate. hydrolysis and esterification reactions in the solid phase," *Transactions of the Faraday Society*, vol. 57, pp. 150–159, 1961.

[13] C. M. Staff, "About PET - PETRA: Information on the use, benefits and safety of PET plastic." `http://www.petresin.org/aboutpet.asp`. Date accessed: 25, Jan 2018.

[14] B. R. et al, "Electroless plating of nip and cu on polylactic acid and polyethylene terephthalate glycol-modified for 3d printed flexible substrates.," *Journal of The Electrochemical Society*, vol. 163, 27 July 2016.

[15] C. M. Staff, "Everything you need to know about the world's most useful plastic (PET and polyester)." `https://www.creativemechanisms.com/blog/everything-about-polyethylene-terephthalate-pet-polyester`. Date accessed: 25, Jan 2018.

[16] Tovatech, "How to select a moisture analyzer for plastic resins." `http://www.tovatech.com/blog/18928/moisture-balance-2/select-a-moisture-analyzer-for-plastic-resins`, Nov 2016. Date accessed: 08, Feb 2018.

[17] J. P. Bentley, *Principles of Measurement Systems*. Prentice Hall, 2004.

[18] Brabender-MT, "Aquatrac-3e moisture meter for plastics." `https://www.brabender-mt.de/en/products-and-solutions/aquatrac-3e-en`. Date accessed: 15, June 2018.

[19] I. MEECO, "Tracer 2 modulator moisture analyzer." `https://meeco.com/meeco/wp-content/themes/mecco/pdf/english/Tracer%202.pdf`. Date accessed: 15, June 2018.

[20] S. Anjo, "The Electrical Impedance Spectroscopy Technique – 3 Case Studies in Chemical and Biological Materials," 2016.

[21] M. I. Carretero, "Assessment of three Spanish clays for their use in peloterapy," vol. 99, pp. 131–143, 2014.

[22] M. Pozo, "Composition and physico-chemical properties of peloids used in Spanish spas: A comparative study," vol. 83-84, pp. 270–279, 2013.

[23] A. C. SANTOS, "Maturação de lamas vulcânicas açorianas e sua aplicação em peloterapia," 2011.

[24] J. Daniela, D. Moraes, S. Raquel, A. Bertolino, S. Lucia, D. Fernando, P. Eriberto, and G. Ricci, "Clay minerals : Properties and applications to dermocosmetic products and perspectives of natural raw materials for therapeutic purposes — A review," vol. 534, no. July, pp. 213–219, 2017.

[25] Exatronic, "edersensæ: a new way for thermal medicine." `http://www.exa4life.com/edersensae/#page`. Date accessed: 06, Jun 2018.

[26] K. A. Samah, M. R. Sahar, M. Yusop, and M. F. Omar, "Phase modification and dielectric properties of a cullet–paper ash–kaolin clay-based ceramic," *International Journal of Minerals, Metallurgy, and Materials*, vol. 25, pp. 350–356, Mar 2018.

[27] J. Pineda-Piñón, "Impedance spectroscopy of chemically enhanced clays used for adobe construction," vol. 76, 2004.

[28] M. M. Martins, "Malaria Diagnosis System Based on Electric Impedance Spectroscopy," 2017.

[29] E. Borges, A. Matos, J. Cardoso, C. Correia, T. Vasconcelos, and N. Gomes, "Early detection and monitoring of plant diseases by bioelectric impedance spectroscopy," in *Bioengineering (ENBENG), 2012 IEEE 2nd Portuguese Meeting in*, pp. 1–4, IEEE, 2012.

[30] N. C. S. Capela, "Impedance cardiography," Master's thesis, 2013.

[31] A. F. V. Cortez, "Application of bioimpedance techniques for physiological states assessment in plant tissues," Master's thesis, 2012.

[32] M. Sequeira, "Broadband excitation for bioelectrical impedance spectroscopy - a comparative study," Master's thesis, 2012.

[33] M. JR, "Impedance spectroscopy," *Ann Biomed Eng.*, vol. 20(3), pp. 289–305, 1992.

[34] A. Lasia, *Electrochemical impedance spectroscopy and its applications*. Springer, 2014.

[35] E. Barsoukov and J. R. Macdonald, *Impedance spectroscopy: theory, experiment, and applications*. Wiley-Interscience, 2005.

[36] L. Callegaro, "The metrology of electrical impedance at high frequency: a review," *Measurement Science and Technology*, vol. 20, no. 2, p. 022002, 2009.

[37] "RLC (LCR) meters." `http://www.digimessinstruments.co.uk/rlcmeters/`. Date accessed: 27, Jul 2018.

[38] "N9041B UXA Signal Analyzer, Multi-touch, 2 Hz to 110 GHz." `https://www.keysight.com/en/pdx-2743415-pn-N9041B/uxa-signal-analyzer-multi-touch-3-hz-to-110-ghz?pm=spc&nid=-32508.1189667&cc=PT&lc=eng`. Date accessed: 27, Jul 2018.

[39] "Bench LCR Meters - Model 895." `https://www.bkprecision.com/products/component-testers/895-1mhz-lcr-meter.html`. Date accessed: 27, Jul 2018.

[40] M. Rafiei-Naeini, P. Wright, and H. McCann, "Low-noise measurement for electrical impedance tomography," in *13th International Conference on Electrical Bioimpedance and the 8th Conference on Electrical Impedance Tomography* (H. Scharfetter and R. Merwa, eds.), (Berlin, Heidelberg), pp. 324–327, Springer Berlin Heidelberg, 2007.

[41] P. J. Yoo, D. H. Lee, T. I. Oh, and E. J. Woo, "Wideband bio-impedance spectroscopy using voltage source and tetra-polar electrode configuration," *Journal of Physics: Conference Series*, vol. 224, no. 1, p. 012160, 2010.

[42] G. J. Saulnier, A. S. Ross, and N. Liu, "A high-precision voltage source for EIT," *Physiological measurement*, vol. 27, no. 5, p. S221, 2006.

[43] R. Buendia, F. Seoane, and R. Gil-Pita, "Experimental validation of a method for removing the capacitive leakage artifact from electrical bioimpedance spectroscopy measurements," *Measurement Science and Technology*, vol. 21, no. 11, p. 115802, 2010.

[44] M. Mojid and H. Cho, "Estimating the fully developed diffuse double layer thickness from the bulk electrical conductivity in clay," *Applied Clay Science*, vol. 33, no. 3, pp. 278 – 286, 2006.

[45] J. K. Mitchell, *Fundamentals of soil behavior*. John Wiley & Sons, Inc, 1976.

[46] A. Kaya, "Electrical spectroscopy of kaolin and bentonite slurries," *Turkish Journal of Engineering and Environmental Sciences*, vol. 25, no. 4, pp. 345–354, 2001.

[47] V. A. Rinaldi and F. M. Francisca, "Impedance analysis of soil dielectric dispersion (1 mhz-1 ghz)," *Journal of Geotechnical and Geoenvironmental Engineering*, vol. 125, no. 2, pp. 111–121, 1999.

[48] H. C. Pullman and March, "Analog Discovery ™ Technical Reference Manual Architectural Overview and Block Diagram," pp. 1–39, 2015.

[49] S. Arora, "Analog discovery 100ms/s usb oscilloscope and logic analyzer (limited time)." `https://store.digilentinc.com/analog-discovery-100msps-usb-oscilloscope-logic-analyzer-limited-time/`. Date accessed: 18, Jul 2018.

[50] Analog Devices, "Adg1409," pp. 1–16, 2009.

[51] T. Instruments, "LM4040 Precision Micropower Shunt Voltage Reference Precision Micropower Shunt Voltage Reference," no. March, pp. 1–19, 2005.

[52] P. Cheremisinoff, *Handbook of engineering polymeric materials*. CRC Press, 1997.

[53] "SQM5-6R8JB2." `http://uk.farnell.com/welwyn/sqm5-6r8jb2/resistor-5w-5-6r8/dp/1687941?ost=sqm5+8ohm&dym=sqm+8ohm&cfm=true&ddkey=http%3Aen-GB%2FElement14_United_Kingdom%2Fsearch`. Date accessed: 24, Jul 2018.

[54] T. Instruments, "LMT86 2.2-V, SC70/TO-92/TO-92S, Analog Temperature Sensors 1," 2017.

[55] A. Devices, "Low Cost Instrumentation Amplifier AD622 * Product Page Quick Links," *AD623 Datasheet*, 2012.

[56] V. Siliconix, "SiRA90DP Vishay Siliconix N-Channel 30 V (D-S) MOSFET SiRA90DP,"

[57] Mixtrónica, "MH1210W - 3w 1.7" screen intelligent digital temperature con." http://www.mixtronica.com/ferramentas-medicao-medicao-termometros-higrometros/7103-mh1210w-3w-1-7-screen-intelligent-digital-temperature-con-mh1210w.html. Date accessed: 30, Jul 2018.

[58] "Fast fourier transform." https://www.mathworks.com/help/matlab/ref/fft.html. Date accessed: 22, May 2018.

[59] "Discrete fourier transform." https://www.mathworks.com/help/signal/ug/discrete-fourier-transform.html. Date accessed: 25, May 2018.

[60] U. Texas, "Discrete fourier transform." http://www.ae.utexas.edu/courses/ase363q/past_projects/StarLiteGVT/Report_html/Appendix_A/Appendix_A_FFT.html. Date accessed: 21, May 2018.

[61] Continente, "Argila verde - seara." https://www.continente.pt/stores/continente/pt-pt/public/Pages/ProductDetail.aspx?ProductId=3046629(eCsf_RetekProductCatalog_MegastoreContinenteOnline_Continente). Date accessed: 22, Jun 2018.

[62] F. Dubelley, E. Planes, C. Bas, E. Pons, B. Yrieix, and L. Flandin, "Water Vapor Sorption Properties of Polyethylene Terephthalate over a Wide Range of Humidity and Temperature," *The Journal of Physical Chemistry B*, vol. 121, no. 8, pp. 1953–1962, 2017.

[63] P. R. Bevington and D. K. Robinson, *Data reduction and error analysis for the physical sciences*. McGraw-Hill, 2010.

[64] J. W. Bartlett and C. Frost, "Reliability, repeatability and reproducibility: Analysis of measurement errors in continuous variables," *Ultrasound in Obstetrics and Gynecology*, vol. 31, no. 4, pp. 466–475, 2008.

[65] A. BenSaïda, "Shapiro-wilk and shapiro-francia normality tests." https://www.mathworks.com/matlabcentral/fileexchange/13964-shapiro-wilk-and-shapiro-francia-normality-tests?focused=3823443&tab=function), 2014. Date accessed: 18, May 2018.

[66] "One-sample kolmogorov-smirnov test." https://www.mathworks.com/help/stats/kstest.html. Date accessed: 18, May 2018.

[67] B. H. Cornish and L. C. Ward, "Data analysis in multiple-frequency bioelectrical impedance analysis," *Physiological Measurement*, vol. 19, no. 2, p. 275, 1998.

[68] "One-sample and paired-sample t-test." `https://www.mathworks.com/help/stats/ttest.html`. Date accessed: 25, Jun 2018.

[69] P. Yang, F. Tian, and Y. Ohki, "Dielectric properties of poly(ethylene terephthalate) and poly(ethylene 2,6-naphthalate)," *IEEE Transactions on Dielectrics and Electrical Insulation*, vol. 21, pp. 2310–2317, Oct 2014.

[70] "DSA800 series — spectrum analyzers." `https://www.rigolna.com/products/spectrum-analyzers/dsa800/`. Date accessed: 19, Jul 2018.

Appendices

APPENDIX A

Física 2018: Abstract

GRAU DE HUMIDADE EM POLYETHYLENE TEREPHTHALATE (PET) POR ESPECTROSCOPIA DE IMPEDÂNCIA ELÉTRICA

Emanuel Duarte[1], J P P Domingues[1,2], João Cardoso[1]

[1] Departamento de Física da Universidade de Coimbra

[2] CIBIT – Universidade de Coimbra

E-mail de contacto: jpd@uc.pt

RESUMO

A Espectroscopia de Impedância Elétrica (EIE) é uma técnica com largo leque de aplicações na caracterização de propriedades físico-químicas de materiais sólidos e líquidos. Consiste na aplicação de uma tensão ou corrente variáveis a uma amostra e consequente medição da corrente induzida ou da queda de tensão na amostra para assim determinarmos a sua impedância – a resposta em módulo e fase - numa gama definida de frequências (Grossi and Riccò, 2017, Callegaro, 2009).

O presente trabalho descreve um método baseado num impedancímetro composto por um dispositivo capaz de gerar/medir/gravar sinais analógicos e digitais – um osciloscópio USB comercial, *Digilent, Inc* - Analog Discovery, - ao qual foi adicionado um *interface* hardware/software que inclui circuitos de controlo e leitura da temperatura. O software de controlo, processamento e interface gráfico com o utilizador é baseado em Matlab.

O resultado é um instrumento portátil, de baixo custo adaptado à caracterização elétrica de um material polimérico, PET, um polyester higroscópico ($C_{10}H_8O_4$) com enorme relevância industrial na área dos vasilhames de água engarrafada, entre outras. Este material primário é usado como dielétrico num contentor que funciona como um condensador integrado num circuito RLC e cuja temperatura pode ser controlada. Provou-se a relação entre essa caracterização elétrica (impedância) e o grau de humidade relativa (HR) contido em amostras desse material, característica importante para a sua aceitação/rejeição no processo industrial. Neste contexto a humidade relativa é definida como a relação entre o conteúdo, em massa, de água relativamente à massa do material seco. Os resultados preliminares apontam para níveis mínimos de deteção de humidade relativa de 0.04%HR uma sensibilidade de 850 Hz/%HR correspondendo a uma variação no pico de ressonância medida através da curva da fase em função da frequência e uma resolução da ordem de 0.02%HR, na zona de variação da humidade relativa que é mais interessante para o estudo em causa (0 - 0.5%).

Independentemente da evolução da sua base de hardware para uma versão totalmente desenvolvida no laboratório (Grupo de Eletrónica e Instrumentação do

LIBPhys, Departamento de Física da Universidade de Coimbra), o instrumento desenvolvido possui características de flexibilidade que permitem que seja adaptável a outro tipo de materiais – bastando para isso alteração da configuração dos elétrodos ou do circuito de controlo de temperatura, por exemplo - como é o caso em curso da caracterização da mobilidade iónica em argilas terapêuticas e outras aplicações que se preveem no futuro.

[1] Marco Grossi and Bruno Riccò, J. Sens. Sens. Syst., 6, 303–325, 2017

[2] Lucca Callegaro, Electrical Impedance: Principles, Measurement and Applications, CRC Press, 2009

[3] Sara Anjo, The Electrical Impedance Spectroscopy Technique - 3 Case Studies in chemical and biological materials, Master Thesis, University of Coimbra, 2016

APPENDIX B

Impedance Meter Box

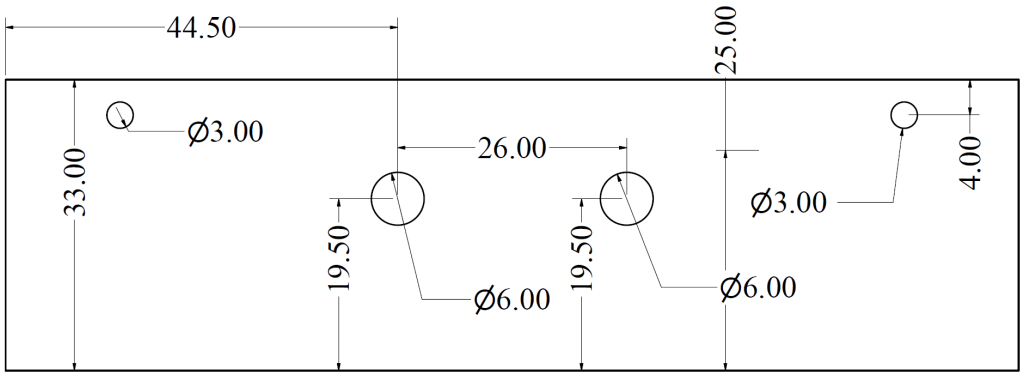

Figure B.1: 2D drawing correspondent to the box designed to protect impedance meter: front view (holes (6.0 *mm* diameter) used for electrodes and PT1000).

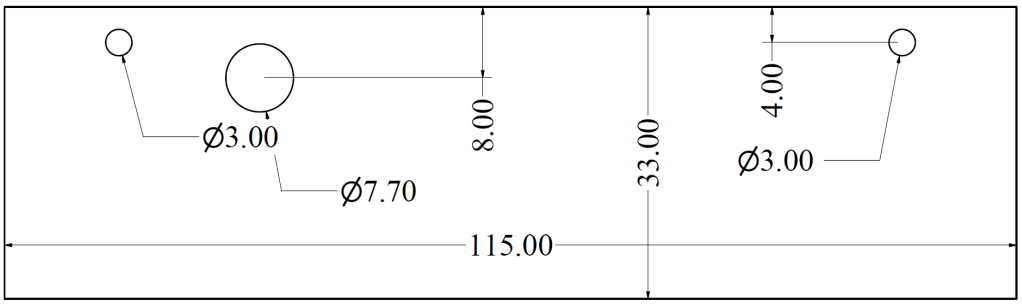

Figure B.2: 2D drawing correspondent to the box designed to protect impedance meter: back view (hole (7.7 *mm* diameter) used for power supply).

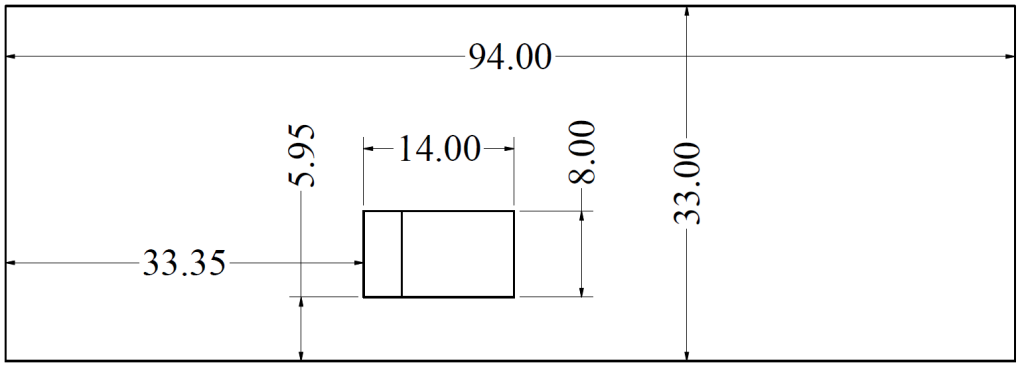

Figure B.3: 2D drawing correspondent to the box designed to protect impedance meter: left view (hole used by micro-USB).

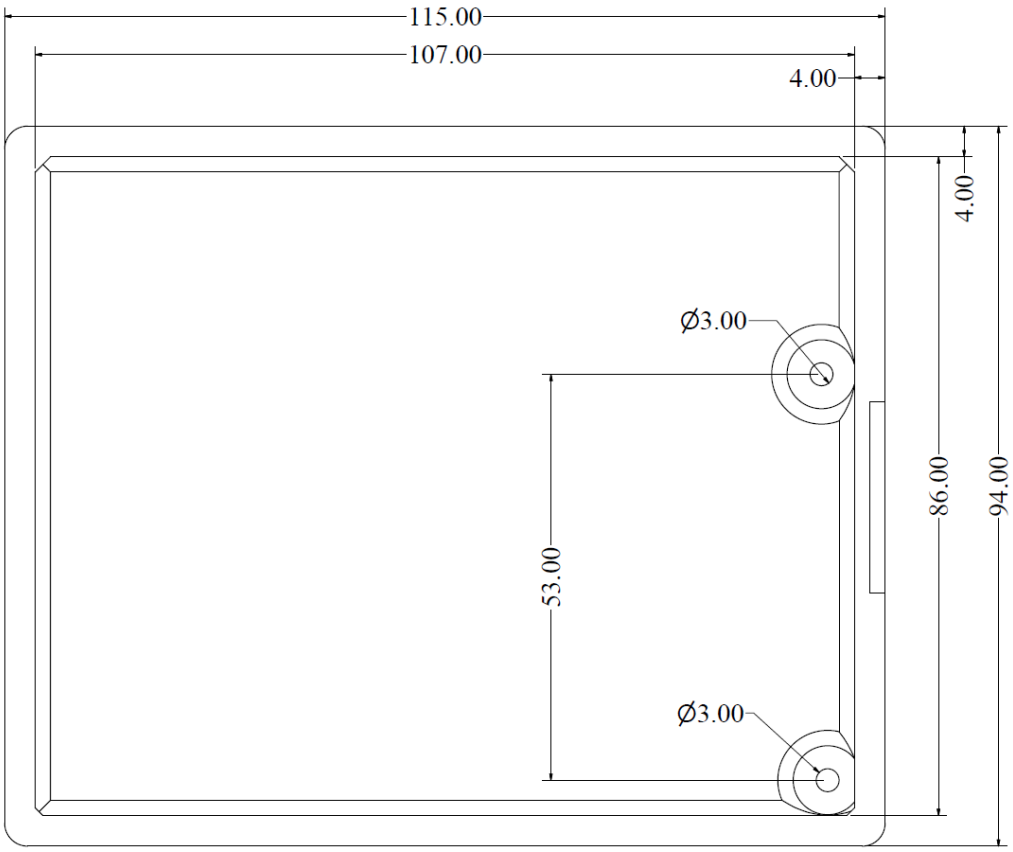

Figure B.4: 2D drawing correspondent to the box designed to protect impedance meter: top view (holes used to screw the PCB into it).

APPENDIX C

Peloids Sample Holder (box system)

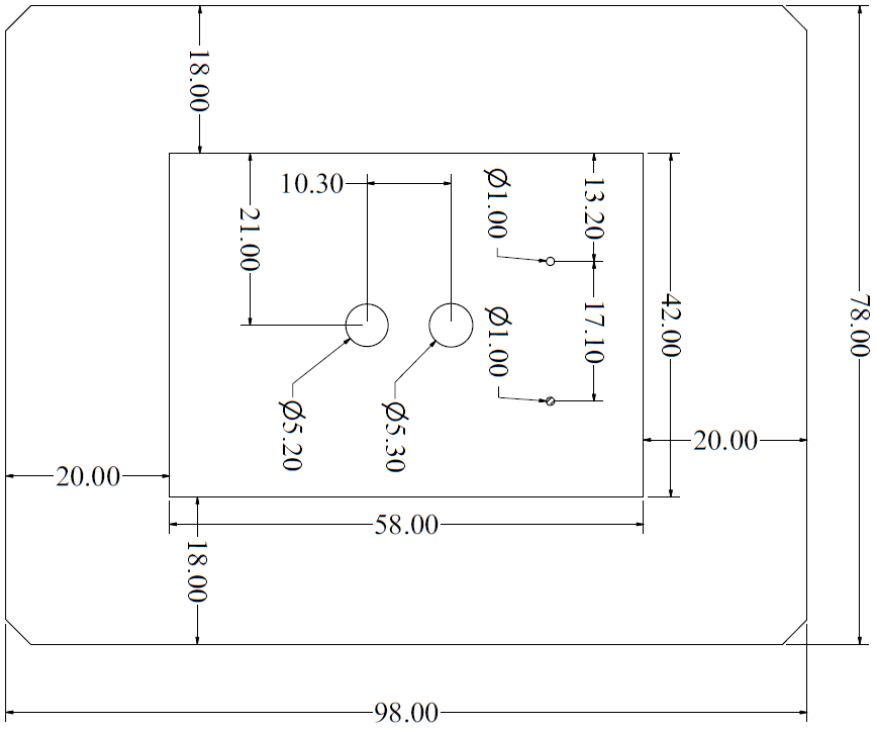

Figure C.1: 2D drawing correspondent to the peloid sample holder: top view (2 holes for temperature measurement (5.20 *mm* and 5.30 *mm* diameter) and 2 holes used by Ni-Cr wire (1.00 *mm* diameter each).

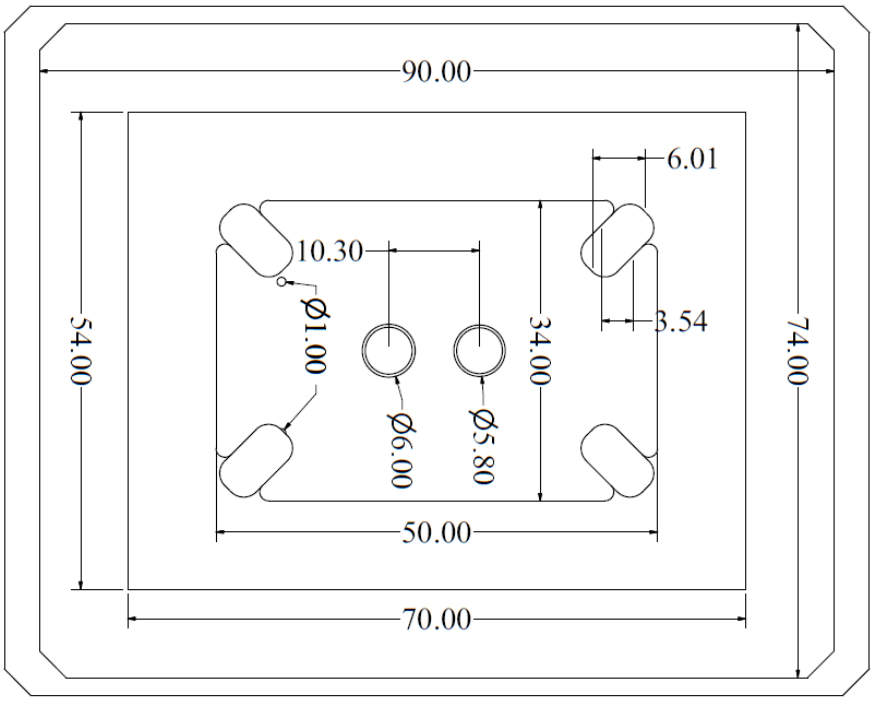

Figure C.2: 2D drawing correspondent to the peloid sample holder: inside top view (2 holes for temperature measurement (6.00 *mm* and 5.80 *mm* diameter) and 2 holes used by Ni-Cr wire (1.00 *mm* diameter each).

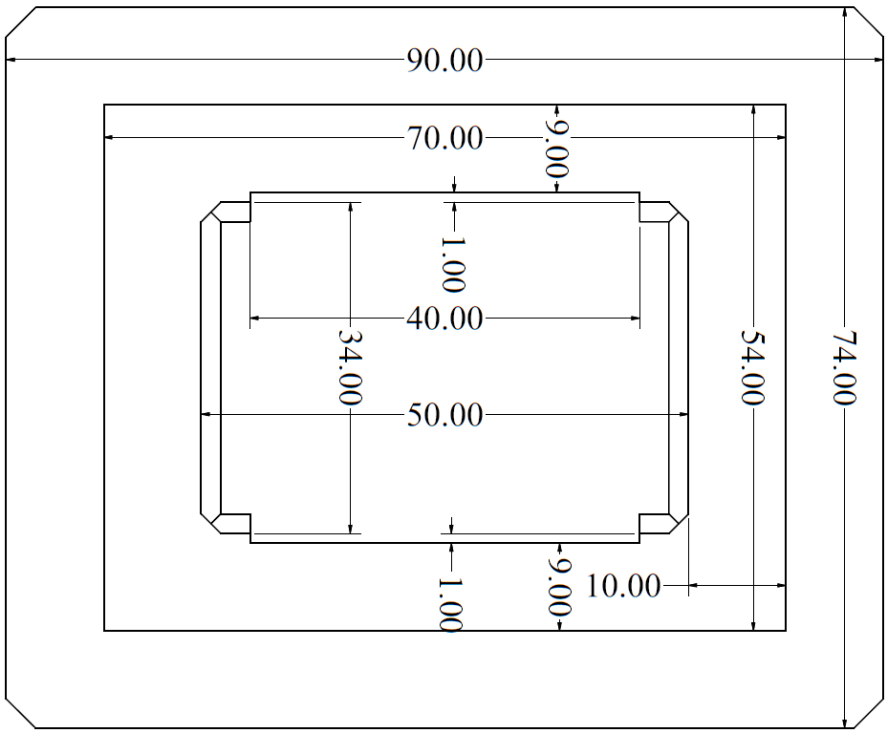

Figure C.3: 2D drawing correspondent to the peloid sample holder: inside bottom view (1 *mm* in each wall to electrodes application).

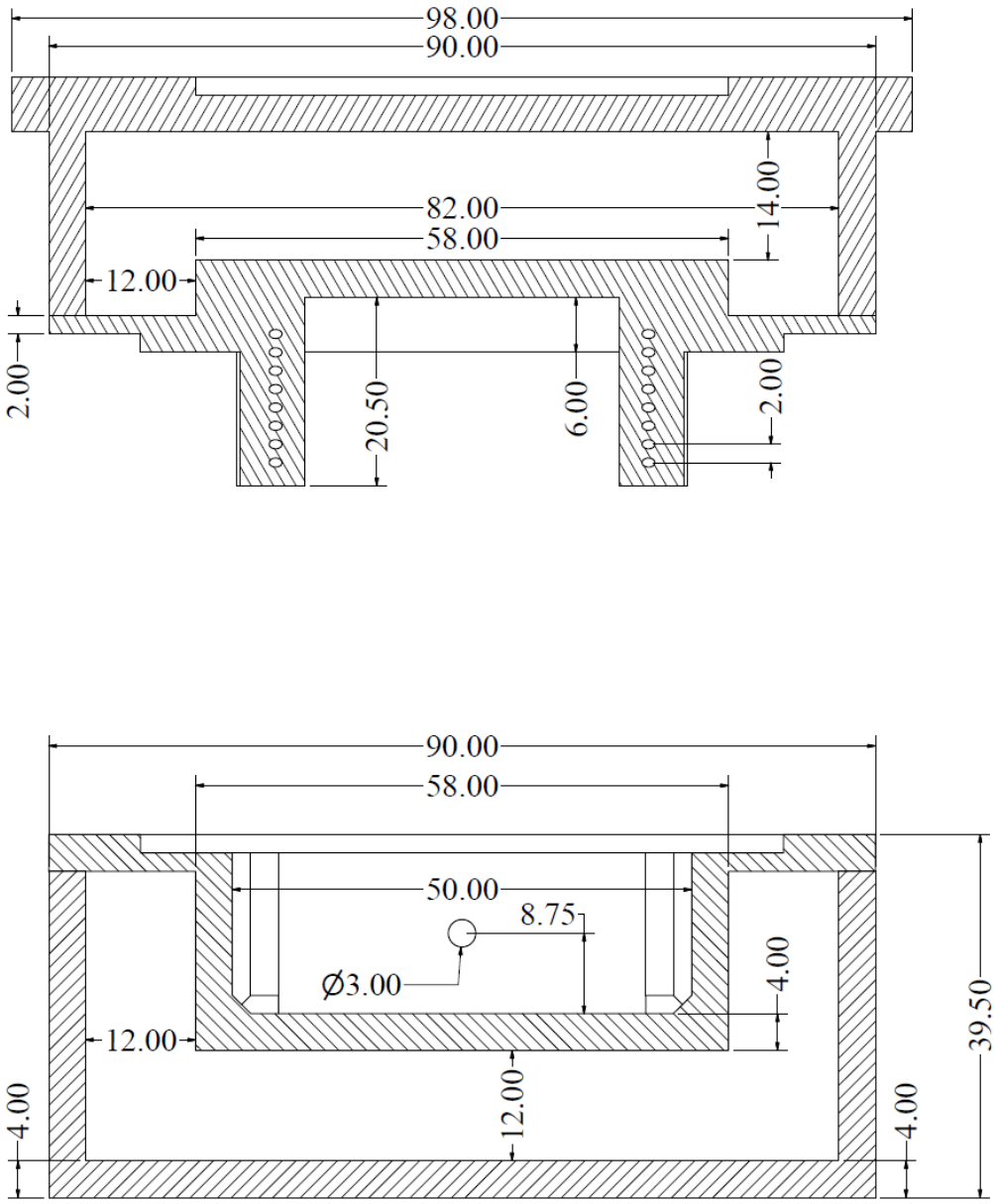

Figure C.4: 2D sectional drawing correspondent to the peloid sample holder: right view (hole (3.0 *mm* diameter) used for electrodes).

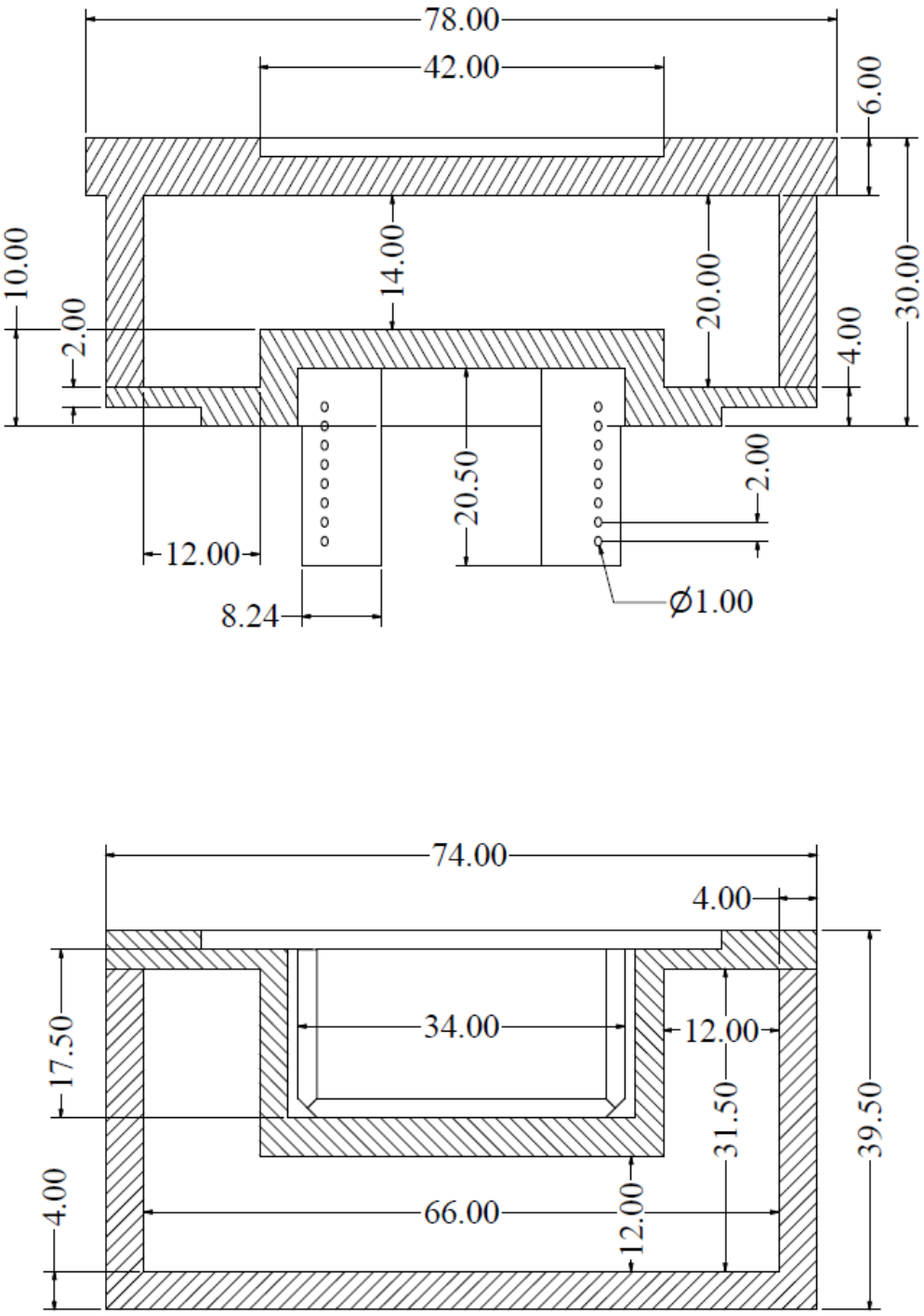

Figure C.5: 2D sectional drawing correspondent to the peloid sample holder: front view (4 column with holes (1.0 *mm* diameter) support the Ni-Cr wire).